IMPROVING THE GPR REFLECTION METHOD FOR ESTIMATING SOIL MOISTURE AND DETECTION OF CAPILLARY FRINGE AND WATER TABLE IN A BOREAL AGRICULTURAL FIELD

by

© CHAMEERA ILLAWATHURE

A Thesis submitted to the

School of Graduate Studies

in partial fulfillment of the requirements for the degree of

Master of Science

School of Science and the Environment

Grenfell Campus

Memorial University of Newfoundland

April 2019

Corner Brook Newfoundland

ABSTRACT

Improving the GPR reflection method for estimating soil moisture and detection of capillary fringe and water table in a boreal agricultural field

by

Chameera Illawathure

Advisor: Dr. Lakshman Galagedara

Committee members: Dr. Mumtaz Cheema & Dr. Adrian Unc

The objective of this thesis was to monitor the soil moisture (SM) and water table depth (WTD) in an agricultural field using ground-penetrating radar (GPR). First, SM was estimated using hyperbola-fitting method (27-50 cm depth range) and compared with vertically installed 30 cm long Time Domain Reflectometry (TDR) probe data. TDR-measured and GPR-estimated SM were not significantly different, and the root mean square error (RMSE) was 0.03 $m^3\ m^{-3}$. Second, the depth of the capillary fringe (D_{CF}) was estimated distinguishing the reflections from the top of the capillary fringe in a GPR radargram. A site-specific strong linear relationship ($R^2 = 0.9778$) of D_{CF} and measured-WTD was developed. RMSE between GPR-based WTD and actual WTD was 0.194 m. Proposed average capillary height for the particular site throughout the growing season (0.741 m) agrees with the existing literature and would be beneficial for the agricultural water management in the region.

Keywords: agricultural, boreal, capillary fringe, GPR, hyperbola fitting, soil moisture, water table depth

ACKNOWLEDGEMENTS

As my advisor, Dr. Lakshman Galagedara, has created an invaluable space for me to take part in this research and improve myself as a researcher in a promising way. I appreciate the freedom he has given me to find my own path and the guidance and support he offered. Financial aid was entirely provided by Dr. Galagedara as well. Many thanks to him and to his research grants funded by Research and Development Corporation, Newfoundland and Labrador (Ignite R&D) and Research office of Grenfell Campus, Memorial University of Newfoundland, Canada.

I extend my sincere gratitude to the committee members, Dr. Mumtaz Cheema and Dr. Adrian Unc for their valuable inputs to this work. Research collaborators from Boreal Ecosystem Research Facility of Grenfell Campus, Department of Fisheries and Land Resources of the Government of Newfoundland, and colleagues from the Memorial University of Newfoundland are highly acknowledged. My past teachers, friends, trainers and, co-workers should necessarily be included in the acknowledgement. I must express my very profound gratitude to my loving family for providing me with unfailing support and continuous encouragement.

This work would not have been possible without the existing methods, instruments, and knowledge. Special thanks should go for the researchers who advanced the relevant research field even without the technology development like nowadays.

Thank you all!

Chameera Illawathure

TABLE OF CONTENTS

LIST OF TABLES

LIST OF FIGURES

LIST OF ABBREVIATIONS AND SYMBOLS

BERF	Boreal Ecosystem Research Facility
BH	Borehole
c	Electromagnetic wave velocity in free space/ speed of light
CMP	Common mid-point
CO	Common offset
D_{CF}	Depth to the capillary fringe
EM	Electromagnetic
GovNL	Government of Newfoundland and Labrador
GPR	Ground Penetrating Radar
max	Maximum
min	Minimum
MMSA	Multiresolution Monogenic Signal Analysis
MOP	Multi offset profile
n	Number of samples
n.d	No date
NL	Newfoundland
PBRS	Pynn's Brook Research Station
r	Correlation coefficient
R	Normal incidence reflection coefficient
RMSE	Root Mean Square Error
Rx	Receiver antenna
SM	Soil moisture

TDR	Time Domain Reflectometry
TRIME	Time-domain Reflectometry with Intelligent Micro Elements
t_{rw}	Reflected wave travel time
TWTT	Two-way travel time of GPR waves
Tx	Transmitter antenna
v	Average radar velocity
v_{rw}	Reflected wave velocity
v_t	Total volume of soil
v_w	Volume of water
WNL	Western Newfoundland
WTD	Water table depth
WTD_m	Measured water table depth
WTD_p	Predicted water table depth
ZOP	Zero offset profile
α	attenuation coefficient/ significance interval
ε	absolute permittivity
ε_0	permittivity of a vacuum
ε_r	Relative permittivity (dielectric constant)
θ_m	Gravimetric soil moisture content
θ_v	Volumetric soil moisture content
σ	Electrical conductivity

LIST OF APPENDICES

CHAPTER 1

Introduction and Overview

1.1 Introduction

Maintaining the ideal soil moisture (SM) in the root zone (unsaturated zone) at each growing phase, and understanding the behavior and contamination possibilities of groundwater (saturated zone) are the main components of sustainable water management in agriculture. Soil moisture is the temporary water storage at the unsaturated condition in between atmosphere and groundwater reservoir; the key factor that helps the growing plants by allowing to uptake their nutrients from the soil. Water table demarcates the boundary between saturated-unsaturated soils.

SM data may also be useful for crop yield forecasting and early warning of droughts, organic matter decomposition, heat transfer at the land-atmosphere interface and, to manage insect and disease control (Agrios, 1997; Champagne *et al*., 2012; Dari *et al*., 2018; Engman, 1991; Ghorbani *et al*., 2008; Koster, 2010; Schwingshackl *et al*., 2017). Additionally, SM also helps to improve agricultural practices without environmental degradation (Engman, 1991) and regulates the distribution of precipitation between runoff and infiltration (Burns, 1974; Li *et al*., 2017). The SM is neither homogeneously dispersed nor static over time, because of the heterogeneity of soil properties, topography, land cover, and the non-uniformity of rainfall and evapotranspiration (Engman, 1991). A large number of data are needed to measure SM in a larger area. Gravimetric SM (θ_m) of a particular soil sample can be derived from mass loss by oven drying a moist sample, which is considered as the direct and the standard method. Destructive, non-repeatable, and time and labor consuming circumstances of the gravimetric method directed researchers toward indirect methods of SM determination (Huisman *et al.,* 2003; Lambot *et al.,* 2004). The indirect method could be either large-scale or point-scale measurements. Remote sensing techniques such as satellites are being used for large-scale SM detection, but has low resolution and restricted to the soil surface (Errico *et al*., 2000). Recognized indirect methods for SM measurements are; neutron probes (Chanasyk & Naeth, 1996; Kodikara *et al.,* 2013) electromagnetic probes (time domain reflectometry/ TDR) (Brandyk *et al.,* 2016; Galagedara *et al.,* 2003b), capacitance sensors (Zotarelli *et al.,* 2011), electrical resistance probes (Williams, 1980), heat pulse sensors (Price, 1982), fiber optic sensors (Ciocca *et al.,* 2012), cosmic-ray sensors (Sigouin *et al*., 2016) and gamma-ray scanners (Baldoncini *et al.,* 2019; Carroll, 1981). Electromagnetic probes among all of them have become dominant and standard during the last few decades, but low sampling volume and limiting to point measurements are the main disadvantages (Fisher *et al*., 1992; Galagedara *et al*., 2003a; Greaves *et al*., 1996; Van Overmeeren *et al*., 1997; Weiler *et al*., 1998).

A reliable indirect method which is repeatable and rapid to obtain high-resolution SM data at large-scales would be worthy than conventional point measurements (Galagedara *et al*., 2005; Huisman *et al*., 2003; Takeshita *et al*., 2004). Ground penetrating radar (GPR) operates in between 10 to 1200 MHz electromagnetic frequency bandwidth and is primarily reliable for determining SM at a sample volume of 1 m^3 or more (Davis & Annan, 1989; Galagedara *et al*., 2003a; Grote *et al*., 2003; Hubbard *et al*., 2002). GPR is a non-destructive, portable and time-effective method for large-scale applications (Alumbaugh *et al*., 2002; Bikowski *et al*., 2010; Doolittle *et al*., 2006; Du & Rummel, 1996; Galagedara *et al*., 2003a, 2003b, 2005; Gao *et al*., 2012; Grote *et al*., 2002; Huisman *et al*., 2001, 2003; Jacob & Hermance, 2004; Jadoon *et al.,* 2010; Minet *et al*., 2010; Parkin *et al*., 2000; Rucker & Ferre, 2004; Stoffregen *et al*., 2002; Wijewardana & Galagedara, 2010).

In addition, GPR is capable of non-intrusively detecting the water table and sub-surface anomalies such as cavities and sub-surface flow paths (Doolittle *et al*., 2006; Gish *et al*., 2002; Paz *et al*., 2017; Shih *et al*., 1986). Irrigation is needed in agriculture if the soil moisture in the unsaturated zone and/or the water table depth (WTD) is not appropriate for the plant root system to absorb water and nutrients. In contrast, a drainage system must be used to control the excess amount of surface/groundwater in agricultural fields. However, intensive agricultural activities contaminate soil and water resources (Heinse & Link, 2013; Nimmo, 2009). When the contaminants get into the groundwater, it is not only harmful to human use but also difficult to control spreading into other areas. Therefore, studying groundwater dynamics is also important with SM measurements. The accuracy of WTD measurements over a large area can be improved by increasing the number of monitoring wells, but it is costly and time-consuming.

When using GPR, the accuracy of WTD estimations depends on the average radar velocity (v) from the surface to the water table (Doolittle *et al*., 2006; Johnson, 1992; Kowalczyk *et al*., 2018). The user should define v during data collection and processing within a range of 0.060 m/ns (wet) to 0.150 m/ns (dry) in common soils (Davis & Annan, 1989). Additionally, in a GPR radargram, a prominent and early reflection can come from the capillary fringe or the transition zone, but not from the actual water table (Daniels *et al*., 2004; Endres *et al.*, 2000; Klenk, 2014; Pyke *et al.*, 2008). These limitations affect the precision of GPR based WTD estimations. However, the importance of knowing radar wave velocity v of subsurface materials, influence of SM on the v, presence of capillary fringe, and tracing water table as a zone on the GPR radargram rather than a sharp boundary are well documented (Annan *et al*., 1991; Bano, 2006; Bevan *et al.*, 2003; Endres *et al*., 2000; Loeffler & Bano, 2004; Nakashima *et al.*, 2001; Paz *et al*., 2017; Takeshita *et al*., 2004; Tsoflias *et al*., 2001). Number of studies related to water table monitoring using GPR have also been reported in agricultural practices and/or groundwater pollution studies during the last two decades (Conant *et al*., 2004; Corbeanu *et al*., 2002; Gish *et al.*, 2002; Lambot *et al.*, 2008; Lunt *et al*., 2005; Mahmoudzadeh *et al.,* 2010; Talley *et al*., 2005; Tsoflias & Becker, 2008). The GPR method has also been used in water table studies in other applications such as studying preferential flows in mining (Grandjean & Gourry, 1996), groundwater dependent ecosystems (Molina-Sánchez *et al*., 2015; Zurek *et al.*, 2015), and civil/structural engineering works (Slowik, 2013).

1.1.1 Rationale of the study

Long-lasting winter permits only one crop season in Newfoundland and Labrador (NL), Canada (Kavanagh, 2014). High soil acidity, and low soil organic matter, cation exchange capacity, nutrients retention and water holding capacity, and poor soil structure with sandy soils are the other major barriers for agricultural production in the region (Department of Fisheries and Land Resources, n.d.). A recent hydrological modelling in western Newfoundland soils showed lower saturation, quicker hydrological responses, and higher infiltration and percolation rates in podzolic soils when compared with most other agricultural soils (Altdorff *et al.*, 2017). Low intensity of farming due to these circumstances has cut down farmers' profits and trends towards agriculture.

Studies have been carried out and ongoing for introducing winter crops (Kavanagh, 2014), alternative fruits and vegetables, forage mixtures for yield and quality (Haverstock, 2014), different soil amendments, and integrated pest management (Madore, 2014). Currently, the Government of Newfoundland and Labrador has engaged in long-term multidisciplinary research projects in collaboration with Memorial University to improve agricultural practices and production in NL. However, the impact of spatio-temporal variations of SM and fluctuation of WTD during the growing period is not well understood in podzolic soils in NL. Without this knowledge, irrigation and drainage practices cannot be improved for increasing the agricultural and water productivity. In addition, groundwater fluctuation and underground flow paths are not well studied at the regional scale to achieve better WTD management and reduce groundwater contamination threats under different agricultural management practices. The present study was conducted to fill this knowledge gap.

1.1.2 Objectives

Therefore, the main goal of this study was to monitor the spatio-temporal variation of SM and WTD using the GPR technique throughout the growing season. Following main objectives were considered in order to accomplish the main goal. These two objectives were achieved by two separate research studies as discussed in the next two chapters. Specific objectives with respect to each study are given in the relevant chapter.

1. To establish a methodology to estimate the spatio-temporal variation of SM in the agricultural root zone using GPR hyperbola analysis.
2. To distinguish the capillary fringe reflection in a GPR profile for precise WTD estimation.

1.1.3 Thesis organization

This thesis encompasses four chapters, including two chapters as research papers.

Chapter One: starts with an overview, rationale of the study and overall objectives. It also provides the theoretical background of GPR for studying SM and WTD.

Chapter Two: establishes a methodology to estimate SM in the crop root zone. This also includes a comparison of the sample area of TDR- and GPR-based SM determination.

Chapter Three: focuses on precise WTD estimation. This chapter shows the capability of WTD estimation using GPR as well as the challenges of distinguishing the water table -reflection from the capillary fringe reflection. The proposed method provides a good augment of precise WTD estimation using GPR.

Chapter Four: includes the general discussion, conclusions, and further directions.

1.2 Theoretical Background

1.2.1 Basic principles of GPR

Estimation of SM and WTD from GPR are based on the transmission and reflection of an electromagnetic wave that is transmitted to the studied medium (Chanzy *et al.*, 1996). The transmitter antenna (Tx) generates a short pulse of radar wave which propagates away in a broad beam (Daniels *et al*., 2004). Electrical properties of the subsurface cause part of the transmitted signal to be reflected, refracted and attenuated. The reflected signal is detected by the receiver antenna (Rx) (Davis & Annan, 1989). As indicated by Figure 1.1, several radar waves may reach the Rx, and wave propagation geometry may vary according to the survey method (Du & Rummel, 1994; Huisman *et al*., 2003; Paz *et al*., 2017). The direct ground wave directly propagates from the Tx to the Rx through the ground. The airwave directly propagates through the air between the Tx and Rx. The reflected or refracted waves characterize energy returned directly at a boundary where different electrical properties are encountered.

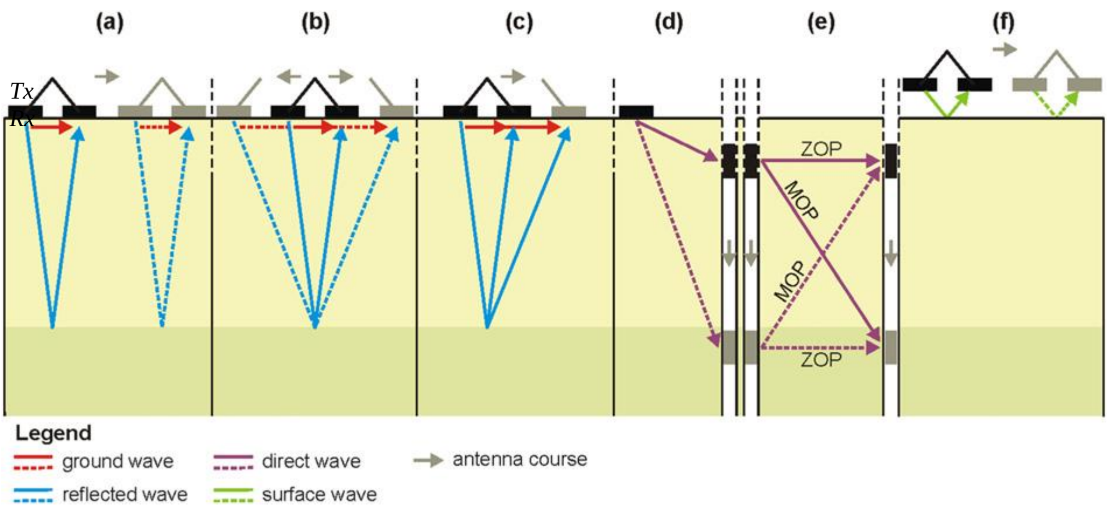

Figure 1.1: Electromagnetic wave propagation paths with respect to different GPR survey methods (after Paz *et al*., 2017). (a) Common offset, (b) Common midpoint, (c) Wide-angle reflection and refraction, (d) Vertical radar profile, (e) Borehole GPR, ZOP being zero-offset profile and MOP multi-offset profile, (f) Surface reflection.

1.2.2 SM estimation from the GPR velocity

SM can be expressed as volumetric water content, θ_v (θ_v = soil bulk density × θ_m) that can be defined as the ratio of the volume of water, v_w, to the total soil volume, v_t as given in Equation 1.1 (Swiss Federal Institute of Technology, 2017).

$$\theta_v = \frac{v_w}{v_t} \tag{1.1}$$

The relative permittivity (ε_r) also known as the dielectric constant of a material is the ratio between its absolute permittivity (ε) and the permittivity of a vacuum (ε_0) as given in Equation 1.2. Permittivity is a material property that affects the Coulomb force between two point charges in a material (IEEE Standard Board, 1998).

$$\varepsilon_r = \frac{\varepsilon}{\varepsilon_0} \tag{1.2}$$

Radar signal velocity (v) of a non-magnetic and low-loss geological material is related to ε_r and the electromagnetic wave propagation velocity in free space (c = 0.3 m/ns) as given in Equation 1.3 (Davis & Annan, 1989; Neal, 2004; Schmelzbach *et al.*, 2012).

$$v = \frac{c}{\sqrt{\varepsilon_r}} \tag{1.3}$$

Several empirical and mixing models have been developed to relate SM to ε_r (Jones & Or, 2002). The relationship between ε_r and θ_v (Eq. 1.4) was suggested by Topp *et al*. (1980) is widely being used in vadose zone hydrology.

$$\theta_v = -5.3 \times 10^{-2} + 2.92 \times 10^{-2}\varepsilon_r - 5.5 \times 10^{-4}\varepsilon_r^2 + 4.3 \times 10^{-6}\varepsilon_r^3 \tag{1.4}$$

Root mean square error (RMSE) is a measure of the differences between the predicted values by a model or an estimator and the observed values and can be calculated by Equation 1.5. To evaluate the accuracy of GPR-based θ_v estimations by comparing with gravimetric SM as the standard method or with TDR as the commonly used indirect method, , RMSE is generally used.

$$\mathrm{RMSE} = \sqrt{\sum_{i=1}^{N} \frac{(p_i - o_i)^2}{N}} \tag{1.5}$$

where p_i is the predicted value, o_i is the observed value and N is the sample size.

1.2.3 Water table determination from the GPR

The amount of pore spaces filled with water generally increases with the depth of a soil profile and reaches the zone of saturation (phreatic zone). The upper surface of the zone of saturation is called water table and, it reflects more than 40% of GPR wave energy (Kowalczyk *et al.*, 2018) in coarse-grained soils. Accordingly, water table can give continuous, mostly flat reflections with high amplitude in GPR radargrams (Davis & Annan, 1989; Greaves *et al.*, 1996; Van Overmeeren, 1998) and has become an essential method in groundwater studies (Beres & Haeni, 1991; Tsoflias *et al.*, 2001).

The real part of the dielectric constant (ε_r) and the electrical conductivity (σ) control the propagation of EM waves. Attenuation coefficient (α) can be derived using Equation 1.6 (Davis & Annan, 1989; Neal, 2004; Algeo *et al.*, 2016).

$$\alpha \approx \frac{1}{2c\varepsilon_0} \frac{\sigma}{\sqrt{\varepsilon_r}} \tag{1.6}$$

Additionally, Bentley & Trenholm (2002) have described that capillary fringe reflection has the opposite to that of airwave. Doolittle *et al*. (2006) reported that oscillations in the reflected radar pulse due to water table result in a series of bands to represent the water table in a radar profile.

The normal incidence reflection coefficient (R) is (Davis & Annan, 1989),

$$R = \frac{\sqrt{\varepsilon_{r_1}} - \sqrt{\varepsilon_{r_2}}}{\sqrt{\varepsilon_{r_1}} + \sqrt{\varepsilon_{r_2}}} \tag{1.7}$$

where the dielectric permittivity above and below the water table reflection are ε_{r_1} and ε_{r_2}, respectively.

1.2.4 Assumptions and limitations

It is assumed in GPR analysis that propagation and reflection of electromagnetic waves occur instead of induction in a material. Because GPR operating frequency bandwidth exceeds the material's transition frequency and displacement currents are dominant in that frequency spectrum (Davis & Annan, 1989). However, this assumption is not acceptable for the materials with high magnetic permeability.

GPR wave propagation is three-dimensional. However, most GPR applications assume that wave propagation in two-dimensions to simplify the analysis. Under natural soil conditions where anisotropic soil matrix is present, this assumption would not be fully accurate.

Empirical derivations in most GPR studies consider dielectric and lossless or low-loss materials. GPR would not be used as a reflection imaging technique if this assumption is not applicable.

1.3 Potential impacts of the study

At the global scale, the world is moving to unpredictable climate changes. Expected extreme weather events may cause food security challenges due to land and water degradation. Local food production is the best option to achieve food security in the region. Natural barriers of inherent soil properties on agriculture in NL have already created a lack of crop production in the province. Therefore, more challenges may happen in the future.

Maintaining the required SM in the root zone results in optimum crop yields. A profitable agricultural industry may invest in novel technologies, research, and developments to increase the local crop production. In contrast, intensive agriculture may cause groundwater pollution. Implementing the best possible water management with a better understanding of groundwater fluctuation of the region will reduce these threats. As a result, sustainable use of land and water resources would be ensured for future generations.

References

Agrios, G.N. 1997. Plant Pathology, Academic Press, San Diego. pp. 200-216

Algeo, J., Van Dam, R.L., Slater, L. 2016. Early-time GPR: a method to monitor spatial variations in soil water content during irrigation in clay soils. *Vadose Zone Journal*, 15(11), doi.org/10.2136/vzj2016.03.0026

Altdorff, D., Galagedara, L., Unc, A. 2017. Impact of projected land conversion on water-balance of boreal soils in western Newfoundland. *Journal of Water and Climate Change*, doi: 10.2166/wcc.2017.016

Alumbaugh, D., Chang, P., Paprocki, L., Brainard, J., Glass, R.J., Rautman, C.A. 2002. Estimating moisture contents in the vadose zone using cross-borehole ground penetrating radar: a study of accuracy and repeatability. *Water Resources Research*, 38, p. 1309

Annan, A.R, Cosway, S.W, and Redman, J.D. 1991. Water table detection with ground penetrating radar: in Expanded Abstracts. 61st Annual International Meeting of the Society of Exploration Geophysicists, *Society of Exploration Geophysics*, pp. 494-496

Baldoncini, M., Albéri, M., Bottardi, C., Chiarelli, E., Raptis, K., Strati, V., Mantovani, F. 2019. Biomass water content effect on soil moisture assessment via proximal gamma-ray spectroscopy. *Geoderma*, 335, pp. 69-77

Bano, M. 2006. Effects of the transition zone above a water table on the reflection of GPR waves. *Geophysical Research Letters*, 33(13), doi:10.1029/2006GL026158

Bentley, L., Trenholm, N. 2002. The accuracy of water table elevation estimates determined from ground penetrating radar data. *Journal of Environmental & Engineering Geophysics*, 7(1), 37-53, doi:10.4133/JEEG7.1.37

Beres, M., Haeni, F.P. 1991. Application of ground penetrating radar methods in hydrogeologic studies. *Ground Water*, 29, pp. 375–386

Bevan, M.J., Endres, A.L., Rudolph, D.L., Parkin, G.W. 2003. The non-invasive characterization of pumping induced dewatering using ground penetrating radar. *Journal of Hydrology*, 281, pp. 55–69

Bikowski, J., van der Kruk, J., Huisman, J.A., Vereecken, H., Vrugt, J.A. 2010. Inversion and sensitivity analysis of GPR data with waveguide dispersion using Markov Chain Monte Carlo simulation. Proceedings of the 8th International Conference on Ground Penetrating Radar, Lecce (Italy). pp. 722–726

Brandyk, A., Kiczko, A., Majewski, G., Kleniewska, M., Krukowski, M. 2016. Uncertainty of Deardorff's soil moisture model based on continuous TDR measurements for sandy loam soil. *Journal of Hydrology and Hydromechanics*, 64(1), pp. 23-29

Burns, I.G. 1974. A model for predicting the redistribution of salts applied to fallow soils after excess rainfall or evaporation. *Journal of Soil Science*, 25(2), pp. 165-178

Carroll, T.R. 1981. Airborne soil moisture measurements using natural terrestrial gamma radiation. *Soil Science*, 132(5), pp. 358-366

Champagne, C., Berg, A., McNairn, H., Drewitt, G., Huffman, T. 2012. Evaluation of soil moisture extremes for agricultural productivity in the Canadian prairies. *Agricultural and forest meteorology*, 165, pp. 1-11

Chanasyk, D.S., Naeth, M.A. 1996. Field measurement of soil moisture using neutron probes. *Canadian journal of soil science*, 76(3), pp.317-323

Chanzy, A., Tarussov, A., Judge. A., Bonn, F. 1996. Soil water content determination using a digital ground-penetrating radar. *Soil Science Society of America Journal*, 60, pp. 1318-1326

Ciocca, F., Lunati, I., van de Giesen, N., Parlange, M.B. 2012. Heated optical fiber for distributed soil-moisture measurements: A lysimeter experiment. *Vadose Zone Journal*, 11(4), doi: 10.2136/vzj2011.0199

Conant Jr., B., Cherry, J.A., Gillham, R.W. 2004. A PCE groundwater plume discharging to a river: influence of the streambed and near-river zone on contaminant distributions. *Journal of Contaminant Hydrology*, 73, pp. 249–279

Corbeanu, R.M., McMechan, G.A., Szerbiak, R.B., Soegaard, K. 2002. Prediction of 3D fluid permeability and mudstone distributions from ground-penetrating radar (GPR) attributes: example from the Cretaceous Ferron Sandstone member, east-central Utah. *Geophysics*, 67, pp. 1495–1504

Daniels, D.J. 2004. Ground Penetrating Radar. Second Ed. *The Institute of Electrical Engineers*, London, United Kingdom

Dari, J., Morbidelli, R., Saltalippi, C., Massari, C., Brocca, L. 2018. Spatial-temporal variability of soil moisture: a strategy to optimize monitoring at the catchment scale with varying topography and land use. Proceedings of the 20th EGU General Assembly, 4-13 April, 2018, Vienna, Austria, p.7632 retrieved from https://www.egu2018.eu

Davis, J.L., Annan, A.P. 1989. Ground-penetrating radar for high-resolution mapping of soil and rock stratigraphy. *Geophysical Prospecting*, 37. pp. 531-551

Department of Fisheries and Land Resources (n.d.). Effect of Biochar Application on Soil Fertility and Crop Productivity in Sandy Soils of Happy Valley-Goose Bay, NL. Retrieved from http://www.faa.gov.nl.ca (accessed on 29.10.2018)

Doolittle, J.A., Jenkinson, B., Hopkins, D., Ulmer, M., Tuttle, W. 2006. Hydropedological investigations with ground-penetrating radar (GPR): Estimating water- table depths and local ground-water flow pattern in areas of coarse-textured soils. *Geoderma*, 131(3), pp. 317-329

Du, S., Rummel, P. 1996. Reconnaissance studies of moisture in the subsurface with GPR. Proceedings of the 5th International Conference on Ground Penetrating Radar. Kitchener, Ont., Canada, *Waterloo Centre for Groundwater Research*, 3. pp. 1241–1248

Endres, A.L., Clement, W.P., Rudolph, D.L. 2000. Ground penetrating radar imaging of an aquifer during a pumping test. *Ground Water*, 38(4), pp. 566-576, doi:10.1111/j.1745-6584.2000.tb00249.x

Engman, E.T. 1991. Applications of microwave remote sensing of soil moisture for water resources and agriculture. *Remote Sensing of Environment*, 35, pp. 213-226

Errico, R.M., Ohring, G., Derber, J., Joiner, J. 2000. Workshop on satellite data assimilation. B. *American Meteorological Society*, 81(10), p. 2457

Fisher, E., McMechan, G.A., Annan, A.P. 1992. Acquisition and processing of wide-aperture ground-penetrating radar data. *Geophysics*, 57(3). pp. 495-504

Galagedara, L., Parkin, G., Redman, J., Von Bertoldi, P., Endres, A.L. 2005. Field studies of the GPR ground wave method for estimating soil water content during irrigation and drainage. *Journal of Hydrology* (Amsterdam), 301(1-4), pp. 182-197, doi:10.1016/j.jhydrol.2004.06.031

Galagedara, L.W., Parkin, G.W., Redman, J.D. 2003a. An analysis of the ground-penetrating radar direct ground wave method for soil water content measurement. *Hydrological Processes*. 17(18), pp. 3615-3628, doi:10.1002/hyp.1351

Galagedara, L.W., Parkin, G.W., Redman, J.D., Endres, A.L. 2003b. Assessment of soil moisture content measured by borehole GPR and TDR under transient irrigation and drainage. *Journal of Environmental and Engineering Geophysics*, 8(2). pp. 77-86

Gao, S., Zhu, Z., Jiao, Q., Du, F. 2012. Application of GPR surface reflection method for estimating soil water content of bare soil. 12th International Conference on GPR, *IEEE*, doi:10.1109/ICGPR.2012.6254941

Ghorbani, R., Wilcockson, S., Koocheki, A. 2008. Soil management for sustainable crop disease control: a review. *Environmental Chemistry Letters*, 6, pp. 149, doi.org/10.1007/s10311-008-0147-0

Gish, T., Dulaney, W., Kung, K., Daughtry, C. 2002. Evaluating use of ground-penetrating radar for identifying subsurface flow pathways. *Soil Science Society of America Journal*, 66(5), pp. 1620-1629, doi:10.2136/sssaj2002.1620

Grandjean, G., Gourry, J.C. 1996. GPR data processing for 3D fracture mapping in a marble quarry (Thassos, Greece). *Journal of Applied Geophysics*, 36, pp. 19–30

Greaves, R.J., Lesmes, D.P., Lee, J.M., Toksoz, M.N. 1996. Velocity variations and water content estimated from multi-offset, ground-penetrating radar. *Geophysics*, 61, pp. 683-695

Grote, K., Hubbard, S., Rubin, Y. 2002. GPR monitoring of volumetric water content in soils applied to highway construction and maintenance. *The Leading Edge*, 21(5), doi:10.1190/1.1481259

Grote, K., Hubbard, S., Rubin, Y. 2003. Field-scale estimation of volumetric water content using ground-penetrating radar ground wave techniques. *Water Resources Research*, 39(11), doi:10.1029/2003WR002045

Haverstock, J. 2014. Forage Mixtures for Yield & Quality and Non-Traditional Forage Identification Trial. Provincial Agrifoods Research & Development Fund Report 2013-2014. Department of Natural Resources Forestry & Agrifoods Agency, Newfoundland and Labrador, Canada

Heinse, R., Link, T.E. 2013. Vadose Zone Processes: A compendium for teaching interdisciplinary modeling. *Journal of Contemporary Water Research & Education*, 152, pp. 22-31

Hubbard, S., Grote, K., Rubin, Y. 2002. Mapping the volumetric soil water content of a California vineyard using high-frequency GPR ground wave data. *The Leading Edge*. 21(6), doi:10.1190/1.1490641

Huisman, J., Hubbard, S.S., Redman, J.D., Annan, A.P. 2003. Measuring soil water content with ground penetrating radar: A review. *Vadose Zone Journal*, 2, pp. 476-491, doi:10.2113/2.4.476

Huisman, J.A., Sperl, C., Bouten, W., Verstraten, J.M. 2001. Soil water content measurements at different scales: Accuracy of time domain reflectometry and ground-penetrating radar. *Journal of Hydrology*. 245(1-4), pp. 48-58, doi:10.1016/S0022-1694(01)00336-5

IEEE Standards Board. 1998. IEEE Standard Definitions of Terms for Radio Wave Propagation. *IEEE*, doi: 10.1109/IEEESTD.1998.87897

Jacob, R.W., Hermance, J.F. 2004. Assessing the precision of GPR velocity and vertical two-way travel time estimates. *Journal of Environmental and Engineering Geophysics*, 9(3), pp. 143-153

Jadoon, K.Z., Lambot, S., Scharnagl, B., van der Kruk, J., Slob, E., Vereecken, H. 2010. Quantifying field-scale surface soil water content from proximal GPR signal inversion in the time domain. *Near Surface Geophysics*, 8, pp. 483-491

Johnson, D.G. 1992. Use of ground-penetrating radar for water table mapping, Brewster and Harwich, Massachusetts. Water Resources Investigations Report 90-4086, U.S. Geological Survey, Marlborough, Massachusetts

Jones, S.B., Or, D. 2002. Surface area, geometrical and configurational effects on permittivity of porous media. *Journal of Non-Crystalline Solids*, 305, pp. 247-254

Kavanagh, V. 2014. Viability of Winter Wheat and Spring Barley Cultivation for Animal Feed Production in Insular Newfoundland, 2013-2014 Year End Report, Department of Natural Resources Forestry & Agrifoods Agency, Newfoundland and Labrador, Canada

Klenk, P., Keicher, V., Jaumann, S., Roth, K. 2014. Current limits for high precision GPR measurements. Proceedings of the 15th International Conference on Ground Penetrating Radar, 30 June-4 July 2014, Belgium, doi:10.1109/ICGPR.2014.6970524

Kodikara, J., Rajeev, P., Chan, D., Gallage, C. 2013. Soil moisture monitoring at the field scale using neutron probe, *Canadian Geotechnical Journal*, 51(3), pp.332-345

Koster, R.D. 2010. Skill in streamflow forecasts derived from large-scale estimates of soil moisture and snow. *Nature Geoscience*, 3, pp. 613-616

Kowalczyk, S., Lejzerowicz, A., Kowalczyk, B. 2018. Groundwater table level changes based on ground penetrating radar images: a case study. Seventh International Conference on Ground Penetrating Radar, *IEEE Xplore Digital Library*, pp. 1-4. doi:10.1109/ICGPR.2018.8441628

Lambot, S., Slob, E., Chavarro, D., Lubczynski, M., Vereecken, H. 2008. Measuring soil surface water content in irrigated areas of southern Tunisia using full-waveform inversion of proximal GPR data. *Near Surface Geophysics*, 6, pp. 403–410

Lambot, S., Slob, E.C., van den Bosch, I., Stockbroeckx, B., Vanclooster, M. 2004. Modeling of ground-penetrating radar for accurate characterization of subsurface electric properties. *IEEE Transactions on Geoscience and Remote Sensing*, 42, pp. 2555-2568

Li, J. *et al*., 2017. Identification of dominating factors affecting vadose zone vulnerability by a simulation method. *Scientific Reports*, 7, p. 45955

Loeffler, O., Bano, M. 2004. GPR measurements in a controlled vadose zone: Influence of the water content, *Vadose Zone Journal*, 3, pp. 1082–1092

Lunt, I.A., Hubbard, S.S., Rubin, Y. 2005. Soil moisture content estimation using ground penetrating radar reflection data. *Journal of Hydrology*, 307, pp. 254–269

Madore, L. 2014. Integrated Pest Management. Forestry and Agrifood, Government of Newfoundland and Labrador, Canada, retrieved from https://www.faa.gov.nl.ca/publications/pdf/Exclusion_Fencing_CRM_2011_2014.pdf

Mahmoudzadeh, M.R., Lambot, S., Frances, A.P., Mohammed, A.A., Lubczynski, M. 2010. Water table detection by GPR in Sardon, Salamanca, Spain. Proceedings of the 8th International Conference on Ground Penetrating Radar, Italy, doi:10.1109/ICGPR.2010.5550217

Minet, J., Lambot, S., Slob, E., Vanclooster, M. 2010. Soil surface water content estimation by full-waveform GPR signal inversion in the presence of thin layers. *IEEE Transactions on Geoscience and Remote Sensing*, 48, pp. 1138-1150

Molina-Sánchez, L., Sánchez-Martos, F., Daniele, L., Vallejos, A., Pulido-Bosch, A. 2015. Interaction of aquifer-wetland in a zone of intensive agriculture: the case of campo de Dalías (Almería, SE Spain). *Environmental Earth Sciences*, 73, pp. 2869–2880

Nakashima, Y., Zhou, H., Sato, M. 2001. Estimation of groundwater level by GPR in an area with multiple ambiguous reflections. *Journal of Applied Geophysics*, 47(3), pp. 241-249, doi:10.1016/S0926-9851(01)00068-4

Neal, A. 2004. Ground penetrating radar and its use in sedimentology: principles, problems and progress. *Earth Science Reviews*, 66, pp. 261–330

Nimmo, J.R. 2009. Vadose Water. In: G. E. Likens, ed. Encyclopedia of Inland Waters. CA, USA: Academic Press, pp. 766-777

Parkin, G., Redman, D., Von Bertoldi, P., Zhang, Z. 2000. Measurement of soil water content below a wastewater trench using ground-penetrating radar. *Water Resources Research*, 36 (8), pp. 2147-2154, doi:10.1029/2000WR900129

Paz, C., Alcalá, F.J., Carvalho, J.M., Ribeiro, L. 2017. Current uses of ground penetrating radar in groundwater- dependent ecosystems research. *Science of the Total Environment*, 595, pp. 868-885, doi:10.1016/j.scitotenv.2017.03.210

Price, J.C. 1982. Estimation of regional scale evapotranspiration through analysis of satellite thermal-infrared data. *IEEE Transactions of Geoscience in Remote Sensing*, 20(3), pp. 286-292

Pyke, K., Eyuboglu, S., Daniels, J., Vendl, M. 2008. A controlled experiment to determine the water table response using ground-penetrating radar. *Journal of Environmental and Engineering Geophysics*, 13(4), pp. 335-342, doi:10.2113/jeeg13.4.335

Rucker, D., Ferre, T. 2004. Correcting water content measurement errors associated with critically refracted first arrivals on zero offset profiling borehole ground penetrating radar profiles. *Vadose Zone Journal*, 3(1), pp. 278-287, doi:10.2113/3.1.278

Schmelzbach, C., Tronicke, J., Dietrich, P. 2012. High-resolution water content estimation from surface-based ground-penetrating radar reflection data by impedance inversion. *Water Resources Research*, 48, doi.org/10.1029/2012WR011955

Schwingshackl, C., Hirschi, M. Seneviratne, S.I. 2017. Quantifying spatiotemporal variations of soil moisture control on surface energy balance and near-surface air temperature. *Journal of Climate*, 30, pp. 7105-7124

Shih, S., Doolittle, J., Myhre, D., Schellentrager, G. 1986. Using radar for groundwater investigation. *Journal of Irrigation and Drainage Engineering*, 112(2), pp. 110-118, doi:10.1061/(ASCE)0733-9437(1986)112:2(110)

Sigouin, J.P., Dyck, M., Si, B.C., Wei, H. 2016. Monitoring soil water content at a heterogeneous oil sand reclamation site using a cosmic-ray soil moisture probe. *Journal of Hydrology*, 543, pp.510-522

Slowik, M. 2013. GPR and aerial imageries to identify the recent historical course of the Obra River and changes of spatial extent of Obrzańskie Lake, altered by hydro-technical works. *Environmental Earth Sciences*, 70, pp. 1277–1295

Stoffregen, H., Zenker, T., Wessolek, G. 2002. Accuracy of soil water content measurements using ground penetrating radar: Comparison of ground penetrating radar and lysimeter data. *Journal of Hydrology* (Amsterdam), 267(3-4), pp. 201-206

Swiss Federal Institute of Technology. 2017. Soil moisture measurements. Climatological and hydrological fieldwork, Retrieved from https://www.ethz.ch/ (accessed on 10.27.2017)

Takeshita, Y., Kobayashi, H., Kazunori Tao, I., Kaihotsu, I. 2004. Measurement of groundwater behavior in sandy soils using surface ground penetrating radar. Proceedings of the 10th International Conference on Grounds Penetrating Radar, The Netherlands, Retrieved from https://ieeexplore.ieee.org/document/1343501 (accessed on 10.29.2018)

Talley, J., Baker, G.S., Becker, M.W., Beyrle, N. 2005. Four-dimensional mapping of tracer channelization in subhorizontal bedrock fractures using surface ground penetrating radar. *Geophysics Research Letters*, 32, doi.org/10.1029/2004GL021974

Topp, G.C., Davis, J.L., Annan, A.P. 1980. Electromagnetic determination of soil water content: Measurements in coaxial transmission lines. *Water Resources Research*, 16(3), pp. 574–582, doi:10.1029/WR016i003p00574

Tsoflias, G.P., Becker, M.W. 2008. Ground-penetrating-radar response to fracture-fluid salinity: why lower frequencies are favorable for resolving salinity changes. *Geophysics*, 73, doi:10.1190/1.2957893

Tsoflias, G.P., Halihan, T., Sharp Jr., J.M. 2001. Monitoring pumping test response in a fractured aquifer using ground-penetrating radar. *Water Resources Research*, 37, pp. 1221–1229

Van Overmeeren, R.A., Sariowan, S.V., Gehrels, J.C. 1997. Ground penetrating radar for determining volumetric water content: results of comparative measurements at two sites. *Journal of Hydrology*, 197, pp. 316-338

Weiler, K.W., Steenhuis, T.S., Boll, J., Kung, J.S. 1998. Comparison of ground penetrating radar and time domain reflectometry as soil water sensors. *Soil Science Society of America Journal*, 62, pp. 1237-1239

Wijewardana, Y.G.N.S., Galagedara, L.W. 2010. Estimation of spatio-temporal variability of soil water content in agricultural fields with ground penetrating radar. *Journal of Hydrology*, 391(1), pp. 24-33, doi:10.1016/j.jhydrol.2010.06.036

Williams, T. 1980. Automatic electrical resistance soil-moisture measuring system: Technical note. *Journal of Hydrology*, 46(3-4), pp 385–390

Zotarelli, L., Dukes, M.D., Scholberg, J.M.S., Femminella, K., Munoz-Carpena, R. 2011. Irrigation Scheduling for Green Bell Peppers Using Capacitance Soil Moisture Sensors, *Journal of Irrigation and Drainage Engineering*, 137(2), pp.73-81

Zurek, A.J., Witczak, S., Dulinski, M., Wachniew, P., Rozanski, K., Kania, J., Postawa, A., Karczewski, J., Moscicki, W.J. 2015. Quantification of anthropogenic impact on groundwater-dependent terrestrial ecosystem using geochemical and isotope tools combined with 3-D flow and transport modelling. *Hydrology and Earth System Sciences*, 19, pp. 1015–1033

CO-AUTHORSHIP STATEMENT

The research objectives were conceived and defined under the supervision of Dr. Lakshman Galagedara (principle supervisor), who also provided the funding for the research. Dr. Mumtaz Cheema (co-supervisor) and Dr. Adrian Unc (committee member) were also collaborators of the same research project on "Hydrogeophysical Characterization of Agricultural Fields in Western Newfoundland using Integrated GPR-EMI", which was led by Dr. Galagedara.

I, Chameera Illawathure as the thesis author, was responsible for data collection, analysis and data interpretation. I personally wrote the first draft of my thesis including the two main chapters (2 & 3) in manuscript format that make up the core of my thesis. Dr. Galagedara provided research plans and guidance for the entire fieldwork. He also guided the data processing and analysis, and comprehensively reviewed and revised my thesis. Dr. Cheema and Dr. Unc reviewed the entire thesis and steered me in the right direction of how to analyze my raw data and the possible output of my data presentation.

CHAPTER 2

Soil moisture estimation from GPR hyperbola fitting in the agricultural root zone

2.1 Introduction

More than 60% of the root biomass of most temperate crops exists within the upper 30 cm of the soil profile (Fan *et al*., 2016). Soil moisture (SM) in this upper soil layer is a key factor that determines plant growth through water and nutrient uptake from the soil (Seneviratne *et al*., 2010). SM also plays a major role in the hydrological cycle as it regulates the distribution of precipitation between storm runoff and water storage (Burns, 1974). Knowledge of the SM in shallow root zones is also useful to optimize sowing depth. SM shows both spatial and temporal variations. Therefore, it is challenging to measure SM with respect to time and space at the field scale, especially in the shallow root zone.

Ground Penetrating Radar (GPR) is capable for large-scale, non-destructive estimation of SM (Davis & Annan, 1989; Galagedara *et al*., 2003; Huisman *et al*., 2003; Lambot *et al*., 2004; Minet *et al*., 2012; Tran *et al*., 2014). The direct groundwave method for determining SM using GPR is well established but has limitations to be applicable for the root zone (Galagedara *et al*., 2005b). Some of the limitations are difficulties of distinguishing the airwave from groundwave and, shallow penetrating depths (Galagedara *et al*., 2005a; Galagedara *et al.*, 2005b). Further, manual picking of the leading edge of the groundwave is associated with errors, and even automatic picking cannot be performed efficiently (Galagedara *et al.*, 2003). The lack of a practical approach to determine SM in the shallow agricultural root zone impedes non-destructive, portable and time-effective advantages of GPR.

The two-way travel time of GPR reflected wave could be used to estimate the SM of a large area in natural field conditions (Lunt *et al*., 2005). Reflection from a sub-surface point reflector (*i.e.*, a drainage pipe or a piece of rock) can trace out a hyperbola in a GPR radargram. The depth and the shape of the object, and the matrix (Maas & Schmalzl, 2013) influence the shape of the hyperbola. SM can be estimated through the reflected wave velocity and corresponding permittivity of the soil matrix if the depth of reflection is well known (Davis & Annan, 1989; Huisman *et al*., 2003; Topp *et al*., 1980). The estimated wave velocity roughly represents an average value of the soil layer from the ground surface to the reflector. Information about the soil volume of which the hyperbola analysis could optimally describe propagation velocity has not been well documented. The estimated moisture from a hyperbola analysis can be validated using a commonly used indirect method such as Time Domain Reflectometry (TDR) (Galagedara *et al.*, 2005; Huisman *et al*., 2001). Gravimetric sampling, which is the direct method, is not feasible due to the comparatively large sample volume of GPR (Dobriyal *et al*., 2012) and due to its destructive nature, which hinders sample repeatability.

Full-wave inverse modeling of the GPR data has demonstrated its benefits in terms of accuracy and automatization for SM mapping (Lambot *et al.*, 2004; Lambot & André, 2014; Minet *et al.*, 2012; Tran *et al.*, 2014). The method relies on a 3D electromagnetic model accounting for the radar-antenna-medium system and its inversion to retrieve the medium permittivity and correlated moisture. This approach requires a specific calibration of the radar instrument. The method has not been made available yet, but is expected to be released soon as an online tool on www.gprsensing.com (S. Lambot & A. De Coster, Université catholique de Louvain, Belgium).

On the other hand, TDR is a commonly used indirect method to measure SM, but still has a comparatively smaller sample volume than GPR (Topp *et al*., 2008).

Therefore, an adequate number of TDR measurements are needed to represent the GPR sample volume. The knowledge of the TDR sample volume that covers the GPR sample volume is essential for GPR data validation. Ferré *et al.* (1998) described the TDR sample volume as a cylindrical shape that contributes to the overall SM measurement. This cylindrical soil volume has a sample radius as a function of the TDR probe separation distance and height equivalent to the length of the TDR probe (Ferré *et al*., 1998). The soil outside the sample volume has no significant input to the total TDR probe response. Introducing TRIME (Time-domain Reflectometry with Intelligent Micro Elements) technology, current TDR probes can measure larger sample volumes than conventional TDR probes (IMKO Micromodultechnik, Germany).

Similar to TDR, the volume of the porous medium that contributes to the GPR wave velocity estimation varies with the configuration of each GPR system. The GPR characterization scale is also influenced by the soil properties themselves. In addition, the GPR sample volume and the resolution of its moisture estimation mainly differs with different survey parameters and different center frequencies (Galagedara *et al.*, 2005). Medium to high frequency (*e.g.*, 250, 500 and 1000 MHz) GPR instruments are sold as transducers in which antennas and electronics are assembled to optimize the performance (Sensors & Software Inc., Canada). They are relatively small and therefore ideal for use throughout the growing season even with the presence of crops. Employing the appropriate GPR frequency with a feasible survey type for data acquisition increases the accuracy of the results as well as the efficiency of the method.

The traditional GPR hyperbola method for SM estimation is applicable only if point reflectors are present in the soil being studied and if clear hyperbolas are visible in the radargram. However, finding shallow hyperbolas in a radargram is a major limitation of this method for use as a practical tool for rapid SM estimation in the root zone. Some recent research has focused on increasing the efficiency of the hyperbola fitting method by minimizing the human error associated with identifying and fitting hyperbolas. Techniques such as MMSA (Multiresolution Monogenic Signal Analysis) are useful to detect hyperbolas accurately (Qiao *et al*., 2015). Real-time detection and fitting of hyperbolas have also been recently investigated (Dou *et al*., 2017). An automated hyperbola detection algorithm has been calibrated to determine the existence of a hyperbola by the '*ambiguity zone for the human brain*,' which is a relatively fast method compared to other methods (Mertens *et al*., 2016). Instead of using the traditional hyperbola fitting method in commercially available software, a modified algorithm such as MMSA would increase the accuracy and efficiency of the proposed GPR method. As noted in the recent review of current GPR-based SM measurement methods by Liu *et al*. (2017), the automated recognition of hyperbolic signals should not only improve the efficiency of the method, but it eliminates the need to know the depth of the reflector. To avoid the dependability of the hyperbola fitting on different analysts (Sham & Lai, 2016), we followed a systematic guideline for GPR data processing. We hypothesized that the same accuracy for SM estimation in the upper 30 cm of the soil profile of an experimental plot could be achieved by analyzing hyperbolas regardless of the depth from 27-50 cm.

Motivated by the recent advancements of the GPR hyperbola analysis and challenges encountered in the field, we aimed at evaluating a straightforward GPR method to estimate SM in the shallow agricultural root zone. TDR data were used as the reference to evaluate GPR data with special consideration given to sample geometry of both methods, which has not yet been well documented. For that purpose, a systematic TDR data collection was introduced to coincide with the GPR sample area. Consequently, the objectives of this study were to use hyperbola fitting method to; (i) determine the soil volume that hyperbolic reflections describe in terms of radar wave velocity and (ii) evaluate a practical GPR-based approach to estimate SM within the upper 30 cm of the soil profile.

2.2 Theoretical Background

The GPR wave propagation velocity (v_{rw}) for a monostatic antenna can be estimated by the depth to the known reflector method (ASTM D6432-11; Daniels *et al*., 2005). Limitations are: depth is not known in most cases, and the two-way travel time (t_{rw}) of radar wave only at the apex of the hyperbola is used for the calculation. Velocity sounding method can be used to determine the radar velocity in a multiple antenna-offset survey (Dix, 1955).

2.2.1 Traditional hyperbola fitting method

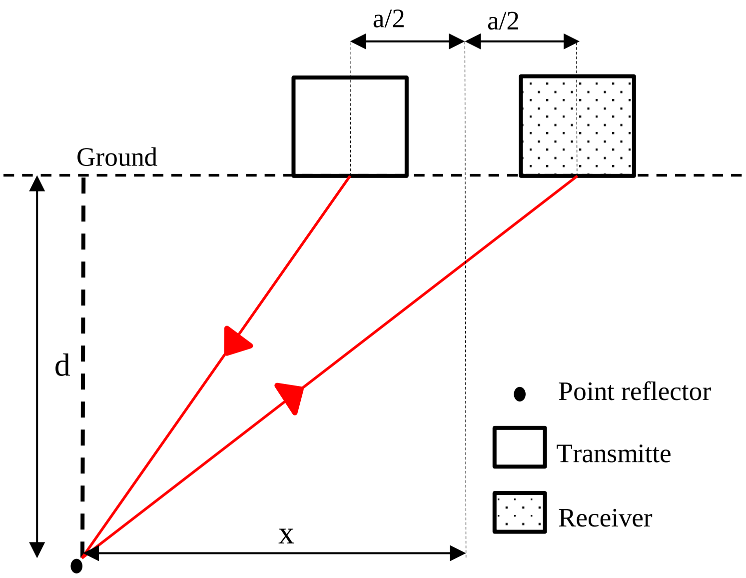

Figure 2.1: Arrow-headed lines represent the wave propagation paths assuming straight-ray propagation.

Equation 2.1 determines the average v_{rw} from the ground surface to a sub-surface point reflector for t_{rw} with respect to horizontal distance from the reflector to the antenna, *x* (Fig. 2.1) (Huisman *et al.*, 2003).

$$v_{rw} = \frac{\sqrt{(x-0.5a)^2 + d^2} + \sqrt{(x+0.5a)^2 + d^2}}{t_{rw,x}} \tag{2.1}$$

Where *a* is the antenna separation and *d* is the depth to the top of the reflector.

2.2.2 Modified hyperbola detection algorithms

Assuming that (i) the electromagnetic properties of the soil above the buried reflector do not vary, (ii) wave propagation follows straight ray paths, (iii) the antenna and antenna-medium coupling do not affect observed propagation times, (iv) the target reduces to a point and (iv) the antenna is at the soil surface, the two-way travel times measured over a point reflector in a monostatic configuration of GPR antennas follow a hyperbolic function (*e.g.*, Mertens *et al.*, 2016). Equation 2.2 which is a general shape of a hyperbola can be derived using the Pythagorean theorem. Hyperbola parameters appearing in Equation 2.2 are illustrated in Figure 2.2.

$$\frac{t^2}{{t_0}^2} - \frac{|y - y_0|^2}{\frac{{t_0}^2 {v_{rw}}^2}{4}} = 1 \tag{2.2}$$

Where v_{rw} is the reflected wave velocity in the soil, a and b in Figure 2.2 are t_0 and ($t_0.v_{rw}/2$), respectively. Therefore, v_{rw} can be estimated for a known b and position of the apex of the hyperbola.

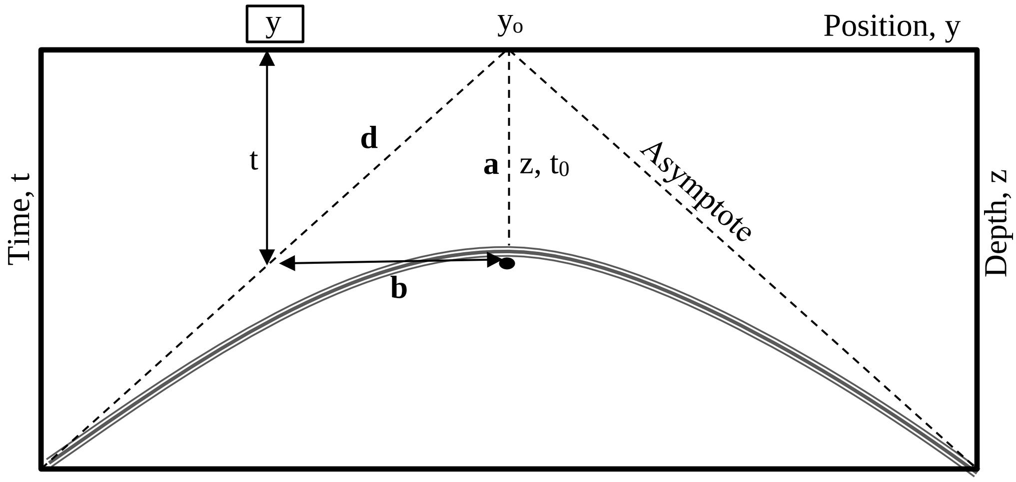

Figure 2.2: Hyperbola parameters appearing in Equation 2.2.

Equation 2.2 can be modified accounting for the radius of the reflector for a common-offset method (CO) with a significant antenna separation (Sham & Lai, 2016). Still, most of the computational algorithms currently used are based on the assumption that the reflector is a point. Otherwise, the calculation would be more complicated. It is, however, worth noting that neglecting the radius or shape of the target is expected to result in errors in the permittivity estimates (Sham & Lai, 2016).

2.3 Method Development

2.3.1 Site description and experimental setup

A field study was conducted in a flat experimental plot of 15 m × 4 m (49.073 N, 57.561 W) at Pynn's Brook Research Station, Pasadena, NL, Canada (Fig. 3). Eroded and dissected lacustrine, glacial veneer and organic deposits are dominant with a shallow unconfined sandy aquifer (Newfoundland & Labrador Geological Survey, 2014). Shallow soil at the adjacent cornfield is gravelly loamy sand (sand 82.0 ± 3.4%, silt 11.6 ± 2.4% and clay 6.4 ± 1.2%) (Badewa *et al*., 2018). Soil textural analysis (*n*=8) at the experimental plot revealed that the shallow soil layer up to a depth of 50 cm is loamy sand which is the same as the 0-15 cm soil profile as described by Sadatcharam

(2019). Laboratory tests for determining basic soil properties were carried out at Boreal Ecosystem Research Facility (BERF) of Grenfell Campus-Memorial University of Newfoundland, Corner Brook, NL, Canada.

2.3.2 Data acquisition

Data collections were carried out in 2017 (September 22, October 3, 20, 24) and 2018 (June 01 and 29). Both CO and Common mid-point (CMP) methods (Davis and Annan, 1989; Huisman *et al.*, 2003) were used for GPR data acquisition. Twelve CO surveys were carried out using 250, 500 and 1000 MHz center-frequency transducers of the PulseEKKO® Pro GPR system (Sensors and Software Inc., Canada) after burying eight different types of point reflectors ranging from 27-70 cm depth below the surface. Buried materials were; three hollow metals, one aluminum can and four plastic bottles filled with three different concentrated salt solutions and one with tap water. Sizes of the reflectors were from a maximum of 4.5 l (30 cm × 15 cm × 10 cm) and to a minimum of 2 l plastic water bottle. These reflectors were buried along two straight lines 2 m apart (Fig. 2.3). GPR grid surveys were performed at 0.5 m spacing resulting in nine grid lines in total and, each grid line was 15 m in length. Two survey lines of each grid survey were done exactly along the traces of the buried objects (Fig. 2.4a).

CMP surveys using 500 MHz transducers were also carried out at each buried location (October 20 and 24, 2017). Thirteen systematic SM measurements were collected using vertically installed 30 cm long TRIME-PICO64 TDR probes (IMKO Micromodultechnik, Germany) at the center and 10, 20 and 30 cm radii from top of each reflector together to coincide with the CMP surveys (Fig. 2.4b). Four TDR measurements at each radius were collected at 0°, 90°, 180° and 270° with respect to the GPR survey direction and one TDR measurement was collected exactly on top of the reflector (Fig. 2.4b). Figure 2.5 illustrates the vertical cross-sectional sample area of systematic TDR data collection over a buried reflector.

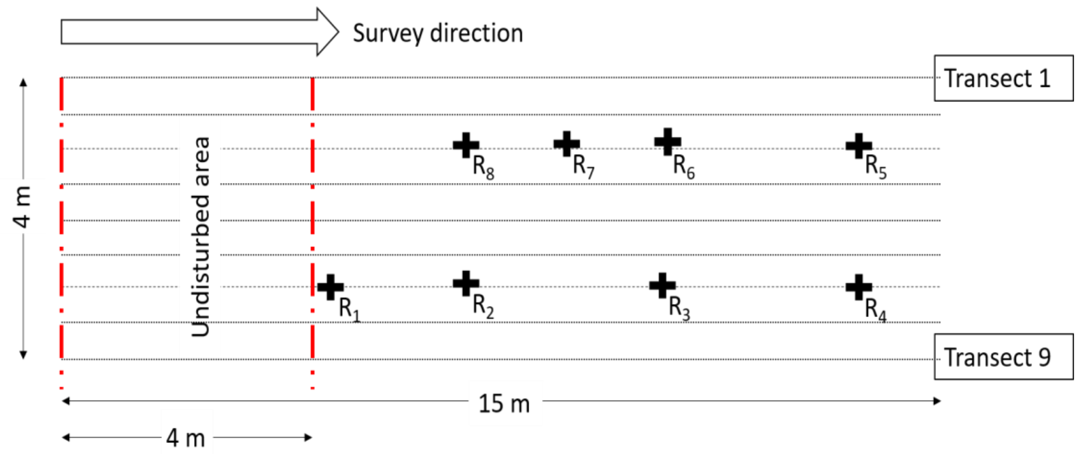

Figure 2.3: Plan view of the experimental setup; R_1-R_8 are buried reflectors (not to scale).

Before winter started, buried reflector locations were marked using plastic pegs, and the level of the ground surface was marked in each peg. In 2018, two field campaigns were performed after the spring thaw. In each day, two GPR lines along the buried reflectors were carried out using all three frequencies with systematic TDR data collection as before. Then buried pits were opened up carefully to verify the depth and positions of the reflectors.

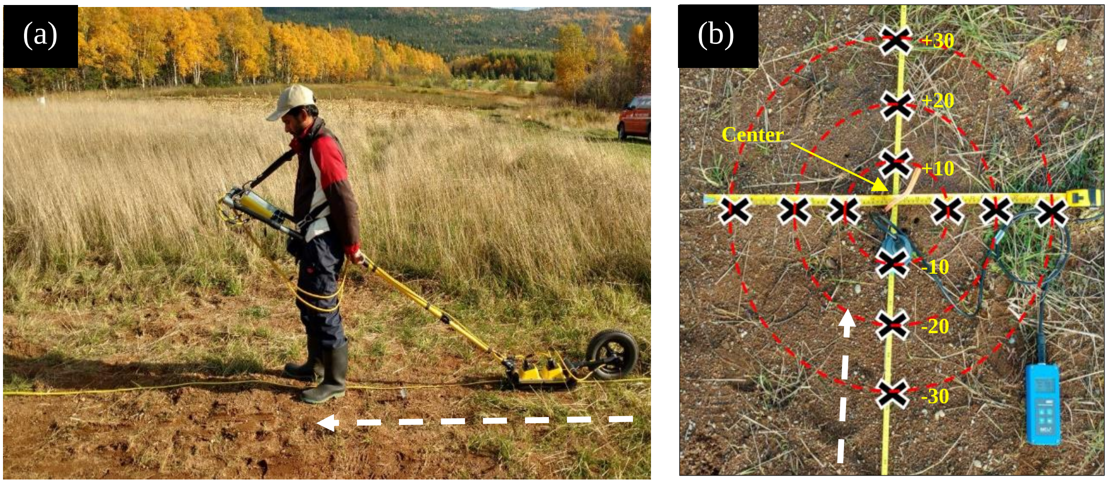

Figure 2.4: (a) A GPR CO survey over the buried objects using 1000 MHz center-frequency transducer fixed to an odometer. (b) A systematic TDR data collection at a buried location; measuring tapes cross at top of the buried object where the center TDR measurement was performed. Dashed arrow line indicates the GPR survey direction.

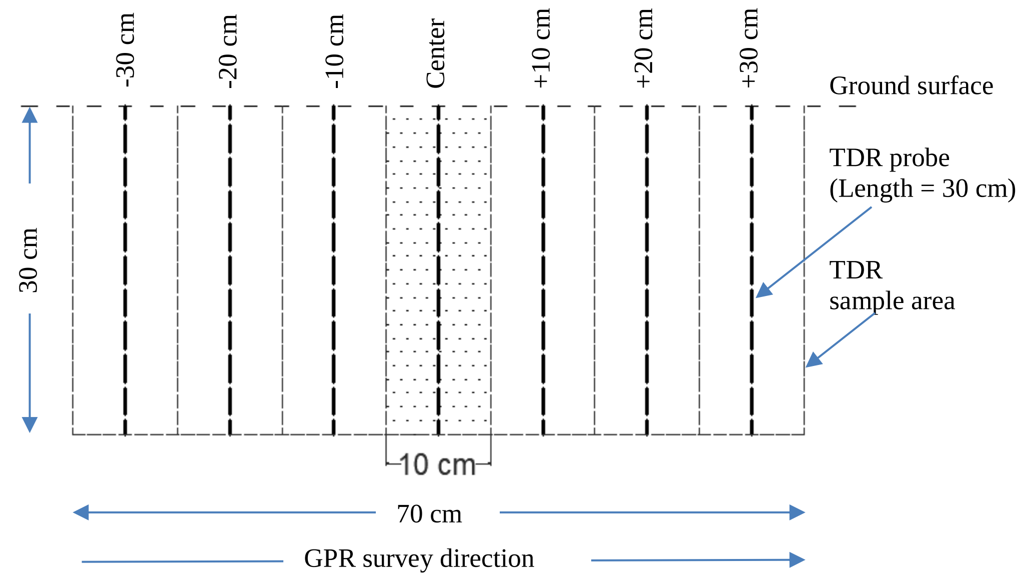

Figure 2.5: Vertical cross section of systematic TDR sampling area over a buried reflector. Sample area of the center TDR probe is shown by the shaded area. Distances represent TDR locations from the center along the transect (see also Fig. 4b).

2.3.3 TDR probe calibration

Twenty-one (21) TDR measurements were collected by vertically installed 30 cm long TDR probes along one GPR transect at each buried object. Just after each TDR measurement, soil samples (2.5 cm in diameter) were collected from 0-30 cm depth using a soil auger (ASTM D1452) from the same location (n=6). Soil bulk density was measured using undisturbed samples collected at the middle and two ends of the experimental plot (ASTM D7263-09). Gravimetric soil moistures were determined by the oven drying method, 105°C for 24h, and then converted to volumetric SM (θ_v) using the average bulk density of the soil.

2.3.4 GPR data processing

GPR data processing was done using *EKKO Project V3 R1* software (Sensors and Software Inc.). SM at each buried location was estimated through the calculation of the relative permittivity (ε_r) (Topp *et al.*, 1980) using v_{rw} obtained from GPR. The data processing methodology is shown in Figure 2.6. The procedure started by checking the major deflections of GPR traces in a particular radargram. The flow chart shown in Figure 2.6 is for a positive first major deflection. If it was negative, re-picking was done with the negative transition, and the negative edges were picked by automatic time picking. When the deflection was not clear and difficult to make a decision, both transitions and relevant auto picking criteria were used. Each trace was shifted to align first-breaks in a line (Fig. 2.7).

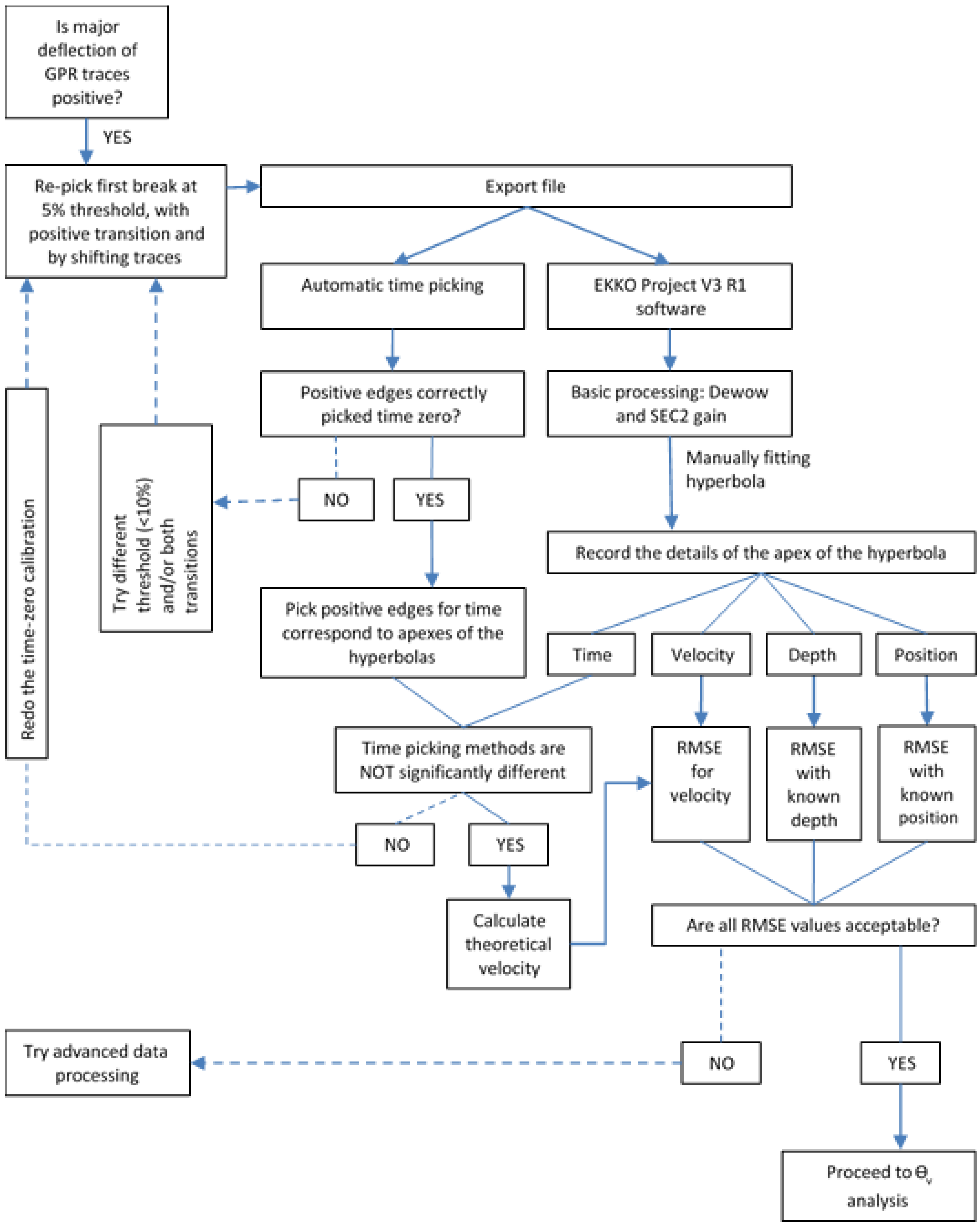

Figure 2.6: Systematic guidelines for GPR data processing (steps illustrated by dashed lines were not followed for this analysis)

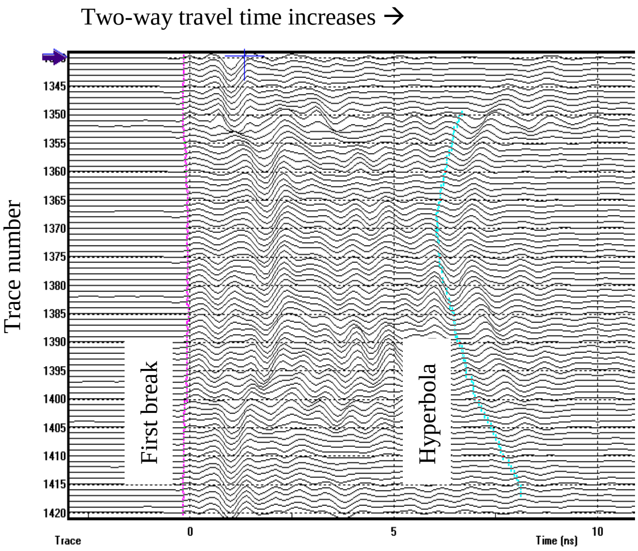

Figure 2.7: Positive edges of both first-break and hyperbolic reflection are picked by automatic time picking after a successful re-pick processing.

If the first break is a positive deflection, all other later reflection events were picked at the positive edge to obtain the actual reflected wave travel time. After this re-picking procedure, each data file was exported, and the time-zero picking was checked by automatic time picking of the positive edge of the airwave. Time zero method described by Galagedara *et al*. (2003) was used for time-zero calibration and, to minimize the error of time-zero drift. Locations of the apex of the hyperbola by automatic picking were used to minimize the subjective error of manual hyperbola fitting.

2.3.5 Testing the hypothesis

A 30 cm long TRIME-PICO64 TDR probe has a sample radius of 5 cm in the plane perpendicular to the probe length (IMKO Micromodultechnik, Germany). We considered a 2-dimensional projection of TDR and GPR sample volumes for the comparison of θ_v estimations from both methods. Therefore, seven TDR measurements, coincided with the GPR sample area for a buried location, were collected along the

GPR transect (Fig. 2.4b and Fig. 2.5). The total TDR sample area for a buried location that is projected to the GPR section is 70 cm × 30 cm = 2100 cm^2 (Fig. 2.5).

A GPR frequency of 500 MHz was used for CMP analysis. First, we compared GPR sample areas of ~30 cm deep hyperbolic reflections from CO and CMP methods. TDR data points along the survey line were only considered for the comparison. We used RMSE to compare GPR and TDR measurements. Only three hyperbolas at 27, 31 and 34 depths (to represent around 30 cm depth) were selected for the comparison in three survey days. Sample area for θ_v estimations from CO and CMP methods are compared in Section 2.4.3. In the second step, we compared the CO survey method of 250 and 500 MHz for θ_v estimations over ~30 cm deep hyperbolic reflections statistically using RMSE value and Mann-Whitney test (Hammer *et al*., 2001; Hettmansperger & Sheather, 1986).

To check the spatial representativeness of using GPR, we compared GPR estimated θ_v with different criteria used to average the TDR data. The TDR averaging criteria used were: (i) TDR1: all TDR measurements (30 cm radius) collected at a buried location (n=13); (ii) TDR2: up to 20 cm radius including the center (n=9); (iii) TDR3: only 10 cm radius (n=4); (iv) TDR4: only at 20 cm (n=4); (v) TDR5: only at 30 cm (n=4); (vi) TDR6: across the transect (n=7); and (vii) TDR7: along the transect (n=7). Finally, to check the hypothesis, we obtained the θ_v estimations by hyperbola fitting regardless of the depth of the hyperbola (27 – 50 cm depth range). For the comparison of GPR-estimated and TDR-measured θ_v, we used above-mentioned statistical methods.

2.4 Results and Discussion

2.4.1 Probe calibration results

Average soil bulk density of 0-30 cm soil profile was 1.39 (±0.09) g cm^{-3} (*n*=6). TDR measured θ_v in m^3 m^{-3} (min=0.1034, max=0.1798, median=0.1298; *n*=21) and gravimetrically measured θ_v in m^3 m^{-3} (min=0.0907, max=0.1618, median=0.1239; *n*=21) were within a RMSE of 0.0161 m^3 m^{-3} (see also Appendix 2.1). Average bulk density of the soil (*n*=28) and the RMSE of θ_v estimation (*n*=10) between TDR and gravimetric methods of a shallow soil were 1.31 g cm^{-3} and 0.018 m^3 m^{-3}, respectively, in a previous study conducted at the same site (Badewa *et al.*, 2018). Table 2.1 compares different TDR criteria used to average θ_v measurements at a buried location. All the averaging criteria agree with the overall average (TDR1) having medium to high positive correlations with TDR1 and TDR2 showing the highest correlation. TDR5 has the lowest correlation with the overall average. TDR2 also shows a high correlation with other criteria except for TDR5.

Table 2.1: Pearson correlation coefficients (p-values within brackets) of TDR measurements with different criteria used to average the TDR data

	TDR1 (n = 13)	TDR2 (n = 9)	TDR3 (n = 4)	TDR4 (n = 4)	TDR5 (n = 4)	TDR6 (n = 7)
TDR2 (n = 9)	0.940 (0.000)					
TDR3 (n = 4)	0.837 (0.000)	0.940 (0.000)				
TDR4 (n = 4)	0.845 (0.000)	0.863 (0.000)	0.650 (0.016)			
TDR5 (n = 4)	0.714 (0.006)	0.432 (0.140)	0.293 (0.332)	0.450 (0.123)		
TDR*6* (n = 7)	0.907 (0.000)	0.851 (0.000)	0.752 (0.003)	0.800 (0.001)	0.645 (0.017)	
TDR7 (n = 7)	0.936 (0.000)	0.876 (0.000)	0.796 (0.001)	0.733 (0.004)	0.679 (0.011)	0.705 (0.007)

2.4.2 Error estimation of the hyperbola fitting method

Time related to apexes (Fig. 2.8) of the hyperbolas (n=59) in all three frequencies for automatic picking (median=7.156 ns) and hyperbola fitting (median=7.410 ns) were not significantly different (*p-value*=0.6167) at the 95% significance level of the Mann-Whitney test. Radar wave velocities obtained by the hyperbola method are close to the theoretical velocities calculated by Equation 2.1 (Appendix 2.2). The RMSE between the actual and the hyperbola method for depth and position of buried objects are within 0.05-0.06 m for all frequencies (Table 2.2; see also Appendices 2.2-2.4). The data processing procedure presented in Section 2.3.4 is associated with these RMSE levels.

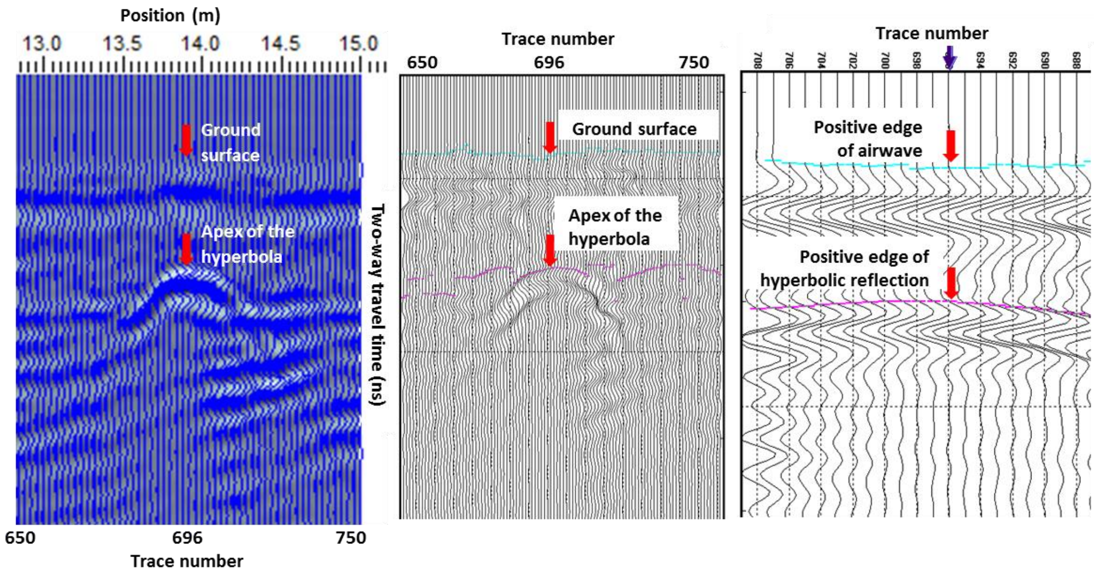

Figure 2.8: A hyperbola traced out in a GPR radargram (left); GPR traces exported to automated time picking software and positive edges of the airwave and reflected wave are picked (middle); magnified view (right). Arrows are aligned exactly on top of the reflector and two-way travel time corresponded to that trace (trace number 696 in this example) was substituted into Equation 1 after time-zero correction for the velocity calculation.

Table 2.2: The root mean square error (RMSE) between hyperbola fitting and automatic time picking (for theoretical calculations) for details of the apex of the hyperbola

Frequency (MHz)	N	Depth (m)	Position (m)	Velocity (m/ns)
1000	11	0.05	0.06	0.02
500	33	0.05	0.05	0.02
250	19	0.06	0.06	0.01

The RMSE of hyperbola-derived velocity was 0.01-0.02 m/ns when compared with the theoretical velocity. A difference of 0.02 m/ns in radar velocity is equivalent to about 0.01 $m^3 m^{-3}$ difference in θ_v in wet soils (within the range of 0.067-0.098 m/ns). In dry soils (within the range of 0.099-0.150 m/ns), a difference of 0.02 m/ns in radar velocity could make a maximum of 0.06 $m^3 m^{-3}$ difference in θ_v. However, the theoretical velocity is based on a measurement of exactly on top of the buried reflector. Hyperbola derived velocity is a measure of an average number of data points and represents an average value within the GPR sample area. Therefore, RMSE of 0.02 m/ns was accepted to proceed to θ_v estimation (Section 2.4.4).

2.4.3 GPR sample area of θ_v estimations with the hyperbola method

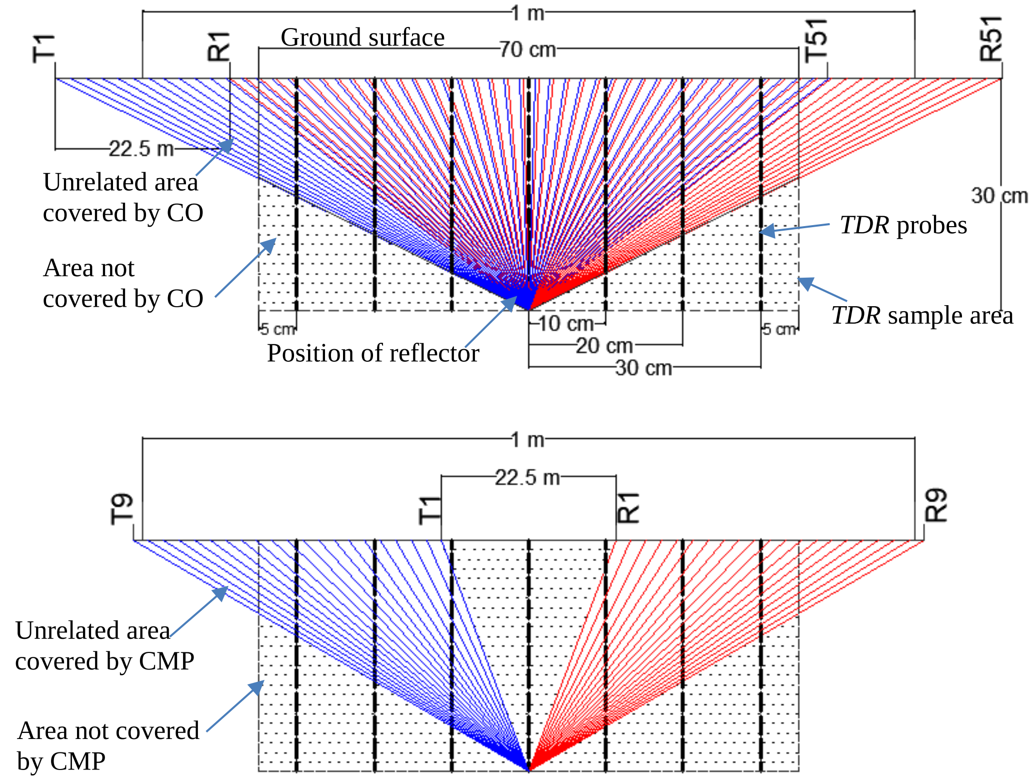

Figure 2.9: Cross section of GPR and TDR sample areas over a 30 cm deep reflector with systematic data collection; comparison of CO (above) and CMP (below). Note: transmitted wave in blue and reflected wave in red. T= Transmitter, R=Receiver.

Figure 2.9 compares sample areas of the TDR with CMP and CO methods for a 500 MHz survey in a default mode. Percentages of TDR sample area covered by the two GPR survey methods are listed in Table 2.3. The GPR sample area for θ_v estimation depends on the depth of the hyperbola used for v_{rw} estimation (Fig. 2.10). Table 2.4 presents the percentage of 30 cm long TDR probes' sample area covered by 30 cm and 70 cm hyperbola depths (70 cm depth was selected to show the full coverage of TDR sample area by GPR sample area).

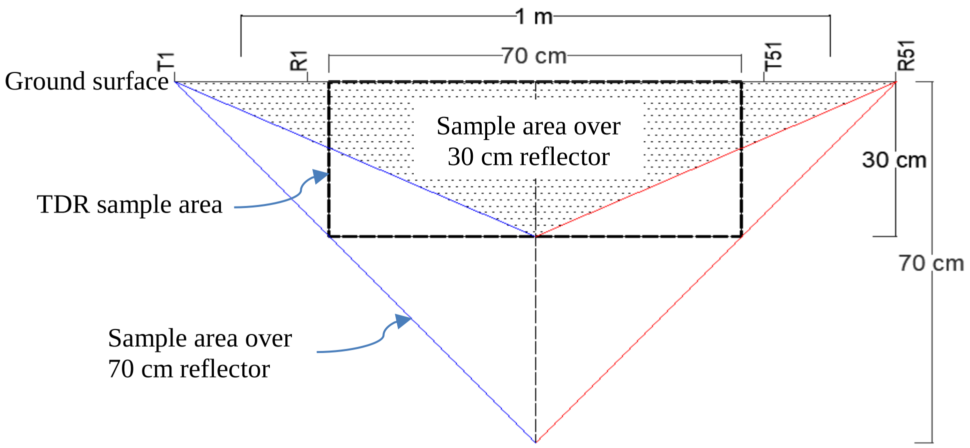

Figure 2.10: Vertical cross-section of GPR and TDR sample areas over 30 cm deep (dotted triangle) and 70 cm deep (outside large triangle) reflectors with TDR sample area (dashed rectangle).

Table 2.3: Percentage of TDR sample area covered by two GPR survey methods (500 MHz)

	Total GPR sample area (cm^2)	TDR sample area* covered by GPR	Unrelated area out of total GPR sample area
CMP	1200.0	49.8 %	12.9 %
CO	1837.5	71.4 %	18.4 %

Table 2.4: Percentage of 30 cm TDR sample area covered by two hyperbola depths

Depth of hyperbola (cm)	TDR sample area covered by GPR	Unrelated area out of total GPR sample area	
		0-30 cm	30-70 cm
30	71.4 %	18.4 %	-
70	100 %	18.4 %	32.6%

* Total TDR sample area (70 cm × 30 cm) = 2100 cm^2

2.4.4 Hyperbola fitting using CMP and CO methods

The software for analyzing GPR data allows fitting half of the hyperbola traced out in a CMP survey output to estimate the average wave velocity to a selected reflector. The correct reflection event should be picked by careful observation. We considered 500 MHz surveys for CMP data analysis (Fig. 2.11c). Table 2.5 presents the RMSE of TDR measured θ_v vs. θ_v estimated by using CO and CMP hyperbola fitting methods for 500 MHz. Three hyperbola depths (<34 cm) selected for the comparison imply that CMP-hyperbola estimated θ_v is less accurate (RMSE = 0.05 m^3 m^{-3}) than CO-hyperbola (Fig. 2.11 a & b) estimated θ_v (RMSE = 0.02 m^3 m^{-3}) when compared to TDR measured θ_v.

Table 2.5: Root mean square error (m^3 m^{-3}) of GPR-estimated and 30 cm TDR-measured θ_v for CO and CMP methods of 500 MHz GPR

GPR Method	Sample size*	Average TDR θ_v along the transect		
		10 cm (n=3)	20 cm (n=5)	30 cm (n=7)
CMP - hyperbola fitting	6	0.054	0.054	0.055
CO – hyperbola fitting	6	0.018	0.021	0.020

* Number of buried locations

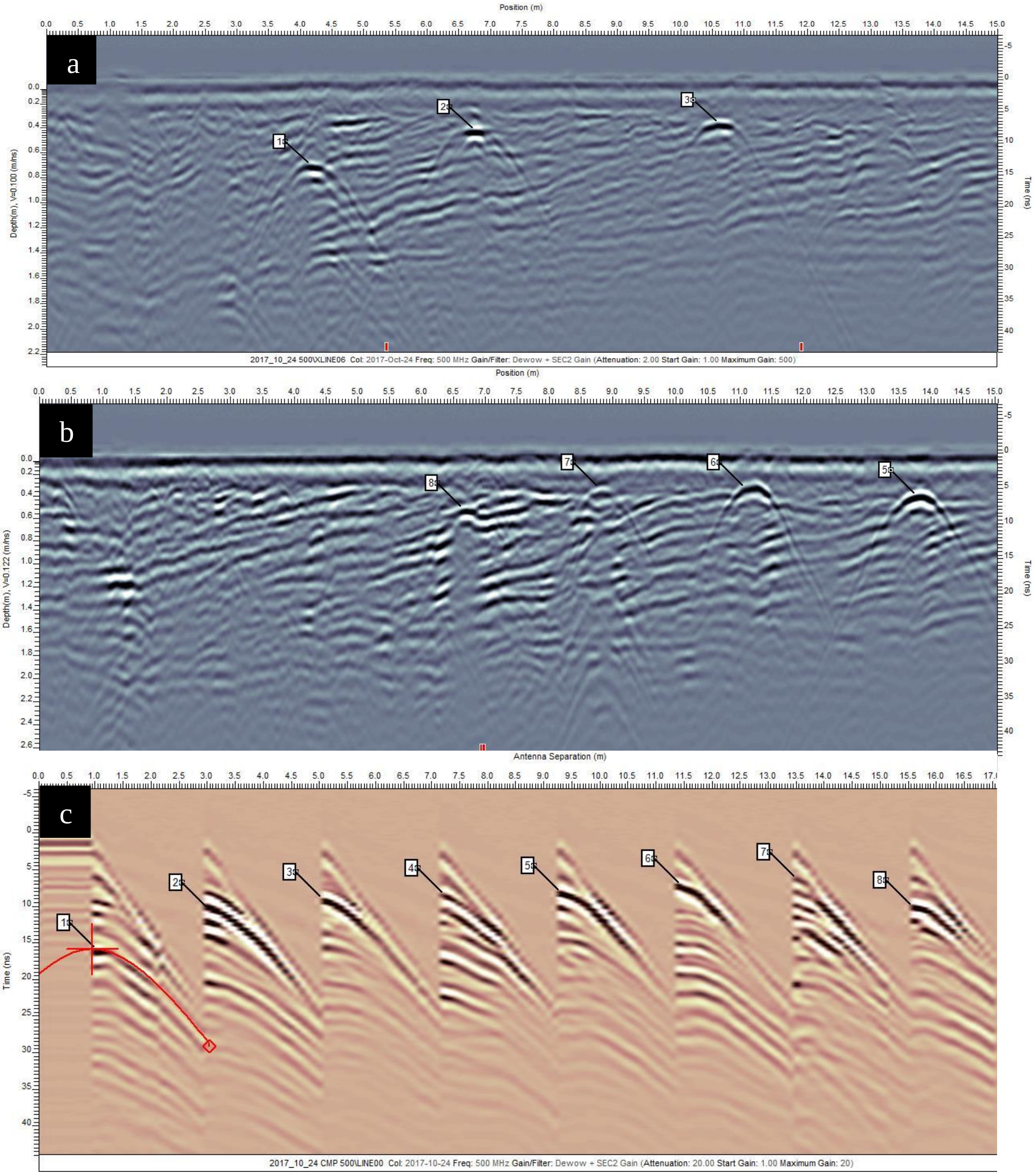

Figure 2.11: Hyperbolas traced out from buried reflectors 1-3 (a) and 5-8 (b) in CO and all reflectors in CMP (c) surveys using 500 MHz on October 24, 2017.

2.4.5 Evaluation of a practical approach to estimate θ_v in the root zone

TRIME-PICO64 TDR probes provide reliable θ_v estimations at point-scale with an RMSE of 0.016 $m^3 m^{-3}$ when compared to the gravimetric method. In addition, the TDR measurements are consistent as Badewa *et al.* (2018) reported similar accuracy (RMSE = 0.018 $m^3 m^{-3}$) during the previous growing season at the same location. This accuracy has allowed TRIME-PICO64 TDR probes (especially in sandy soils) to be used as a common used indirect method of θ_v estimation (IMKO Micromodultechnik, 2017). Many researchers have argued the low representativeness of the point-scale measurements of TDR (Hignett *et al.*, 2008). Therefore, apart from the advantage of the increased sample volume of TRIME-PICO technology (IMKO Micromodultechnik, Germany), a systematic TDR data collection was introduced in this study to be compatible with the large sample volume of the GPR hyperbola analysis method. However, the high spatial variability of the field water content, high gravel content and the artificial compaction due to human and machinery activities within very shallow depths can have a negative impact of the θ_v estimation using the proposed GPR method (Badewa *et al.*, 2018).

We compared the sample areas of TDR and GPR considering a 1 m longitudinal section along the GPR transect. In the CO method, the default mode of 500 MHz records a GPR trace every 2 cm, so that there will be 51 data points for a 1 m long transect. If the antenna step size is 2 cm, CMP data collection will have 21 traces for a 1 m length. The sample area of a 500 MHz GPR-hyperbola for θ_v estimation over a point reflector at 30 cm depth is higher in the CO method (1837.5 cm^2) than the CMP method (1200.0 cm^2). Consequently, the CO method produced more accurate θ_v estimation (RMSE = 0.02 $m^3 m^{-3}$) than the CMP method (RMSE = 0.05 $m^3 m^{-3}$) with

500 MHz (Table 2.5). It should also be noted that the unrelated area considered for the θ_v estimation is higher in CO than CMP, which could potentially increase the error in CO method under high spatial variability of θ_v. When the minimum antenna separation was used, 500 MHz had 11.25 cm (antenna separation/2) distance from the center to either transmitter or receiver. Since two antennas in a CMP survey were moving apart from the center, this initial cone-shaped soil volume of 11.25 cm radius and 30 cm height would not be accounted for in the velocity estimation (Fig. 2.8). Though the accuracy of estimated θ_v by CMP-hyperbola would increase by increasing the survey distance, the maximum distance could be limited depending on the strength of the signal received by the receiver (Greaves *et al*., 1996). Therefore, despite the practicability of the CO-hyperbola fitting method, it also provides a reliable θ_v estimation (RMSE = 0.02 m^3 m^{-3}) along a survey line when the appropriate frequency and the survey parameters are used (Galagedara *et al*., 2003).

Selection of the best GPR frequency for estimating field θ_v has always been a trade-off. Higher frequencies penetrate only shallow depths and give a higher resolution while low frequencies penetrate deeper but give a lower resolution. Our preliminary data showed that it would not be possible to use 1000 MHz transducers in such a field survey. Because of the low weight and smaller footprint (0.08 m × 0.25 m approx.) of 1000 MHz transducers, it would not guarantee the proper ground coupling, and they would result in noisy data due to the inherent surface roughness. In such cases, 250 MHz would be a better alternative. However, the resolution aspect plays a major role in the accuracy of θ_v estimation. In a default mode 250 MHz (antenna separation = 38 cm) has 5 cm sampling interval whereas 500 MHz (antenna separation = 22.5 cm) has 2 cm sampling interval. For instance, 1 m length of a CO GPR transect (50 cm horizontal distance to both sides of a buried reflector) will have 21 and 51 GPR traces for 250 MHz and 500 MHz, respectively. All the TDR averaging criteria agreed that 500 MHz had a lower error (max RMSE = 0.03 $m^3 m^{-3}$) than 250 MHz (RMSE = 0.06 $m^3 m^{-3}$) for hyperbola depths < 34 cm (Table 2.6). In most cases, agricultural fields have low spacing between crop rows, which do not allow operating long/larger instrumentation in-between them. Approximate transducer footprints of 250 MHz and 500 MHz are 0.30 m × 0.70 m and 0.15 m × 0.40 m, respectively.

Table 2.6: Statistical comparison of 30 cm long TDR average θ_v and GPR-hyperbola estimated θ_v

GPR frequency (MHz)	n	Test*	*TDR* average						
			TDR1	TDR2	TDR3	TDR4	TDR5	TDR6	TDR7
			13	9	4	4	4	7	7
250	6	(a)	0.056	0.056	0.057	0.055	0.057	0.058	0.056
		(b)	0.005	0.005	0.005	0.081	0.005	0.005	0.005
500†	9	(a)	0.023	0.024	0.026	0.022	0.023	0.023	0.024
		(b)	0.427	0.348	0.653	0.236	0.391	0.270	0.178
500‡	9	(a)	0.036	0.041	0.045	0.037	0.027	0.033	0.039
		(b)	0.185	0.057	0.185	0.133	0.426	0.157	0.157
500§	18	(a)	0.030	0.033	0.037	0.031	0.025	0.029	0.032
		(b)	0.117	0.079	0.159	0.069	0.200	0.103	0.079

As per the limitations mentioned in Section 2.4.4, we evaluated a practical approach of 500 MHz to estimate θ_v within the agricultural root zone (30 cm). Eighteen hyperbolas ranging from 27-50 cm depth that collected from three field campaigns were used for the comparison. Statistical comparison of GPR-estimated θ_v and TDR-

* (a) Root mean square error (RMSE)/ ($m^3 m^{-3}$), (b) Mann-Whitney test, p-value
† hyperbola depths = 27, 31, 34 cm
‡ hyperbola depths = 40, 45, 50 cm
§ hyperbola depth range = 27-50 cm

measured θ_v is summarized in Table 2.6. The *p-values* for the Mann-Whitney test are less than the significance level ($\alpha = 0.05$) in all cases except TDR4 for 250 MHz. Therefore, the data support the hypothesis that there is a difference between the population medians. Meanwhile, the *p-values* for Mann-Whitney test for all cases tested are higher than the significance level ($\alpha = 0.05$) for 500 MHz. Therefore, the data support the hypothesis that there is no difference between the medians of GPR and TDR measured θ_v.

Reflections from the shallow hyperbolas do not represent the complete TDR sample area (Fig. 2.10). If the hyperbola depths were more than 70 cm, 100% of the 30 cm TDR sample area would be covered by GPR (Table 2.4). However, additional unrelated sample area would be added to the GPR sample area. Unrelated sample area within 0-30 cm out of the total GPR sample area was the same whether hyperbola depth was 30 or up to 70 cm. Nevertheless, additional larger sample area was added for GPR θ_v estimation from deeper hyperbola. Even taking advantage of the fully covered TDR sample area, additional sample area from 30-50 cm layer would significantly affect the total GPR response. This sampling area coverage resulted in a lowered RMSE (max 0.04 $m^3\ m^{-3}$) for deeper hyperbolas.

Further, this RMSE level was higher than the RMSE error obtained by Lunt *et al.* (2005) for θ_v estimations from a GPR reflection study. They used a calibrated neutron probe to compare the θ_v estimations of GPR and acquired RMSE of 0.018 $m^3\ m^{-3}$. However, they conducted the survey using 100 MHz antennas and used detailed borehole information for their analysis, which would not always be practical in an agricultural field. It should be noted that the sources of errors associated with the proposed method are not only due to the experimental setup but also due to the assumptions based on straight-ray wave propagation. Estimating the ε_r using a mixing model such as Topp's equation (Topp *et al.*, 1980) may also readily result in 1-2% errors in terms of absolute moisture (Mukhlisin & Saputra, 2013).

The need for prior knowledge of the shallow soil profile might be a constraint of this proposed method (Grote *et al*., 2002). Also, this method might not be applicable if texturally different soil layers exist within the shallow depths. As mentioned by Lunt *et al.* (2005), transient reflector geometry and inconsistency of GPR reflection amplitude under wet conditions are also challenges for the accuracy of this method. The proposed approach can be used to estimate θ_v in the root zone with a priori knowledge such as geological strata, the presence of shallow soil horizons, and the thickness of A_P horizon in the shallow soil profile. CO surveys carried out in a silage-corn field adjacent to the experiment plot using the same 500 MHz transducers in the same configuration showed both well- or ill-shaped shallow hyperbolas in a radargram without burying reflectors. Integrated or segregated application of modern hyperbola fitting algorithms (Dou *et al.*, 2017; Mertens *et al.*, 2016; Qiao *et al.*, 2015) would increase the efficiency and the accuracy (avoiding the subjective error of hyperbola fitting) of this proposed method. The capability of this approach to be used in the spatial and temporal variation of θ_v in managed agricultural fields for efficient water management will be our next research question.

2.5 Conclusion

We proposed a noninvasive practical approach to estimate SM rapidly in shallow soils with relatively large samples volumes. GPR data were evaluated using a systematic TDR data collection with special reference to sampling geometry of both methods. According to our understanding, this approach has not yet been discussed in the literature. Besides, the subjective error of hyperbola fitting was minimized by following a data processing guideline. Our field experiment revealed that SM measurement using the proposed hyperbola fitting method agreed with 30 cm long TDR probe data with an RMSE of 0.02 $m^3 m^{-3}$ for shallow (< 34 cm), and an RMSE of 0.04 $m^3 m^{-3}$ for deeper hyperbola analysis. We calculated the representative sample areas of GPR CO and CMP methods with respect to TDR sample area. Reflections over a 30 cm deep point reflector along a 1 m GPR survey length of CO and CMP methods were compared. The CO method covered larger (71.4 %) TDR sample area (30 cm × 70 cm) than the CMP method (49.8 %).

Further, we showed that deeper hyperbolic reflections cover a larger sample area for θ_v estimation than shallower hyperbolic reflections when comparing with the TDR method. Our analysis showed that the CO method (RMSE = 0.02 $m^3 m^{-3}$) was more accurate than the CMP method (RMSE = 0.05 $m^3 m^{-3}$) when the velocity was estimated using shallow hyperbolas. It was also revealed that 1000 MHz transducers were not successful due to poor ground coupling in irregular surfaces of crop fields. In a comparison of the CO method, 500 MHz (RMSE = 0.02 $m^3 m^{-3}$) gave better SM estimations than 250 MHz (RMSE = 0.06 $m^3 m^{-3}$) for shallow hyperbolas, mainly due to the higher resolution and higher compatibility with the TDR sample area. The error of 500 MHz SM estimations, when compared to 30 cm long TDR probe data, were considerably different for two depth ranges (27-34 cm or 40-50 cm) of hyperbolas tested. These results do not support our hypothesis that the same accuracy for θ_v estimation in 30 cm deep shallow soil profile of the experimental plot could be achieved by fitting the hyperbolas regardless of the depth from 27-50 cm. However, the estimated

θ_v using the proposed GPR hyperbola fitting (27-50 cm) is still within an RMSE of 0.03 m^3 m^{-3} and is not statistically different from the TDR measurements in this study. Therefore, evaluating the GPR estimated θ_v with a systematic TDR probes arrangement along the GPR transect is recommended. Probe arrangement should be compatible with the GPR sample geometry (i.e., long TDR probes at the top of the reflector and shallow probes towards both sides of the transect).

References

Agrios, G.N. 1997. Plant Pathology, *Academic Press,* San Diego. pp. 200-216

ASTM D1452 / D1452M-16. 2016. Standard practice for soil exploration and sampling by auger borings. *ASTM International*, West Conshohocken, PA. www.astm.org

ASTM D6432-11. 2011. Standard guide for using the surface ground penetrating radar method for subsurface investigation. *ASTM International*, West Conshohocken, PA. www.astm.org

ASTM D7263-09. 2018. Standard test methods for laboratory determination of density (unit weight) of soil specimens. *ASTM International*, West Conshohocken, PA. www.astm.org

Badewa, E., Unc, A., Mumtaz, C., Kavanagh, V., Galagedara, L. 2018. SM mapping using multi-frequency and multi-coil electromagnetic induction sensors on managed podzols. *Agronomy* 8(10), p 224

Burns, I.G. 1974. A model for predicting the redistribution of salts applied to fallow soils after excess rainfall or evaporation. *Journal of Soil Science* 25 (2), pp. 165-178

Daniels, J.J., Allred, B., Binley, A., Labrecque, D., Alumbaugh, D. 2005. Hydrogeophysical case studies in the vadose zone. IN: Rubin, Y., Hubbard, S.S. (Eds.), Hydrogeophysics. Springer, pp. 413–440

Davis, J.L., Annan, A.P. 1989. Ground-penetrating radar for high-resolution mapping of soil and rock stratigraphy. *Geophysical prospecting* 37, pp. 531-551

Dix, C. 1955. Seismic velocities from surface measurements. *Geophysics* 20(1), pp. 68–86

Dobriyal, P., Qureshi, A., Badola, R., Hussain, S.A. 2012. A review of the methods available for estimating SM and its implications for water resource management. *Journal of Hydrology* 458–459, pp. 110-117

Dou, Q., Wei, L., Magee, D., Cohn, A. 2017. Real-time hyperbolae recognition and fitting in GPR data. *IEEE Transactions on Geoscience and Remote Sensing* 55(1), pp. 51-62

Engman, E.T. 1991. Applications of microwave remote sensing of SM for water resources and agriculture. *Remote Sensing of Environment* 35, pp. 213-226

Fan, J., McConkey, B., Wang, H., Janzen, H. 2016. Root distribution by depth for temperate agricultural crops. *Field Crops Research* 189, pp. 68-74

Ferré, P.A., Knight, J.H., Rudolph, D.L., Kachanoski, R. G. 1998. The sample areas of conventional and alternative time domain reflectometry probes. *Water resources research* 34(11), pp. 2971-2979

Galagedara, L. W., J. D. Redman, G. W. Parkin, A. P. Annan, and A. L. Endres. 2005. Numerical modeling of GPR to determine the direct ground wave sampling depth. Vadose Zone Journal (4), pp. 1096-1106. doi:10.2136/vzj2004.0143

Galagedara, L.W, Parkin, G.W., Redman, J.D., Von Bertoldi, A.P., Endres, A.L. 2005a. Field studies of the GPR ground wave method for estimating soil water content during irrigation and drainage. *Journal of Hydrology (Amsterdam)* 301(1-4), pp. 182-197

Galagedara, L.W., Parkin, G.W., Redman, J.D. 2003. An analysis of the ground-penetrating radar direct ground wave method for soil water content measurement. *Hydrological Processes* 17(18), pp. 3615-3628

Galagedara, L.W., Parkin, G.W., Redman, J.D. 2005b. Measuring and modeling of direct ground wave depth penetration under transient SM conditions. *Subsurface Sensing Technologies and Applications* 6, p 193. https://doi.org/10.1007/s11220-005-0006-z

Ghorbani, R., Wilcockson, S., Koocheki, A., Leifert, C. 2008. Soil management for sustainable crop disease control: a review. *Environmental Chemistry Letters* 6, pp. 149-162

Greaves, R.J., Lesmes, D.P., Lee, J.M., Toksoz, M.N. 1996. Velocity variations and water content estimated from multi-offset, ground-penetrating radar. *Geophysics* 61, pp. 683-695

Grote, K., Hubbard, S., Rubin, Y. 2002. GPR monitoring of volumetric water content in soils applied to highway construction and maintenance. *The Leading Edge* 21(5), pp. 482-485

Hammer, Ø., Harper, D.A.T., Ryan, P.D. 2001. PAST: Paleontological statistics software package for education and data analysis. *Palaeontologia Electronica* 4(1), p 9. http://palaeo-electronica.org/2001_1/past/issue1_01.htm

Hettmansperger, T.P., Sheather, S.J. 1986. Confidence intervals based on interpolated order statistics, *Statistics and Probability Letters*, 4, pp.75–79

Hignett, C., Evett, S. 2008. Direct and surrogate measures of soil water content. *International Atomic Energy Agency, Soil and Water Management and Crop Nutrition Section, Vienna (Austria)*. No. IAEA-TCS-30

Huisman, J., Hubbard, S.S., Redman, J.D., Annan, A.P. 2003. Measuring soil water content with ground penetrating radar: A review. *Vadose Zone Journal* 2, pp. 476-491

Huisman, J.A., Sperl, C., Bouten, W., Verstraten, J.M. 2001. Soil water content measurements at different scales: accuracy of time domain reflectometry and ground-penetrating radar. *Journal of Hydrology* 245(1-4), pp. 48-58

IMKO Micromodultechnik GmbH. 2017. User manual TRIME-PICO_64-32, version 2.0, Ettlingen, Germany, http://www.imko.de (accessed on 13.04.2019)

Lambot, S., Slob, E.C., van den Bosch, I., Stockbroeckx, B., Vanclooster, M. 2004. Modeling of ground-penetrating radar for accurate characterization of subsurface electric properties. IEEE Transactions on Geoscience and Remote Sensing 42(11), pp. 2555-2568

Lambot, S., André, F. 2014. Full-wave modeling of near-field radar data for planar layered media reconstruction. *IEEE Transactions on Geoscience and Remote Sensing* 52(5), pp. 2295-2303

Liu, X., Chen, J., Cui, X., Liu, Q., Cao, X., Chen, X. 2017. Measurement of soil water content using ground-penetrating radar: a review of current methods. *International Journal of Digital Earth*, pp. 1-24

Lunt, I.A., Hubbard, S.S., Rubin, Y. 2005. Soil moisture content estimation using ground penetrating radar reflection data. *Journal of Hydrology*, 307, pp. 254–269

Maas, C., & Schmalzl, J. 2013. Using pattern recognition to automatically localize reflection hyperbolas in data from ground penetrating radar. *Computers & Geosciences* 58, pp. 116-125

Mertens, L., Persico, R., Matera, L., Lambot, S. 2016. Automated detection of reflection hyperbolas in complex GPR images with no a priori knowledge on the medium. *IEEE Transactions on Geoscience and Remote Sensing* 54(1), pp. 580-596

Minet, J., Bogaert, P., Vanclooster, M., Lambot, S. 2012. Validation of ground penetrating radar full-waveform inversion for field scale SM mapping. Journal of Hydrology 424, 112-123

Mukhlisin, M., Saputra, A. 2013. Performance evaluation of volumetric water content and relative permittivity models. *The Scientific World Journal*, p. 421762, doi:10.1155/2013/421762

Newfoundland and Labrador Geological Survey. 2014. Surficial Geology - Detailed 1:50 000 Scale. *Newfoundland and Labrador GeoScience Atlas online*. Last update: 2014. http://geoatlas.gov.nl.ca (accessed on 10.21.2018)

Zhang, P. 2003. A simple formula for sample size calculation in equivalence studies. *Journal of Biopharmaceutical Statistics* 13, pp. 529-538

Qiao, L., Qin, Y., Ren, X., Wang, Q. 2015. Identification of buried objects in GPR using amplitude modulated signals extracted from multiresolution monogenic signal analysis. *Sensors (Switzerland)* 15(12), pp. 30340-30350

Sadatcharam, K. 2019. Assessing potential applications of multi-coil and multi-frequency electromagnetic induction sensors for agricultural soils in Western Newfoundland (Unpublished master’s thesis). Memorial University of Newfoundland, St. John’s, NL, Canada

Seneviratne, S.I., Corti, T., Davin, E.L., Hirschi, M., Jaeger, E.B., Lehner, I., Orlowsky, B., Teuling, A.J. 2010. Investigating soil moisture–climate interactions in a changing climate: a review. *Earth Science Reviews* 99, pp. 125-161

Sham, J.F.C., Lai, W.W.L. 2016. Development of a new algorithm for accurate estimation of GPR's wave propagation velocity by common-offset survey method. *Tunneling and Underground Space Technology* 83, pp. 104-113

Topp, G.C., Davis, J.L., Annan A.P. 1980. Electromagnetic determination of soil water content: Measurements in coaxial transmission lines. *Water Resources Research* 16(3), pp. 574–582

Topp, G.C., Parkin, G.W., Ty Ferré, P.A. 2008. Soil Water Content. IN: Soil Sampling and Methods of Analysis (2^{nd} Ed) Carter, M.R., Gregorich, E.G. (Eds.), CRC Press, pp. 939-962

Tran, A., André, F., Lambot, S. 2014. Validation of near-field ground-penetrating radar modeling using full-wave inversion for soil moisture estimation. *IEEE Transactions on Geoscience and Remote Sensing* 52(9), pp. 5483-5497

CHAPTER 3

Distinguish the capillary fringe reflection in a ground penetrating radar profile for precise water table depth estimation

3.1 Introduction

Knowledge of the water table depth (WTD) is essential for many environmental prospects including water management in agriculture. WTD, where hydraulic pressure equals atmospheric pressure, demarcates the saturated-unsaturated soil boundary. Naturally, a transition zone called capillary fringe presents on top of the water table, which is nearly saturated but having negative water pressure (de Marsily, 1986). Capillary fringe in the vadose zone provides space, water and nutrients for plants and soil organisms (Selker *et al*., 1999; Tindall *et al*., 1999). Both WTD and the depth to the top of the capillary fringe (D_{CF}) are subjected to seasonal fluctuations resulting in diverse water management practices in agricultural lands throughout the growing season.

WTD can be measured through a borehole (BH), but generally unfeasible at large field-scales. High-resolution subsurface images of ground penetrating radar (GPR) can be used to measure shallow WTD especially in coarse-grained soils (Doolittle *et al.*, 2006; Paz *et al.*, 2017; Shih *et al*., 1986). In GPR, a transmitter antenna (Tx) transmits high frequency (10 to 1200 MHz) short pulses of electromagnetic (EM) energy into the subsurface and a receiver antenna (Rx) captures the transmitted energy (Davis & Annan, 1989). Transmitted EM energy (from now on referred to as GPR wave) can be reflected, refracted or attenuated (Annan, 2005; Daniels *et al.*, 2004; Strobach *et al.*, 2010). GPR wave propagation through the subsurface is highly sensitive to soil moisture (SM) (Agliata *et al.*, 2018; Algeo *et al.*, 2016; Annan, 2005; Huisman *et al.*, 2003). Water table reflects more than 40% of GPR wave energy in coarse-grained soils (Kowalczyk *et al.*, 2018). Accordingly, the water table can give continuous, mostly flat reflections with high amplitude in GPR radargrams (Greaves *et al.*, 1996; Gueting *et al.*, 2015; Khalil *et al.*, 2010; Mahmoudzadeh *et al.*, 2010 & 2012; Seger & Nashait, 2011; Van Overmeeren, 1998). Based on this advantage, GPR has become an essential method in groundwater studies (Beres & Haeni, 1991; Tsoflias *et al.*, 2001). Early researches, for example, Johnson (1992), Livari & Doolittle (1994), van Overmeeren (1994 & 1998), reported the capability of GPR method to detect water table.

GPR field techniques for water table studies have been developed over the decades. Annan *et al.* (1991) suggested that it would be essential to have a sharp boundary between saturated and unsaturated zones in a GPR profile for precise WTD estimation. Longer wavelengths (i.e., lower frequencies) are recommended even though the resolution of the radar profile decreases with increasing wavelength (Annan *et al.*, 1991). Loeffler & Bano (2004) have also found that GPR frequencies higher than 900 MHz do not identify the top of the saturated zone due to the effect from the capillary fringe and the transition zone. Therefore, most of the studies have been carried out using GPR frequencies lower than 250 MHz (Bano, 2006). Nakashima *et al.* (2001) and Takeshita *et al.* (2004) used common-midpoint (CMP) data acquisition of GPR to explain the multiple reflections from the water table. Besides, Nakashima *et al.* (2001) concluded that CMP data allow estimating the variation of relative permittivity (ε_r) and therefore calculating the radar wave velocity (v) along the soil profile. However, common-offset (CO) survey method with 100 MHz has been mostly used for the water table studies (Paz *et al.*, 2017). GPR techniques were employed during pumping tests to measure the temporal fluctuation of WTD (Bevan *et al.*, 2003; Endres *et al.*, 2000; Tsoflias *et al.*, 2001). Further, GPR has been used for various groundwater studies

(Corbeanu *et al.*, 2002; Conant *et al.*, 2004; Doetsch *et al.*, 2012; Gish *et al.*, 2002; Lambot *et al.*, 2008; Lunt *et al.*, 2005; McClymont *et al.*, 2012; Oliver & Woodroffe, 2016; Schmelzbach *et al.*, 2011 & 2012; Słowik, 2014; Talley *et al.*, 2005; Tsoflias & Becker, 2008; Yang *et al.*, 2013).

However, shallow water table associated with closely spaced soil horizons is challenging to interpret only with the aid of GPR outputs (van Overmeeren, 1998). With the advances in sophisticated sensor technology, real-time WTD and SM data would help to improve the GPR outputs (Doolittle *et al.*, 2006). Still, a site-specific GPR data validation is needed to distinguish the accurate water table reflection. Therefore, the objective of this study was to calibrate and validate a site-specific relationship between GPR-estimated D_{CF} and measured-WTD data in an agricultural field.

3.2 GPR theory

There are three characteristics to consider when interpreting WTD from a GPR profile (Fig. 3.1). First, saturation decreases from bottom to top of the capillary fringe (within the transition zone) subsequently increasing the radar wave velocity (Daniels *et al.*, 2005). The thickness of this zone depends on the amount, size (diameter) and interconnectivity of soil pores (Bear, 1972; Doolittle, 2006). Second, the oscillations of the reflected radar pulse due to the transition zone result in a series of bands to represent the water table in a radar profile (Doolittle *et al.*, 2006). Top of the capillary fringe gives an early and robust reflection than the actual water table (Bentley & Trenholm, 2002; Igel *et al.*, 2016). The wetting front also has the same reflection as the water table (Rejiba *et al.*, 2012). Third, two-way travel time (TWTT) correspondence to the maximum absolute amplitude of the airwave (t_{air}) is opposite from that of a reflection event ($t_{reflect}$) (Bentley & Trenholm, 2002) (Fig. 3.1). In addition to the above characteristics, the maximum absolute amplitude occurs at the second half of the respective GPR wavelet (Booth *et al*., 2010).

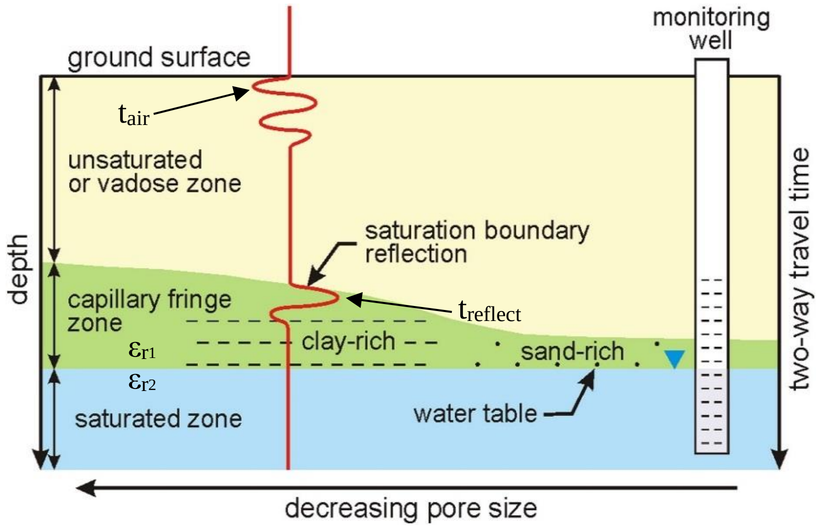

Figure 3.1: Increment of capillary rise with decreasing pore size resulting a comparatively more substantial difference between the WTD measured in a borehole, and saturation boundary reflection observed using a GPR profile in clay-rich soils than that of sand-rich soils (modified from Paz *et al*., 2017)

Equation 3.1 gives radar signal velocity (v) of a non-magnetic and low-loss geological material.

$$v = \frac{c}{\sqrt{\varepsilon_r}} \tag{3.1}$$

Where ε_r is the relative permittivity and c is the electromagnetic wave propagation velocity in free space (= 0.3 m/ns) (Davis & Annan, 1989; Neal, 2004; Schmelzbach *et al*., 2012).

In addition, depth to a known reflector method (Daniels *et al*., 2004) can be used to calculate the GPR reflection wave velocity (v_{rw}) of a monostatic antenna using Equation 3.2.

$$v_{rw} = \frac{2D}{t} \tag{3.2}$$

Where t is the TWTT of the reflected GPR wave from a reflection boundary and D is the depth to the boundary (*ASTM D6432-11*).

ε_r of the soil just below the ground surface can be calculated using GPR direct groundwave method using Equation 3.3 (Huisman *et al*., 2003).

$$\varepsilon_r = \left[\frac{c\ (t_{GW} - t_{AW}) + x}{x}\right]^2 \tag{3.3}$$

Where t_{GW} and t_{AW} are direct groundwave and airwave arrival time, respectively, from Tx to Rx antenna and x is the antenna separation.

ε_r can be derived from SM measured as volumetric water content, θ_v using an empirical model. Topp *et al.* (1980) suggested the first and well-known model (Mukhlisin & Saputra, 2013) as given in Equation 3.4.

$$\varepsilon_r = 3.03 + 9.3\theta_v + 146.0\theta_v - 76.7\theta_v \tag{3.4}$$

3.3 Materials and Methods

3.3.1 Study area

The experimental site was located at a silage cornfield and a grass field in Pynn's Brook Research Station (PBRS), Pasadena, NL, Canada. The area is gently sloping with a 2-5% slope, and depth to the bedrock is >1 m from the surface (Kirby, 1988). Details of the observed shallow soil profile are given in Table 3.1. The top soil (ε_{r1}, t_1) is an organic soil layer with gravels. Immediately below the top layer is the Ap horizon (ε_{r2},

t_2) and be classified as loamy sand (sand = 82.0 ± 3.4%; silt = 11.6 ± 2.4%; clay = 6.4 ± 1.2%) (Badewa *et al.*, 2018). The average bulk density and porosity of the loamy sand layer (n=28) is 1.31 g cm^{-3} (±0.07) and 51% (±0.03), respectively (Badewa *et al*., 2018). A well-sorted sandy soil layer was observed from 0.35-3.47 m depth by hand auguring. The average capillary height was approximated as 0.70 m for unsaturated sandy layer (ε_{r3}, t_3) according to Liu *et al*. (2014). The average WTD measured in all GPR survey days (n=16) was 2.55 m. Therefore, the average t_3 was considered as 1.50 m (2.55-0.70-(0.05+0.30)). The average precipitation is 1113 mm per year with 410 mm falling as snow, and annual mean temperature is 4 °C as recorded at the nearest weather station, Deer Lake, NL for last 30 years (https://weather.gc.ca).

Table 3.1: Details of different soil layers

Soil layer	Depth range (m)	Layer thickness (m)	Relative permittivity
Top soil	0 - 0.05	t_1 = 0.05	ε_{r1}
Loamy sand	0.05 - 0.35	t_2 = 0.30	ε_{r2}
Sand (unsaturated)	0.35 - top of the capillary fringe	t_3 = WTD_m-0.7-0.35	ε_{r3}

3.3.2 Site preparation and data collection

Following materials and instruments were used for data acquisition, processing and interpretation of this study.

PulseEKKO® Pro GPR system (Sensors and Software Inc., Canada) with 100 and 250 MHz center frequencies

Decagon Em50 data logger, and water level, electrical conductivity-, temperature- and SM-probes (METER group Inc., USA)

EKKO Project V3 R1 and IcePicker V3 R7 GPR data processing Software (Sensors and Software Inc., Canada)

The silage cornfield was relatively flat and 43 m long. The main GPR survey line was marked between the cornfield and the grassland using wooden pegs (Fig. 3.2 left). A shallow groundwater monitoring BH (3.47 m deep) was constructed at 19 m position of the GPR survey line. The perpendicular distance between BH and the survey line was 0.5 m (Fig. 3.2 right). A water level-, electrical conductivity- and temperature-sensor, connected to a data logger (Em50 – Meter Group Inc., USA), was installed at the bottom of the BH. The water level sensor measures the height of the water column in the BH. Three SM probes (probe length = 5 cm each) were installed horizontally at 0.1 m, 0.2 m and 0.3 m depths and connected to the same data logger (Fig. 3.3 left). An additional temperature-sensor was installed together with the SM probe at 0.2 m depth. GPR surveys were carried in between the locations of SM probes and the BH (Fig. 3.3 right). The probes were oriented perpendicular to the GPR survey direction.

Background GPR surveys were carried out; (i) before construction of the BH, (ii) after the construction of the BH, but before installation of the water level sensor, and (iii) after installation of the water level sensor. Sixteen 250 MHz GPR CO surveys (43 m in length, antenna separation = 0.38 m, sampling interval = 0.05 m) were performed in 2017 and 2018. Three 100 MHz GPR CO surveys (~30 m in length, antenna separation = 1.0 m, sampling interval = 0.25 m) were also conducted under wet, median and dry conditions in 2018 along the same GPR line.

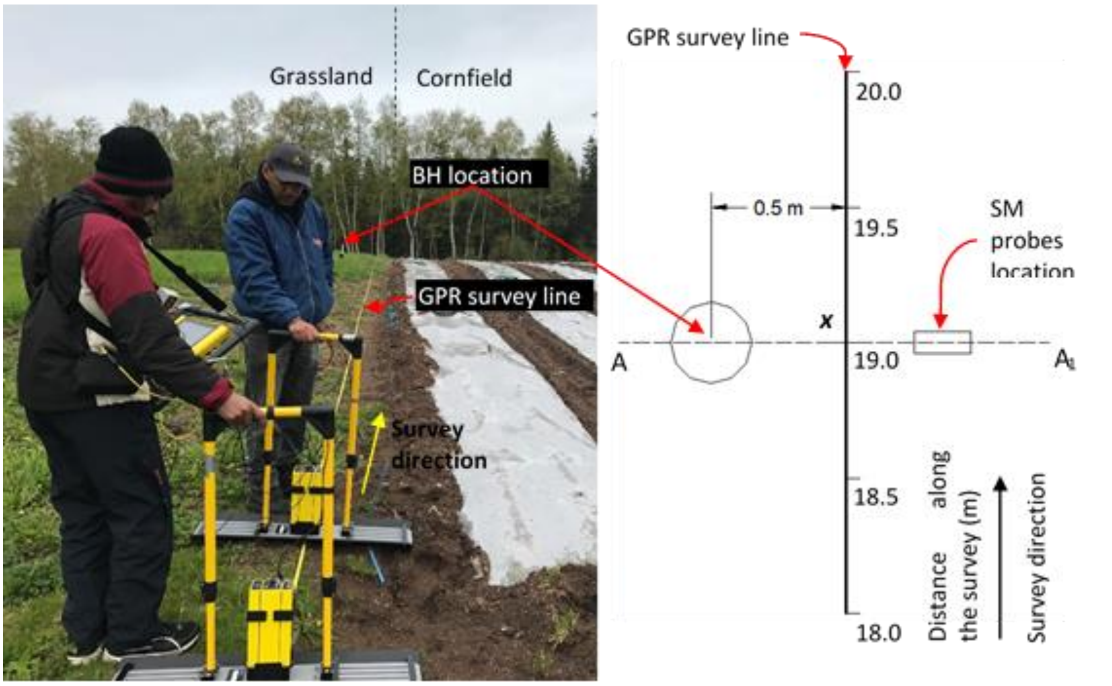

Figure 3.2: Photograph captured during a 100 MHz survey at the starting point of the GPR survey line (left). Plan view of the borehole (BH) location with GPR survey line and the location of soil moisture (SM) probes (right). A-A$_1$ cross section is illustrated in Figure 3.3. The intersection of the A-A$_1$ section and GPR survey line is marked as "*x*."

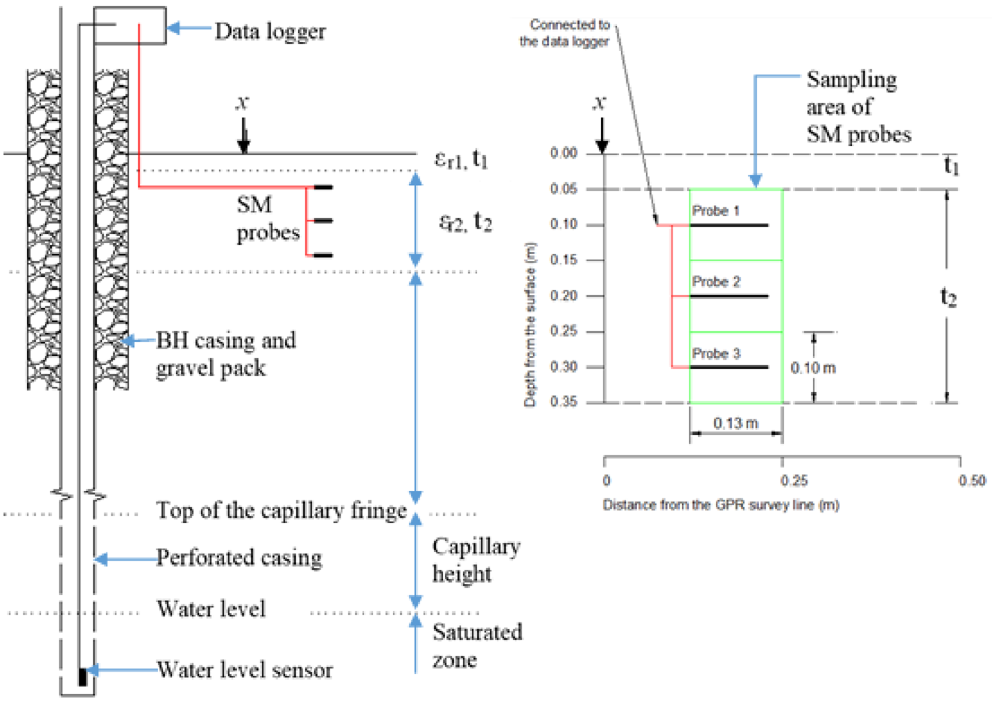

Figure 3.3: A-A$_1$ vertical cross-sectional view of the soil profile and the details of the borehole (BH) (Left). The sampling areas of soil moisture (SM) probes (Right). "*x*" marks the position of the GPR survey line.

Three basic GPR data processing steps were applied using EKKO Project V3 R1 Software (Sensors and Software Inc., Canada) as listed below.

Edit the first-break

Apply dewow and SEC2 gain

Background subtraction – full filter length

After completing above basic processing, GPR files were exported to IcePicker V3 R7 software (Sensors and Software Inc., Canada) for automatic time picking.

3.3.3 Defining the average GPR velocity

The average ε_r from the surface to the top of the capillary fringe ($\overline{\varepsilon_r}$) is needed to define an average v_{rw} when using Equation 3.1. Three soil layers (ε_{r1}, $\varepsilon_{r2,}$ and ε_{r3}) were considered to get $\overline{\varepsilon_r}$. First, the ε_r of 0-0.05 m soil depth (ε_{r1}) was calculated using the GPR direct groundwave (Eq. 3.3). Twelve GPR traces near the SM probes were considered for groundwave analysis (Fig. 3.4).

SM data logging interval was 60 min. Therefore, one daily mean SM datum had 24 replicated measurements. Each SM probe has a cylindrical sampling volume (radius ~ 0.05 m, volume = 0.715 L) that covers 0.05 m soil heights both above and below the probe (Fig. 3.3 right) (https://www.metergroup.com; Sakaki *et al*., 2008). Daily mean SM at three depths was converted to daily mean ε_r value using Equation 3.4. An average ε_r for the soil layer between 0.05-0.35 m (ε_{r2}) was obtained from those ε_r values at three SM probe depths.

ε_r of the soil layer from 0.35 m depth to the top of the capillary fringe (ε_{r3}) was assumed based on the literature and onsite weather data (Table 3.2 and Appendix 3.1).

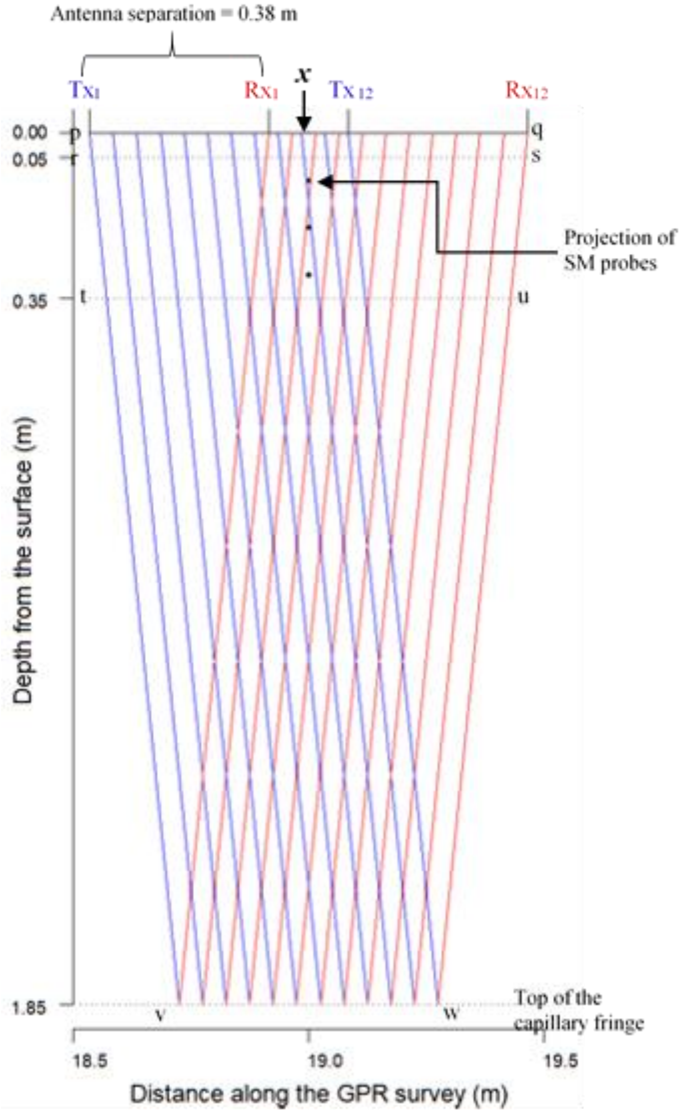

Figure 3.4: GPR wave paths related to twelve GPR traces at the intersection of the GPR survey line and the A-A$_1$ plane. A 250 MHz CO survey with 0.38 m antenna separation and 0.05 m sampling interval was considered. Tx$_1$ and Tx$_{12}$ = transmitter positions, Rx$_1$ and Rx$_{12}$ = receiver positions, corresponding to first and twelfth trace. *x* = intersection of A-A$_1$ plane (refer to Fig. 3.2). Note that GPR wave paths assumed to be straight.

Table 3.2: Relative permittivity (ε_r) values for the assumed moisture condition of the sand layer below 0.35 m depth and above the top of the capillary fringe

Assumed moisture condition	ε_r	Soil moisture (SM) % (Topp *et al.*, 1980)	Reference for ε_r
Dry	3-5	3-8	Davis & Annan, 1989
Mostly dry	6-7	10-13	Cihlar & Ulaby, 1974
Slightly dry	8-9	15-17	Martinez, 2001
Median	10-11	19-21	Cihlar & Ulaby, 1974
Slightly wet	12-15	23-28	Charlton, 2008; Reynolds, 1997
Mostly wet	16-18	29-32	Martinez, 2001
Saturated	20-30	~40	Davis & Annan, 1989

Then the weighted average of ε_{r1}, ε_{r2}, and ε_{r3} was considered as the $\bar{\varepsilon_r}$. For this purpose, the percentage sample area of each layer was calculated with respect to total GPR sample area (Fig. 3.4 and Table 3.3).

Table 3.3: Percentage sample area of each soil layer out of total GPR sample area on the B-B_1 plane related to twelve GPR traces collected top of the SM probes

Soil layer	Polygon (refer to Fig. 3.4)	Area (m^2)	Percentage out of total GPR sample area (%)
Top soil	pqsr	0.0462	3.4
Loamy sand	rsut	0.2667	19.5
Sand (unsaturated)	tuwv	1.0561	77.1
Total	pqwv	1.3690	100.0

Let w to be the weight and x to be the data number, then weighted average ($\bar{x}$) equals to;

$$\bar{x} = \frac{\sum_{i=1}^{n} w_i \times x_i}{\sum_{i=1}^{n} w_i} \tag{3.5}$$

e.g. estimation of the $\bar{\varepsilon_r}$ on 6/23/2017 (first data row in Table 3.4)

$$\bar{\varepsilon_r} = \frac{(3.4\% \times \varepsilon r_1) + (19.5\% \times \varepsilon r_2) + (77.1\% \times \varepsilon r_3)}{100\%}$$

$$\bar{\varepsilon_r} = \frac{(3.4 \ \times 23.0) + (19.5 \times 10.5) + (77.1 \times 10.5)}{100}$$

$$\bar{\varepsilon_r} = 10.9$$

Table 3.4: Calculation of the average reflected wave velocity (v_{rw}) through the estimation of the average relative permittivity ($\bar{\varepsilon_r}$) from surface down to the top of the capillary fringe

Date	WTD (m)	t_3 (m)	ε_{r1}	ε_{r2}	ε_{r3}	$\bar{\varepsilon_r}$	Calculated v_{rw} (m/ns)
6/23/2017	2.47	1.42	23.0	10.5	10.5	10.9	0.091
7/6/2017	2.55	1.50	4.0	12.2	6.0	7.1	0.112
7/28/2017	2.74	1.69	13.2	7.5	6.0	6.5	0.117
8/18/2017	2.85	1.80	10.9	7.8	6.0	6.5	0.117
8/29/2017	2.90	1.85	19.5	8.1	4.0	5.3	0.130
9/15/2017	2.91	1.86	14.0	11.2	4.0	5.7	0.125
10/3/2017	2.77	1.72	6.2	11.6	7.0	7.9	0.107
11/7/2017	2.63	1.58	13.1	13.7	10.5	11.2	0.090
6/1/2018	2.24	1.19	15.2	12.2	13.5	13.3	0.082
6/20/2018	2.33	1.28	14.0	12.5	8.0	9.1	0.100
6/29/2018	2.31	1.26	19.5	12.1	7.0	8.4	0.103
7/20/2018	2.54	1.49	20.0	8.6	6.0	7.0	0.113
8/9/2018	2.61	1.56	6.5	12.8	4.0	5.8	0.125
9/7/2018	2.75	1.70	4.0	12.8	4.0	5.4	0.129
10/2/2018	2.56	1.51	8.0	12.4	10.5	10.8	0.091
10/31/2018	1.86	0.81	23.3	13.1	17.0	16.5	0.074

3.3.4 Estimating the D_{CF} from GPR

GPR traces that used for v_{rw} calculation were considered for the D_{CF} estimation as well. Accordingly, the mean TWTT to the capillary fringe reflection (mean t_{CF}) was obtained from twelve GPR traces. The subjective error was high when picking the leading edge of the wavelet (Galagedara *et al*., 2003). Therefore, TWTT related to the absolute maximum amplitude of the airwave (t_{air}) and the reflection event ($t_{reflect}$) were picked. This procedure was similar to the direct groundwave analysis by Grote *et al.* (2003). The correct t_{CF} was determined by using Equation 3.6.

$$t_{CF} = t_{reflect} - t_{air} \tag{3.6}$$

D_{CF} was then estimated from the mean t_{CF} and the calculated v_{rw} using Equation 3.2. D_{CF} of eight GPR surveys in 2017 were calibrated using a linear regression model. WTD measured by the water level sensor (WTD_m) at the same time of GPR survey was used for the calibration. Next, the WTD was predicted for eight survey days in 2018 using the calibration equation obtained. The predicted WTD (WTD_p) and WTD_m were compared using a 1:1 plot and root mean square error (RMSE). In a second step, WTD_m and D_{CF} for all 16-survey days were plotted in a linear regression plot to examine an average capillary height. Slope and the intercept of the regression line as well as the prediction line were compared statistically with that of the 1:1 line.

3.4 Results and Discussion

3.4.1 Site-specific relationship for WTD_m vs. D_{CF}

D_{CF}, which derived using Equation 3.2 for all 16 GPR survey days are given in Table 3.5. The WTD_m fluctuation related to GPR survey days (*n*=16) was from 1.85 m to 2.91 m. For the entire period of the study covering growing seasons in 2017 and 2018 (496 days), the WTD_m varied between 1.58 – 2.95 m. The shallowest WTD_m (1.58 m) was observed in the spring of 2018 (April 30, 2018), and the deepest WTD_m (2.95 m) was found in the summer of 2017 (Sept 10-12 2017). Throughout the studied period, the average WTD_m was 2.48 m with an annual average of 2.69 m in 2017 and 2.34 m in 2018 during the growing season (from May to the end of October). These data imply that 2017 had a relatively dry growing season was also confirmed with the onsite weather data collected (Appendix 3.1).

Table 3.5: GPR estimated depth to the top of the capillary fringe (D_{CF}) which is derived from the mean two-way travel time (TWTT) to the capillary fringe reflection (t_{CF}) using Equation 3.2 for all GPR surveys. Standard error (SE) of mean, and minimum (Min), median and maximum (Max) of t_{CF} time picks are also given.

Date	Mean t_{CF} (ns)	SE of mean	t_{CF} (ns)			D_{CF} (m)
			Min	Median	Max	
6/23/2017	35.07 ±1.70	0.43	32.65	35.08	38.04	1.59
7/6/2017	29.21 ±1.93	0.58	27.97	28.51	34.80	1.62
7/28/2017	32.40 ±5.39	1.44	27.71	28.82	39.78	1.90
8/18/2017	36.43 ±2.87	0.70	32.11	37.81	39.67	2.13
8/29/2017	33.59 ±2.90	0.70	30.21	32.29	39.16	2.17
9/15/2017	34.31 ±3.86	1.11	27.70	35.23	38.83	2.14
10/3/2017	36.84 ±3.69	1.02	32.80	36.26	42.15	1.96
11/7/2017	40.23 ±4.53	1.26	33.09	39.45	44.36	1.81
6/1/2018	38.08 ±2.06	0.47	35.64	39.35	40.59	1.56
6/20/2018	33.35 ±3.82	0.83	30.18	31.38	40.54	1.67
6/29/2018	31.18 ±1.35	0.33	30.07	30.73	34.40	1.60
7/20/2018	32.89 ±3.33	0.77	28.07	35.20	37.56	1.85
8/9/2018	30.25 ±2.01	0.44	28.15	28.80	32.69	1.89
9/7/2018	30.05 ±2.67	0.67	27.78	29.29	36.47	1.96
10/2/2018	36.93 ±2.65	0.61	34.33	35.42	41.31	1.68
10/31/2018	31.64 ±2.78	0.61	27.93	31.27	35.56	1.18

The WTD_m at the same time of GPR survey, and corresponding D_{CF} are plotted in Figure 3.5 (left). Linear regression of the WTD_m vs. D_{CF} for GPR surveys in 2017 implies that there is a strong linear regression with an R^2 of 0.9778 (WTD_m = 0.6956 D_{CF} + 1.3884) between these two parameters.

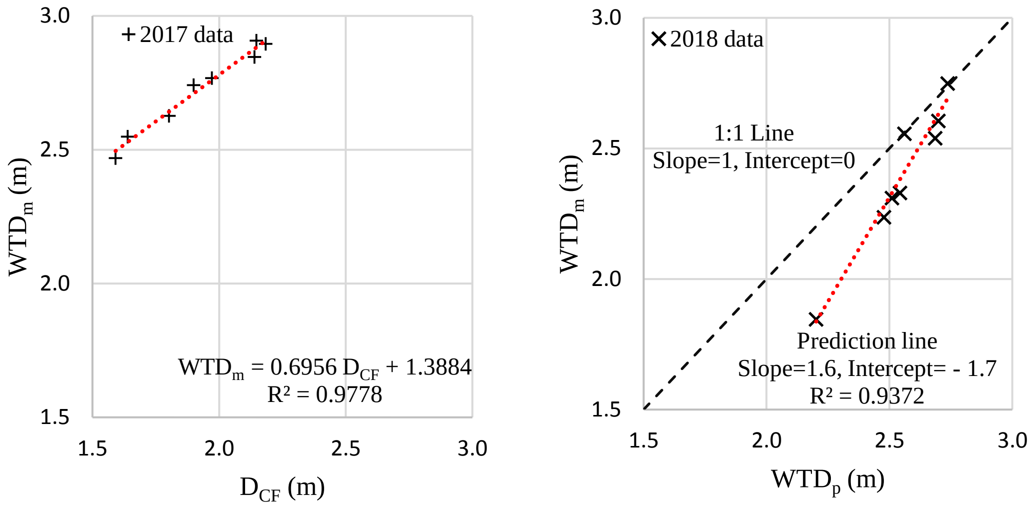

Figure 3.5: Linear regression plot of measured water table depth (WTD_m) vs. GPR estimated depth to the capillary fringe (D_{CF}) for 2017 data (n=8) (left). The 1:1 plot of the predicted water table depth (WTD_p) vs. WTD_m in 2018 (n=8) (right).

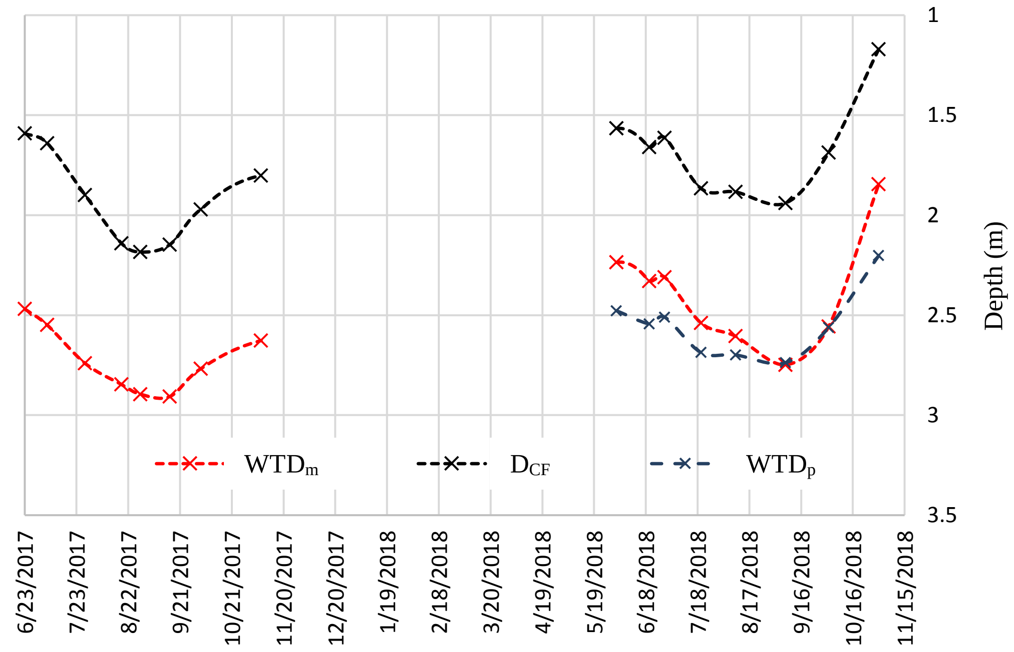

Figure 3.6: Temporal variability of the measured water table depth (WTD_m) and the estimated depth to the capillary fringe using GPR (D_{CF}) for both years and, the predicted water table depth (WTD_p) for 2018.

WTD_p for 2018 based on the D_{CF} and the regression model vs. WTD_m in 2018 were plotted in a 1:1 plot (Fig. 3.5 right). The slope of the prediction line (1.5967) and the slope of 1:1 line (1.000) are significantly different at α=0.05 (p-value= 0.004, df= 12, t critical= 2.179 < t=3.536) (Appendix 3.2). The error of WTD predication is high during the wet survey days and overestimated from the 1:1 line (Fig. 3.5 right). This behaviour could be due to the fact that the capillary fringe would not fluctuate uniformly with the WTD fluctuation. As Bentley & Trenholm (2002) stated, the capillary height is higher when the WTD is increasing (during discharging) while it is lower when the WTD is decreasing (during recharging). This feature could not be captured by a regression equation (Fig. 3.6). Therefore, the regression model might not be suitable when there is a sudden decrease in WTD like during heavy or long-lasting rain events. The rain event at the end of the growing season of 2018 was unexpectedly high (Appendix 3.1); consequently, resulted the maximum error of WTD prediction on Oct 2018 (Fig. 3.6). However, it is worth noting that the RMSE of WTD_m vs. WTD_p (0.194 m) is possibly acceptable for the scale of application in most agricultural practices.

In general, the D_{CF} cannot be measured directly under field conditions (Salim, 2016). The proposed method provides a non-invasive approach to estimate D_{CF}, which is more beneficial in agricultural fields especially during the growing season. The advantage of the proposed method is that both WTD and D_{CF} could be estimated in real time. The results would have been improved if a broader range of measured data were available under different SM conditions.

As seen in Figure 3.7, WTD_m vs. D_{CF} for all survey days have a linear relationship (WTD_m = 1.0123 D_{CF} + 0.741) with an R^2 of 0.911. The slopes of the regression line (1.012) and the slope of 1:1 line (1.000) are not significantly different at α=0.05 (p-value= 0.885, df= 28, t critical= 2.048 > t=0.146) (Appendix 3.2).

Therefore, the intercept of the regression line (0.741 m, n=16) can be considered as the average capillary height within these two growing seasons in 2017 and 2018. This analysis allows defining an average capillary height for the study site throughout the growing season. The average value agrees with the value of ~0.70 m capillary height for the same soil conditions described by Liu *et al*. (2014).

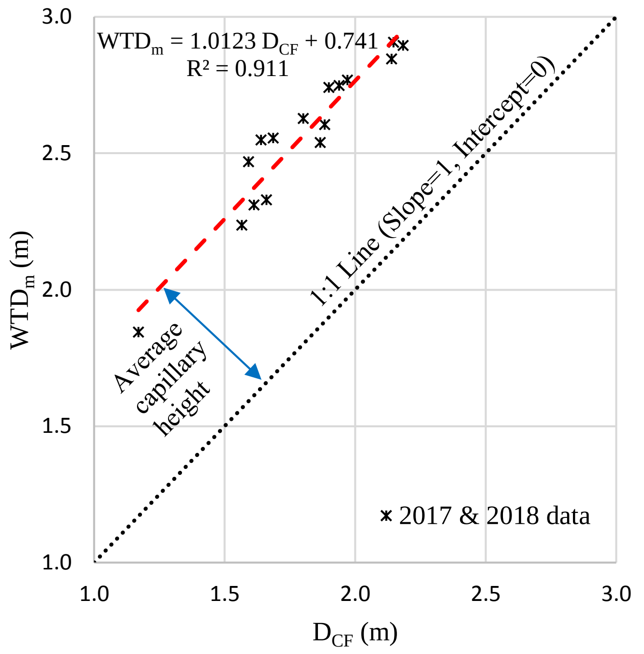

Figure 3.7: Comparison of the measured water table depth (WTD_m) and the estimated depth to the capillary fringe (D_{CF}) based on GPR data for all 16 GPR surveys. 1:1 line indicates the measured and GPR based water table depth.

3.4.2 Challenges of the proposed method

In GPR, the Rx only records different amplitudes of the receiving signals with respect to time. The GPR interpreter observes the radar events in a radargram and obtains relevant TWTTs. Without knowing the v_{rw}, it is impossible to derive D_{CF} (*e.g.*, using Eq. 3.2). Under these circumstances, there are two challenges to estimating the D_{CF} in a GPR radargram. First, picking the TWTT of the capillary fringe reflection correctly. Second, knowing or properly assuming the average v_{rw} from the surface down to the top of the capillary fringe reflection.

Procedures available in the literature were combined to overcome the challenge of picking the correct TWTT. The standard error of the mean t_{CF} was >1 other than 4 cases in 2017: 1.44 (July 28), 1.26 (Nov 7), 1.11 (Sept 15) and 1.02 (Oct 3). Standard deviation (SD) of the mean t_{CF} was above 3 ns for those four survey days. The error associated with these four surveys is mostly due to a high signal-noise ratio in the data acquisition. The lowest SDs of the mean t_{CF} were 1.70 and 1.35 for June 23, 2017 and June 29, 2018, respectively. The inconsistency of GPR reflection amplitude under wet conditions as stated by Lunt *et al.* (2005) could be a reason for the error of time picking.

The challenge of defining v_{rw} is determining the average ε_r of the material above the capillary fringe. ε_r controls the v_{rw} and the reflection coefficients at interfaces. Common v_{rw} values suggested from the literature may not be accurate for heterogeneous soil profiles. In addition, seasonal fluctuation of WTD and capillary height can remarkably change the average ε_r. However, v_{rw} can be measured by using multi-offset GPR survey methods such as CMP and WARR (wide-angle reflection and refraction). Nevertheless, it is time- and labor- consuming to carry out multi-offset surveys in every field campaign (Huisman *et al*., 2003; Paz *et al.*, 2017). In the present study, three different ε_r values were used for different soil layers. A weighted average of ε_r was calculated based on the GPR sampling geometry in order to minimize the error of assuming an average ε_r.

The average capillary height considered (0.70 m) based on the study of Liu *et al*. (2014) to estimate the ε_{r3} is closer to the average capillary height obtained from this study (0.741 m). It should mention that taking an average capillary height would be reasonable under static conditions, but not always suitable if the seasonal fluctuation of WTD is high during the time of interest.

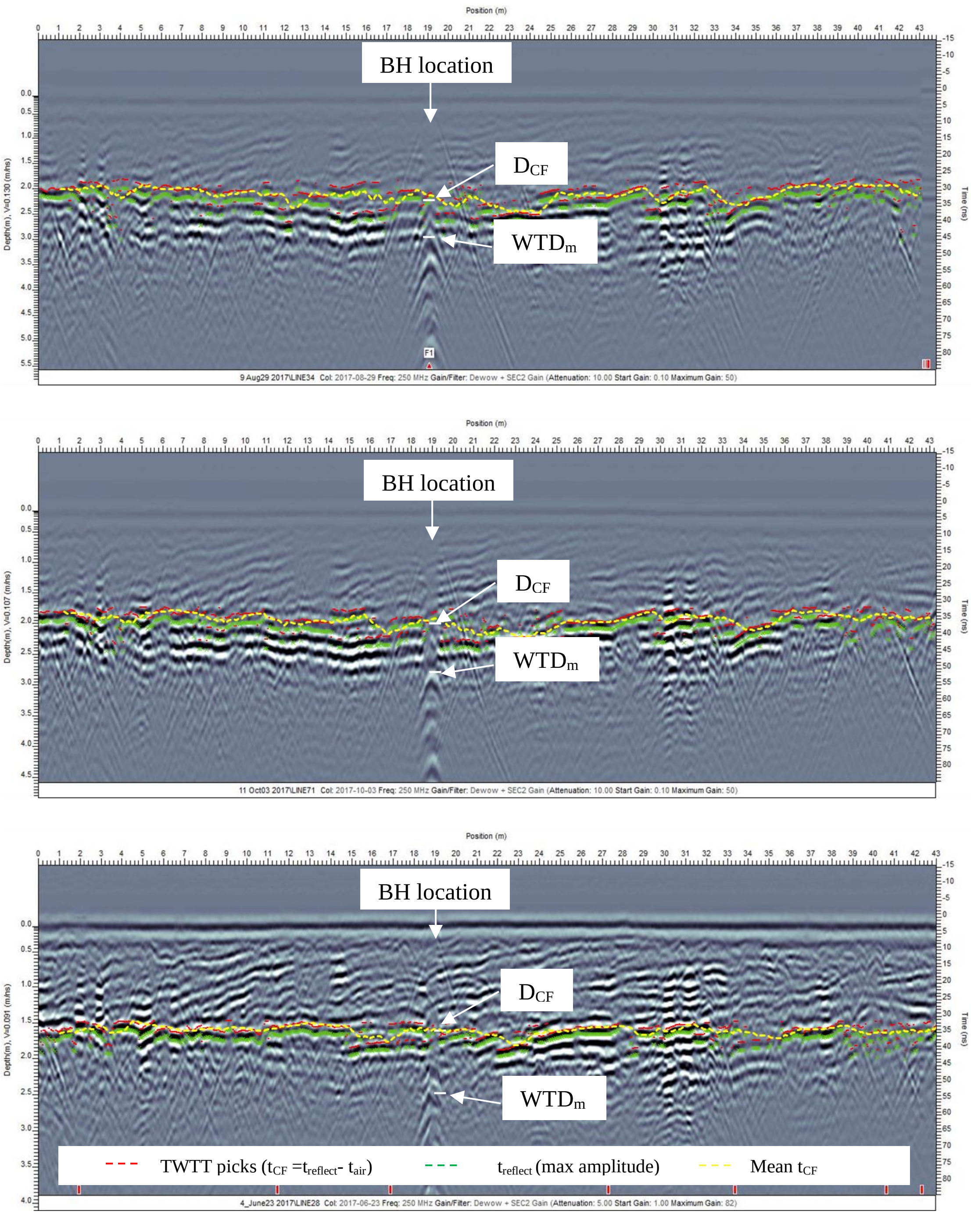

Figure 3.8: Two-way travel time (TWTT) picks of the maximum amplitude of the reflection ($t_{reflect}$), after time-correction (t_{CF}), and the mean t_{CF}. GPR-estimated (250 MHz) depth to the capillary fringe (D_{CF}) and the measured water table depth (WTD_m) at the borehole (BH) are presented under dry soil moisture condition on Aug 29 (above), under median soil moisture condition on Oct 03 (middle), and under wet soil moisture condition on June 23 (below), in the growing season of 2017.

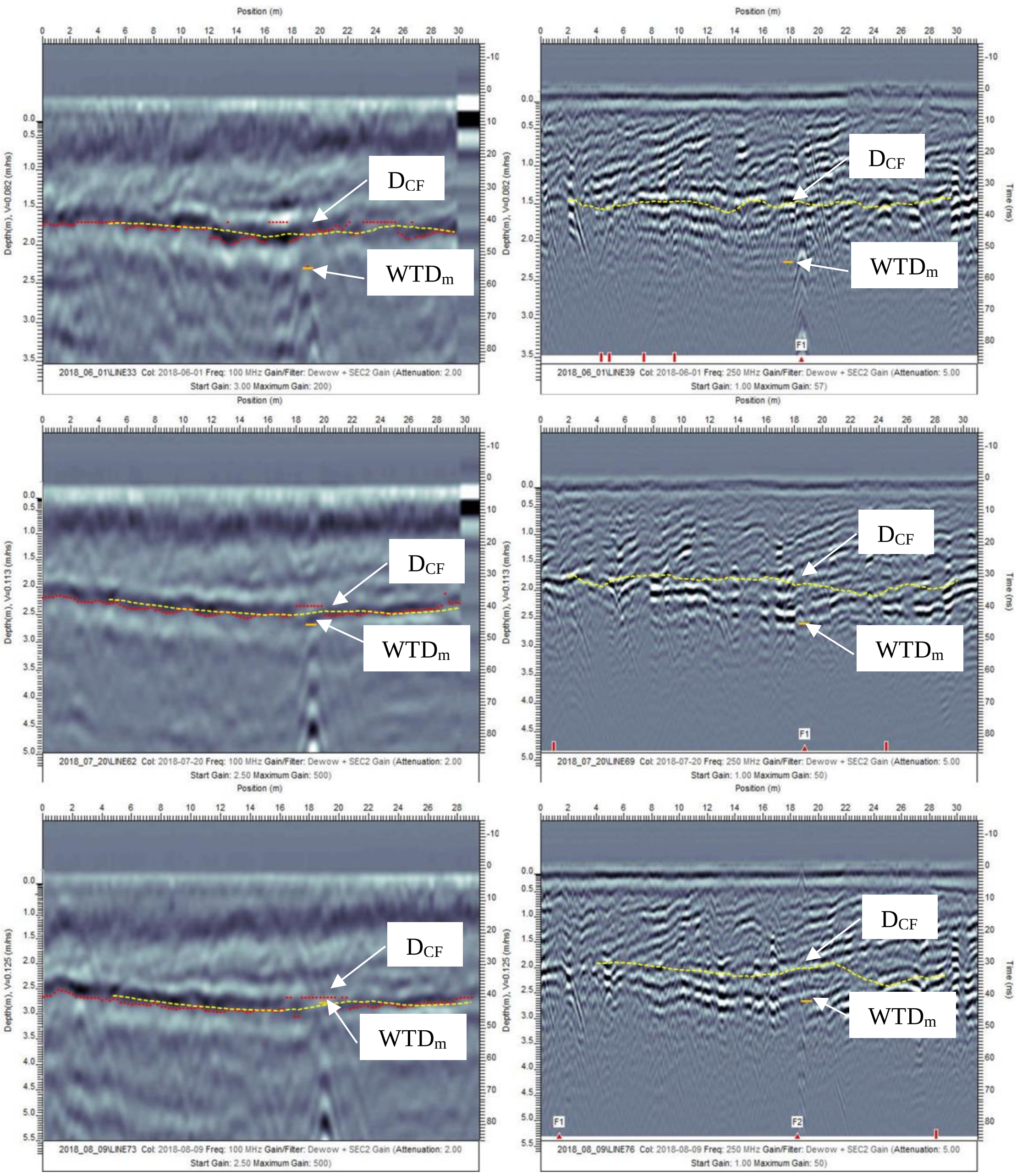

Figure 3.9: Comparison of 100 MHz (left) and 250 MHz (right) GPR radargrams. Two-way travel time (TWTT) picks after time-correction (t_{CF}), and the mean t_{CF} are shown. Measured water table depth WTD_m at the borehole (BH) are presented under wet soil moisture condition on June 01 (above), under median soil moisture condition on July 20 (middle), and under dry soil moisture condition on Aug 09 (below), in the growing season of 2018.

The GPR velocity is independent of the frequency (for frequencies above 100 MHz) and dependent only on the dielectric permittivity and the magnetic permeability (Reppert *et al.*, 2000). Therefore, the same velocity derived from 250 MHz could be used to analyze 100 MHz data on the same day. GPR profiles from 250 MHz give high-resolution than 100 MHz. Thus, multiple reflections near the water table can be clearly observed (Fig. 3.8). However, those reflections give an undulated boundary. In contrast, 100 MHz give low-resolution images with a relatively flat and clear boundary for the water table zone and with less multiple reflections. The water table reflections picked in a 100 MHz radargram are closer to WTD_m than that of 250 MHz (Fig. 3.9). Figure 3.9 clearly shows that the error between the GPR water table and the actual water table (WTD_m) is low under dry conditions and the error increases when deceasing WTD. Both frequencies perform well under dry SM conditions than wet SM conditions because of low signal attenuation under dry SM conditions (Daniels, 2004). Present results imply that 250 MHz is suitable to examine shallow D_{CF} whereas 100 MHz is suitable to examine deeper WTD.

3.5 Conclusion

The shallow water table in a sandy aquifer, with the presence of shallow soil horizons, was difficult to interpret only with GPR data. Real-time WTD data were used to aid the validation of GPR based WTD data. ε_r of shallow soil was determined using continuously measured SM data. GPR sampling geometry was also considered to improve the radar velocity assumptions. A site-specific strong linear relationship (R^2 = 0.9778) between D_{CF} and WTD_m was developed ($WTD_m = 0.6956\ D_{CF} + 1.3884$) using eight GPR surveys throughout the growing season of 2017. The regression model was validated using eight monthly GPR surveys in the same location in 2018. Low RMSE (0.194 m) of predicted- and measured- WTD implies that the proposed non-invasive method would be beneficial for precise WTD and D_{CF} estimations in agricultural fields.

A regression model was developed using all GPR data collected for two growing seasons using the same approach. As a result, an average capillary height of 0.741 m was suggested for the particular site throughout the growing season. The suggested capillary height not only has a strong linear relationship (R^2 =0.911, n=16) but also comparable with the existing literature. The developed model is recommended to modify using the data collected for many growing seasons covering a wider variability of water table. Then the knowledge of the local variation of WTD and D_{CF} throughout the growing season would be transferred to end users of the agricultural sector in the region.

References

Agliata, R., Bogaard, T. A., Greco, R., Mollo, L., Slob, E. C., Steele-Dunne, S. 2018. Non-invasive estimation of moisture content in tuff bricks by GPR. *Construction and Building Materials*, 160, pp. 698-706

Algeo, J., Van Dam, R.L., Slater, L. 2016. Early-Time GPR: A method to monitor spatial variations in soil water content during irrigation in clay soils. *Vadose Zone Journal*, 15, doi:10.2136/vzj2016.03.0026

Annan, A.P. 2005. GPR methods for hydrogeological studies, IN: Hydrogeophysics, edited by Y. Rubin, and S. Hubbard, pp. 185–213, *Springer*, New York

Annan, A.R., Cosway, S.W., Redman, J.D. 1991. Water table detection with ground penetrating radar: in Expanded Abstracts. 61st Annual International Meeting of the Society of Exploration Geophysicists, *Society of Exploration Geophysics*, pp. 494-496

Badewa, E., Unc, A., Mumtaz, C., Kavanagh, V., Galagedara, L. 2018. Soil moisture mapping using multi-frequency and multi-coil electromagnetic induction sensors on managed podzols. *Agronomy* 8 (10). p. 224

Bano, M. 2006. Effects of the transition zone above a water table on the reflection of GPR waves. *Geophysical Research Letters,* 33(13), doi:10.1029/2006GL026158

Bear, J. 1972. Dynamics of Fluids in Porous Media, p. 764, *Elsevier*, New York

Bentley, L., Trenholm, N. 2002. The accuracy of water table elevation estimates determined from ground penetrating radar data. *Journal of Environmental & Engineering Geophysics, 7*(1), pp. 37-53. doi:10.4133/JEEG7.1.37

Beres, M., Haeni, F.P. 1991. Application of ground penetrating radar methods in hydrogeologic studies, *Ground Water*, 29, pp. 375–386

Bevan, M.J., Endres, A.L., Rudolph, D.L., Parkin, G.W. 2003. The non-invasive characterization of pumping induced dewatering using ground penetrating radar. *Journal of Hydrology*, 281, pp. 55–69

Booth, A., Clark, R., Murray, T. 2010. Semblance response to a ground penetrating radar wavelet and resulting errors in velocity analysis. *Near Surface Geophysics,* 2010, 8, pp. 235-246

Byrne, M.P., O'Gorman, P.A. 2015. The response of precipitation minus evapotranspiration to climate warming: Why the "Wet-Get-Wetter, Dry-Get-Drier" scaling does not hold over land. *American Meteorological Society*, 28, pp. 8078–8092, doi: org/10.1175/JCLI-D-15-0369.1

Charlton, M.B. 2008. Principles of ground-penetrating radar for soil moisture assessment, Retrieved from: *MBCharlton.com Research Note 3*, 2nd June 2008

Cihlar, J., Ulaby, F.T. 1974. Dielectric properties of soils as a function of moisture content. Technical report, document ID 19750018483, NASA, United States. Retrieved from: https://ntrs.nasa.gov

Conant Jr., B., Cherry, J.A., Gillham, R.W. 2004. A PCE groundwater plume discharging to a river: influence of the streambed and near-river zone on contaminant distributions. *Journal of Contaminant Hydrology*, 73, 249–279

Corbeanu, R.M., McMechan, G.A., Szerbiak, R.B., Soegaard, K. 2002. Prediction of 3D fluid permeability and mudstone distributions from ground-penetrating radar (GPR) attributes: example from the Cretaceous Ferron Sandstone member, east-central Utah. *Geophysics*, 67, pp. 1495–1504

Daniels, D.J. 2004. Ground Penetrating Radar. Second Ed. *The Institute of Electrical Engineers*, London, United Kingdom

Daniels, J.J., Allred, B., Binley, A., Labrecque, D., Alumbaugh, D. 2005. Hydrogeophysical case studies in the vadose zone. IN: Rubin, Y., Hubbard, S.S. (Eds.), Hydrogeophysics, *Springer*, pp. 413–440

Davis, J.L., Annan, A.P. 1989. Ground-penetrating radar for high-resolution mapping of soil and rock stratigraphy. *Geophysical Processes*, 37, pp. 531-551

de Marsily, G. 1986. Quantitative Hydrology, 440 pp., Elsevier, New York

Doetsch, J., Linde, N., Pessognelli, M., Green, A.G., Günther, T. 2012. Constraining 3-D electrical resistance tomography with GPR reflection data for improved aquifer characterization. *Journal of Applied Geophysics*, 78, pp. 68–76

Doolittle, J.A., Jenkinson, B., Hopkins, D., Ulmer, M., Tuttle, W. 2006. Hydropedological investigations with ground-penetrating radar (GPR): Estimating water- table depths and local ground-water flow pattern in areas of coarse-textured soils. *Geoderma, 131* (3), pp. 317-329. doi:10.1016/j.geoderma.2005.03.027

Endres, A. L., Clement, W. P., Rudolph, D. L. 2000. Ground penetrating radar imaging of an aquifer during a pumping test. *Ground Water, 38*(4), pp. 566-576, doi:10.1111/j.1745-6584.2000.tb00249.x

Galagedara, L.W., Parkin, G.W., Redman, J.D. 2003. An analysis of the ground-penetrating radar direct ground wave method for soil water content measurement. *Hydrological Processes* 17(18), pp. 3615-3628

Gish, T., Dulaney, W., Kung, K., Daughtry, C. 2002. Evaluating use of ground-penetrating radar for identifying subsurface flow pathways. Soil Science Society of America Journal, 66 (5). pp. 1620-1629, doi:10.2136/sssaj2002.1620

Grandjean, G., Gourry, J.C. 1996. GPR data processing for 3D fracture mapping in a marble quarry (Thassos, Greece). *Journal of Applied Geophysics*, 36, pp. 19–30

Greaves, R.J., Lesmes, D.P., Lee, J.M., Toksoz, M.N. 1996. Velocity variations and water content estimated from multi-offset, ground-penetrating radar. *Geophysics*, 61, pp. 683-695

Grote, K., Hubbard, S., Rubin, Y. 2003. Field-scale estimation of volumetric water content using ground-penetrating radar ground wave techniques, *Water Resources Research*, 39, p. 1321, doi:10.1029/2003WR002045

Gueting, N., Klotzsche, A., Kruk, J.V.D., Vanderborght, J., Vereecken, H., Englert, A. 2015. Imaging and characterization of facies heterogeneity in an alluvial aquifer using GPR full-waveform inversion and cone penetration tests. *Journal of Hydrology,* 524, pp. 680–695

Huisman, J., Hubbard, S.S., Redman, J.D., Annan, A.P. 2003. Measuring soil water content with ground penetrating radar: A review. *Vadose Zone Journal 2*, pp. 476-491, doi:10.2113/2.4.476

Igel, J., Stadler, S., Günther, T. 2016. High-resolution investigation of the capillary transition zone and its influence on GPR signatures. 16th International Conference on Ground Penetrating Radar (GPR), Hong Kong, 2016, pp. 1-5, doi: 10.1109/ICGPR.2016.7572603

Johnson, D.G. 1992. Use of ground-penetrating radar for water table mapping, Brewster and Harwich, Massachusetts: Water Resources Investigations Report 90-4086, U.S. Geological Survey, Marlborough, Massachusetts

Khalil, M.A., Hafez, M.A., Monteiro Santos, F., Ramalho, E.C., Mesbah, H.S.A., El-Qady, G.M. 2010. An approach to estimate porosity and groundwater salinity by combined application of GPR and VES: a case study in the Nubian sandstone aquifer. *Near Surface Geophysics*, 8, pp. 223–233

Kirby, G.E. 1988. Soils of the Pasadena-Deer Lake area, Newfoundland. St. John’s. Retrieved from http://sis.agr.gc.ca/cansis/publications/surveys/nf/nf17/nf17_report.pdf

Klenk, P., Keicher, V., Jaumann, S., Roth, K. 2014. Current limits for high precision GPR measurements. Proceedings of the 15th International Conference on Ground Penetrating Radar, 30 June-4 July 2014, Belgium, doi:10.1109/ICGPR.2014.6970524

Kowalczyk, S., Lejzerowicz, A., Kowalczyk, B. 2018. Groundwater table level changes based on ground penetrating radar images: a case study. Seventh International Conference on Ground Penetrating Radar, *IEEE Xplore Digital Library*, pp. 1-4. doi:10.1109/ICGPR.2018.8441628

Lambot, S., Slob, E., Chavarro, D., Lubczynski, M., Vereecken, H. 2008. Measuring soil surface water content in irrigated areas of southern Tunisia using full-waveform inversion of proximal GPR data. *Near Surface Geophysics*, 6, pp. 403–410

Liu, Q., Yasufuku, N., Miao, J., Ren, J. 2014. An approach for quick estimation of maximum height of capillary rise. *Soil and foundations*, 54, 6, pp. 1241-1245

Livari, T.A., Doolittle, J.A. 1994, Computer simulations of depths to water table using ground-penetrating radar in topographically diverse terrains: IN: Kovar, K., Soveri, J. (Eds.), Groundwater Quality Management, IAHS Publication No. 220, 11-20

Loeffler, O., Bano, M. 2004. GPR measurements in a controlled vadose zone: Influence of the water content, *Vadose Zone Journal*, 3, pp. 1082–1092

Lunt, I.A., Hubbard, S.S., Rubin, Y. 2005. Soil moisture content estimation using ground penetrating radar reflection data. *Journal of Hydrology*, 307, pp. 254–269

Mahmoudzadeh, M.R., Francés, A.P., Lubczynski, M., Lambot, S. 2012. Using ground-penetrating radar to investigate the water table depth in weathered granites - Sardon case study, Spain. *Journal of Applied Geophysics*, 79, pp. 17–26

Mahmoudzadeh, M.R., Lambot, S., Frances, A.P., Mohammed, A.A., Lubczynski, M. 2010. Water table detection by GPR in Sardon, Salamanca, Spain. Proceedings of the 13th International Conference on Ground Penetrating Radar, Lecce, Italy, 2010. *IEEE*, doi: org/10.1109/ICGPR.2010.5550217

Martinez, A.R. 2001. Q&A with Anibal R. Martinez. *Society of Petroleum Engineers*. doi:10.2118/1201-0016-JPT

McClymont, A.F., Hayashi, M., Bentley, L.R., Liard, J. 2012. Locating and characterizing groundwater storage areas within an alpine watershed using time-lapse gravity, GPR and seismic refraction methods. *Hydrological Processes*, 26, pp. 1792–1804

Miles, O.W., Novakowski, K.S. 2016. Large water- table response to rainfall in a shallow bedrock aquifer having minimal overburden cover. *Journal of Hydrology, 541*, pp. 1316-1328. doi:10.1016/j.jhydrol.2016.08.034

Mohammad, H.M. 2004. Integrating gpr and geostatistical techniques to map the spatial extent of a shallow groundwater system. *Journal of Geophysics and Engineering, 1*(1), 56-62. doi:10.1088/1742-2132/1/1/007

Molina-Sánchez, L., Sánchez-Martos, F., Daniele, L., Vallejos, A., Pulido-Bosch, A. 2015. Interaction of aquifer-wetland in a zone of intensive agriculture: the case of campo de Dalías (Almería, SE Spain). *Environmental Earth Sciences*, 73, pp. 2869–2880

Mukhlisin, M., Saputra, A. 2013. Performance evaluation of volumetric water content and relative permittivity models. *The Scientific World Journal*, p. 421762

Nakashima, Y., Zhou, H., Sato, M. 2001. Estimation of groundwater level by GPR in an area with multiple ambiguous reflections. *Journal of Applied Geophysics, 47*(3), pp. 241-249. doi:10.1016/S0926-9851(01)00068-4

Neal, A. 2004. Ground penetrating radar and its use in sedimentology: principles, problems and progress. *Earth Science Reviews*, 66, pp. 261–330

Oliver, T.S.N., Woodroffe, C.D. 2016. Chronology, Morphology and GPR-imaged Internal Structure of the Callala Beach Prograded Barrier in Southeastern Australia. IN: Vila-Concejo, A.; Bruce, E.; Kennedy, D.M., McCarroll, R.J. (Eds.), Proceedings of the 14th International Coastal Symposium (Sydney, Australia). *Journal of Coastal Research*, Special Issue, No. 75, pp. 318–322

Paz, C., Alcalá, F.J., Carvalho, J.M., Ribeiro, L. 2017. Current uses of ground penetrating radar in groundwater- dependent ecosystems research. *Science of the Total Environment*, 595, pp. 868-885. doi:10.1016/j.scitotenv.2017.03.210

Pyke, K., Eyuboglu, S., Daniels, J., Vendl, M. 2008. A controlled experiment to determine the water table response using ground penetrating radar. *Journal of Environmental and Engineering Geophysics,* 13(4), pp. 335-342. doi:10.2113/jeeg13.4.335

Rejiba, F., Bobée, C., Maugis, P., Camerlynck, C. 2012. GPR imaging of a sand dune aquifer: A case study in the niayes ecoregion of tanma, senegal. *Journal of Applied Geophysics, 81*, pp. 16-20. doi:10.1016/j.jappgeo.2011.09.015

Reppert, P., Morgan, F., Toksoz, M. 2000. Dielectric constant determination using ground-penetrating radar reflection coefficients. *Journal of Applied Geophysics*, 43, pp. 189–197

Reynolds, J.M. 1997. An Introduction to Applied and Environmental Geophysics. 2nd edition, John Wiley & Sons, Ltd, West Sussex, UK

Sakaki, T., Limsuwat, A., Smits, K. M., Illangasekare, T.H. 2008. Empirical two-point α-mixing model for calibrating the ECH_2O EC-5 soil moisture sensor in sands, *Water Resources Research*, 44, doi:10.1029/2008WR006870

Salim, R.L. 2016. Extent of Capillary Rise in Sands and Silts. Master's Thesis (published online), Western Michigan University, Retrieved from: https://scholarworks.wmich.edu/masters_theses/688

Schmelzbach, C., Tronicke, J., Dietrich, P. 2011. Three-dimensional hydrostratigraphic models from ground-penetrating radar and direct-push data. *Journal of Hydrology*, 398, pp. 235–245

Schmelzbach, C., Tronicke, J., Dietrich, P. 2012. High-resolution water content estimation from surface-based ground-penetrating radar reflection data by impedance inversion. *Water Resources Research*, 48, doi.org/10.1029/2012WR011955

Seger, M.A., Nashait, A.F. 2011. Detection of water table by using Ground Penetration Radar (GPR). *Journal of Engineering Technology*, 29, pp. 554–566

Selker, J.S., Keller, C.K., McCord, J.T. 1999. An Introduction to the Vadose Zone. Vadose Zone Processes. 1st edition, CRC Press LLC, Florida, USA, pp. 3-20

Shih, S., Doolittle, J., Myhre, D., Schellentrager, G. 1986. Using radar for groundwater investigation. *Journal of Irrigation and Drainage Engineering*, 112(2), pp. 110-118

Słowik, M. 2014. Analysis of fluvial, lacustrine and anthropogenic landforms by means of ground-penetrating radar (GPR): field experiment. *Near Surface Geophysics*, 12, pp. 777–791

Slowik, M. 2013. GPR and aerial imageries to identify the recent historical course of the Obra River and changes of spatial extent of Obrzańskie Lake, altered by hydro-technical works. *Environmental Earth Sciences*, 70, pp. 1277–1295

Strobach, E., Harris, B.D., Dupuis, J.C., Kepic, A.W., Martin, M.W. 2010. GPR for large-scale estimation of groundwater recharge distribution. Proceedings of the 13th International Conference on Ground Penetrating Radar, Lecce, Italy, 2010. *IEEE*, doi.org/10.1109/ICGPR.2010.5550189

Takeshita, Y., Kobayashi, H., Tao, K., Kaihotsu, I. 2004. Measurement of groundwater behavior in sandy soils using surface ground penetrating radar. IN: Slob, E., A. Yarovoy, A., Rhebergen, J. B. (Eds.), Proceedings of the 10th International Conference Ground Penetrating Radar, The Netherlands, pp. 517-520

Talley, J., Baker, G.S., Becker, M.W., Beyrle, N. 2005. Four dimensional mapping of tracer channelization in sub horizontal bedrock fractures using surface ground penetrating radar. *Geophysical Research Letters*, 32, http://dx.doi.org/10.1029/2004GL021974

Tindall, J.A., Kunkel, J.R., Anderson, D.E. 1999. Unsaturated water flow in soil. IN: R. A. McConnin (Ed.), Unsaturated Zone Hydrology for Scientists and Engineers. New Jersey: Prentice-Hall, Inc., pp. 183-199

Topp, G.C., Davis, J.L., Annan, A.P. 1980. Electromagnetic determination of soil water content: Measurements in coaxial transmission lines. *Water Resources Research*, 16 (3). pp. 574–582

Tsoflias, G.P., Becker, M.W. 2008. Ground-penetrating-radar response to fracture-fluid salinity: why lower frequencies are favorable for resolving salinity changes. *Geophysics*, 73

Tsoflias, G.P., Halihan, T., Sharp Jr., J.M. 2001. Monitoring pumping test response in a fractured aquifer using ground-penetrating radar. *Water Resources Research*, 37, pp. 1221–1229

Van Overmeeren, R.A. 1994. Georadar for hydrogeology. *First Break*, 12 (8), pp. 401-408

Van Overmeeren, R.A. 1998, Radar facies of unconsolidated sediments in The Netherlands: A radar stratigraphic interpretation method for hydrogeology. *Journal of Applied Geophysics*, 40, pp. 1-18

Yang, X., Klotzsche, A., Meles, G., Vereecken, H., van der Kruk, J. 2013. Improvements in crosshole GPR full-waveform inversion and application on data measured at the Boise Hydrogeophysics Research Site. *Journal of Applied Geophysics*, 99, pp. 114–124

Zurek, A.J., Witczak, S., Dulinski, M., Wachniew, P., Rozanski, K., Kania, J., Postawa, A., Karczewski, J., Moscicki, W.J. 2015. Quantification of anthropogenic impact on groundwater-dependent terrestrial ecosystem using geochemical and isotope tools combined with 3-D flow and transport modelling. *Hydrology and Earth System Sciences*, 19, pp. 1015–1033

CHAPTER 4

Summary

4.1 Summary and Future Work

Both drought and flooded or waterlogged farmlands are challenges for agricultural producers in Canada. Long winters, as well as the high soil moisture (SM) levels due to heavy spring rains or rapid snowmelt, can make saturated soil conditions. As a result, agricultural fields become unreachable or difficult to work delaying start of the growing season. A late growing season reduce the crop growth and development and eventually yield of the crops. Proper seed germination and seedling establishment cannot be guaranteed since wet soils are slow to warm up. During the early growing stage, if the SM conditions are still not favorable, the plant root system may be stunted. Further, oxygen demand in the root zone goes high under waterlogging conditions, which may cause death or low productivity of plants having underdeveloped root systems. During the later growing season with dry SM conditions, the root systems should be deep enough to optimize the plant nutrient and water uptake from the soil. Therefore, the SM condition in the root zone, behavior of the water table and capillary zone throughout the growing season are important parameters for water and nutrient management in agricultural fields. The present study proposed a non-invasive method to measure SM and water table depth (WTD) in the agricultural fields using ground-penetrating radar (GPR).

The receiver antenna (Rx) of GPR detects the radar signals that reflected from the interfaces having different relative permittivity (ε_r). GPR records the radar wave travel time from the Tx back to the Rx with respect to the amplitude of the reflected wave. This phenomenon provides a basis to estimate the depth of the reflection interface. However, the reflected wave velocity (v_{rw}) from the surface down to the reflection interface should be known. On the other hand, if the depth to the reflection is known, the v_{rw} can be estimated. Major advantages of the GPR method are non-invasive and time-effective data collection ability in large-scale. Therefore, the GPR technology is suitable to use in the agricultural fields.

The first study obtained v_{rw} from hyperbola fitting in GPR to estimate the SM in the agricultural root zone. Most published studies focused on groundwave velocity to estimate the SM. Groundwave propagates from the Tx to the Rx through the immediately below the ground surface, so that the SM estimation from the groundwave method is applicable for very shallow depths. Since this study focused on the agricultural root zone, the depth of investigation should be at least 30 cm from the surface. Hyperbola fitting method is also challenged by finding shallow hyperbolas in a radargram.

Therefore, this study hypothesized that the same accuracy for SM estimation in 30 cm deep soil profile of the experimental plot could be achieved by fitting the hyperbolas in the depth range from 27 to 50 cm. A systematic TDR data collection was introduced in this study, which could reduce the bias of different sampling volumes of GPR and time domain reflectometry (TDR). Thirteen TDR samples (vertically installed 30 cm long) per one hyperbola location at a maximum radius of 30 cm expected to be a good representation for GPR sample volume and GPR estimated SM data evaluation. In addition, a comparison of the sample areas of the systematic TDR collection and GPR in a 2D plan provides useful information to select the appropriate GPR survey type. The subjective error associated with the hyperbola fitting was reduced by following predefined data processing guidelines. The proposed method would be more efficient when it combines with the latest hyperbola-fitting algorithms (*e.g.*, Dou *et al.*, 2017; Lambot & André, 2014; Mertens *et al*., 2016; Minet *et al*., 2012; Qiao *et al*., 2015; Tran *et al*., 2014).

The second study estimates the WTD throughout the growing season. There are some limitations in GPR, sometimes can be advantageous. Limitation one is centimeters-scale accuracy of WTD is difficult due to the interference from the capillary fringe in GPR data profile. The advantage is distinguishing the water table- and capillary fringe-reflections allows estimation of both WTD and the depth to the capillary fringe (D_{CF}) simultaneously. WTD and D_{CF} are important parameters to ensure the ideal water availability to the crop root system or identification of potential water logging conditions at each growing phase of a crop.

Limitation two is that the direct groundwave velocity is only valid for very shallow depths as mentioned earlier. The advantage is ε_r of a shallow soil layer can be derived from the direct groundwave velocity (Huisman *et al*., 2003; Galagedara *et al*., 2003; Galagedara *et al*., 2005). The shallow soil layer is the most sensitive to the SM variation (*i.e*., for ε_r variation) which can influence the v_{rw} of shallow depths.

Limitation three is that a GPR radargram needs an accurate v_{rw} from the surface down to the water table/capillary fringe for precise depth estimations. GPR multiple-offset surveys are capable of estimating v_{rw}, but they are time and labor consuming. Therefore, v_{rw} was assumed based on ε_r estimations. However, for deep reflections or rough estimations of ε_r, the straight ray path assumption would be valid. The above assumption can add a significant error for the shallow reflections. This limitation was addressed by considering a weighted average of ε_r from different soil layers. ε_r of a deep soil layer was assumed based on the literature. ε_r of a middle soil layer was calculated based on measured SM at different depths. ε_r of the topsoil was determined using the GPR direct-groundwave method.

One GPR center frequency should have been performed well in both studies to monitor SM and WTD simultaneously. However, there is a trade-off between the resolution of the GPR image and the signal penetrating depth. Consequently, 500 MHz high-resolution data acquisition was compatible with SM estimations at the root zone whereas the penetration depth (< 2.5 m under particular conditions) of 500 MHz radar frequency was not sufficient to capture the WTD depths at the study site. However, this thesis focused on three main objectives. Two of them were achieved by the study described in Chapter 2, and the other objective was achieved by the study described in Chapter 3.

	Objective	Conclusion(s)
1	To examine the soil volume that hyperbolic reflections describe in terms of radar wave velocity	Reflections over a 30 cm deep point reflector along 1 m GPR survey length were compared. The CO method covered larger (71.4 %) TDR sample area (30 cm × 70 cm) than the CMP method (49.8 %).
2	To evaluate a practical GPR-based approach to estimate θ_v within the upper 30 cm of the soil profile	SM measurement using the proposed hyperbola fitting method agreed with 30 cm long TDR probe data with an RMSE of 0.02 $m^3\,m^{-3}$ for shallow (< 34 cm), and an RMSE of 0.04 $m^3\,m^{-3}$ for deeper hyperbola analysis.
3	To calibrate and validate a site-specific relationship between GPR-estimated D_{CF} and measured-WTD (WTD_m)	A site-specific relationship was developed $WTD_m = 0.6956\ D_{CF} + 1.3884$ ($R^2 = 0.9778$, n=8). RMSE = 0.194 m for predicted- and measured- WTD.

	An average capillary height (0.741 m) throughout the growing season is suggested for the particular site which is comparable with the literature.

Future Works

The tested systematic TDR probes arrangement could be modified. It is recommended having more TDR sampling locations along the GPR survey line. Probe arrangement should be compatible with the GPR sample geometry (i.e., long TDR probes at the top of the reflector and shallow probes towards both sides of the survey line).

During the data analysis, it was observed in GPR radargrams, that the groundwater reflections near the borehole were free from the capillary fringe, and represented the correct WTD. Thus, the observed height of capillary fringe can be used to correct the GPR measured WTD. However, this observation could not be evaluated with the present study. Therefore, it is recommended to continue the study related to Chapter 3 with an additional two observation boreholes along the GPR survey line.

The second study revealed a methodology to estimate both D_{CF} and WTD within a same GPR profile while the first study discussed the uncertainty/accuracy of estimating SM within the root zone using the hyperbola reflection method. A future study should focus on developing and testing a methodology to measure shallow SM-using the direct groundwave, SM within the root zone-using hyperbola fitting, together with D_{CF} and WTD simultaneously in one GPR profile. If this can be achieved, GPR can be used to derive and map hydrological properties within the vadose zone over larger areas in achieving sustainable agricultural water management.

APPENDICES

APPENDIX 2.1: One to one (1:1) plot of volumetric water content (θ_v) measured by TDR and gravimetric sampling

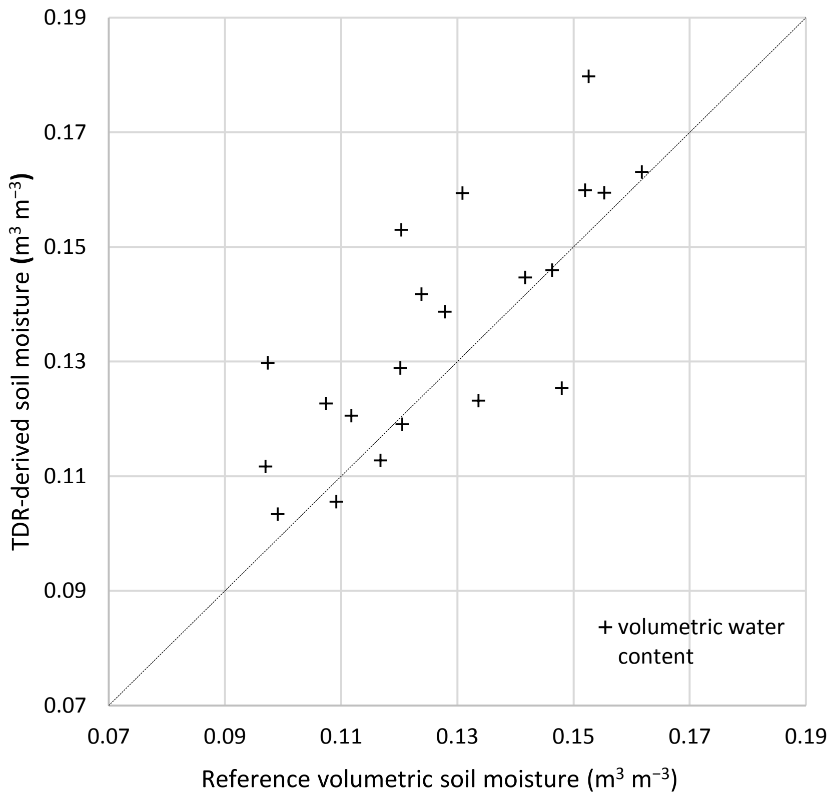

APPENDIX 2.2: One to one (1:1) plot of GPR measured radar wave velocity (v_{rw}) (m/ns) by hyperbola fitting and theoretical calculation using two-way wave travel time (t_{rw})

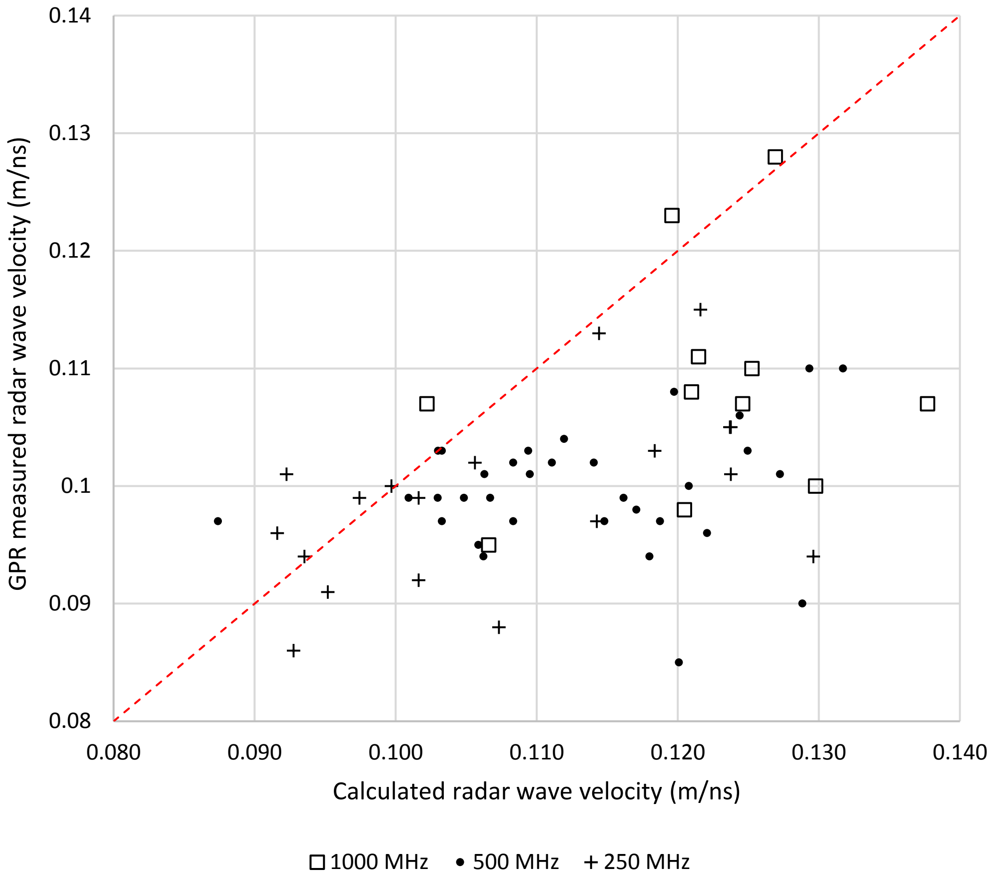

APPENDIX 2.3: One to one (1:1) plot of GPR estimated position (m) vs. actual position (m) of buried location along the GPR transect

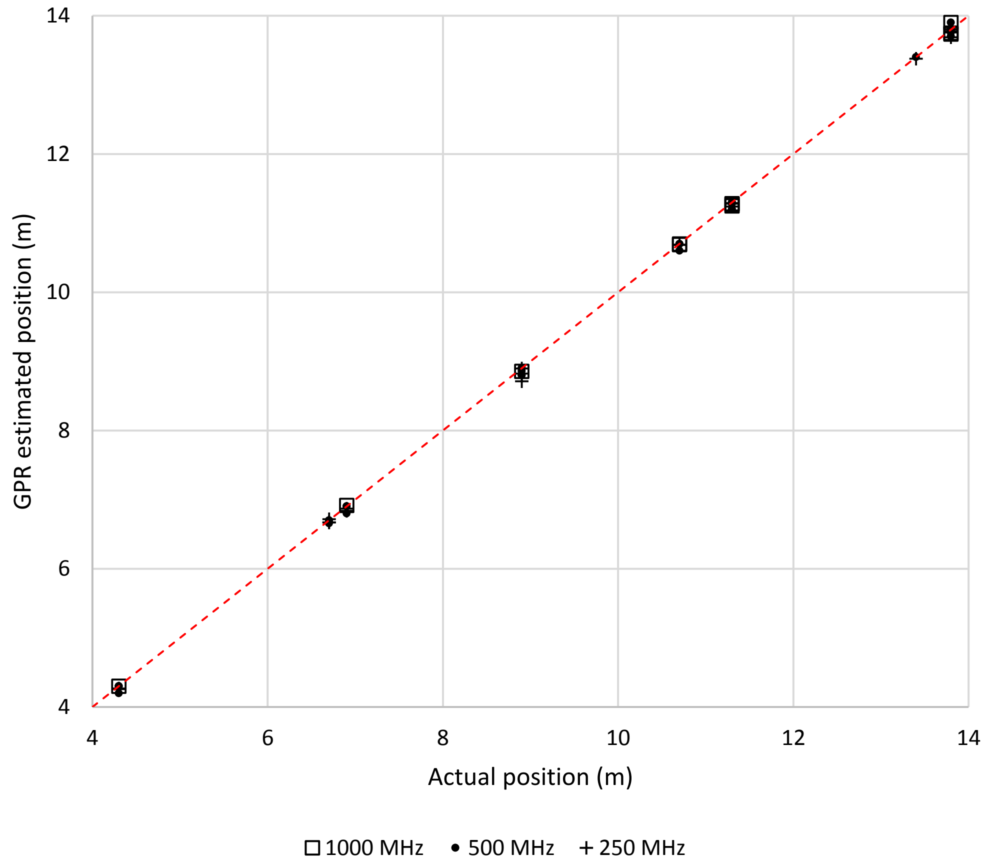

APPENDIX 2.4: One to one (1:1) plot of GPR estimated depth (m) vs. actual depth (m) of buried reflector

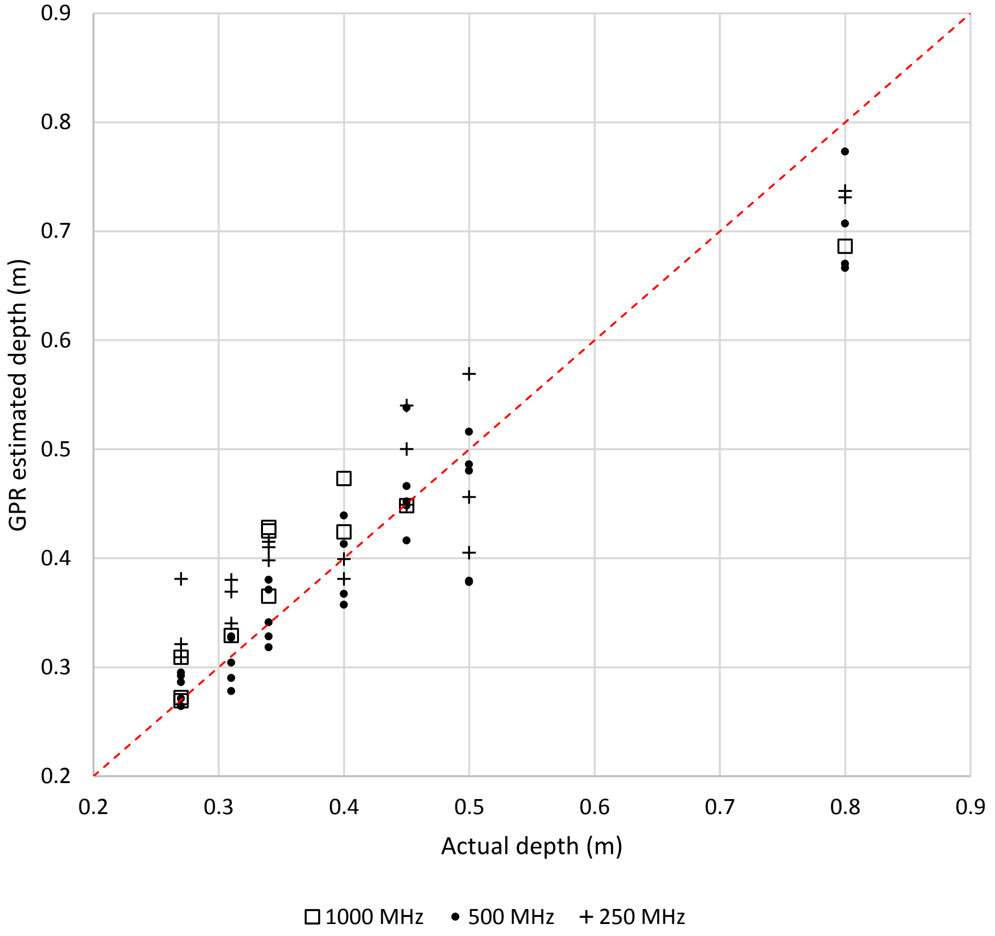

APPENDIX 2.5: Statistical analysis of Chapter 2: outputs of Minitab® 17

Mann-Whitney Test and CI: GPR estimated θ_v, Overall TDR (Depth 27-50 cm)

```
          N   Median
VWC-GPR  18  0.16476
Overall  18  0.15115


Point estimate for η1 - η2 is 0.01010
95.2 Percent CI for η1 - η2 is (-0.00156,0.02442)
W = 383.0
Test of η1 = η2 vs η1 ≠ η2 is significant at 0.1173
The test is significant at 0.1171 (adjusted for ties)
```

Mann-Whitney Test and CI: GPR estimated θ_v, Overall TDR (Depth 27-34 cm)

```
           N   Median
VWC-GPR S  9  0.15776
overall S  9  0.15187


Point estimate for η1 - η2 is 0.00934
95.8 Percent CI for η1 - η2 is (-0.00820,0.02818)
W = 95.0
Test of η1 = η2 vs η1 ≠ η2 is significant at 0.4268
The test is significant at 0.4265 (adjusted for ties)
```

Mann-Whitney Test and CI: GPR estimated θ_v, Overall TDR (Depth 40-50 cm)

```
           N   Median
VWC-GPR D  9  0.17209
overall D  9  0.15043


Point estimate for η1 - η2 is 0.01433
95.8 Percent CI for η1 - η2 is (-0.00700,0.04467)
W = 101.0
Test of η1 = η2 vs η1 ≠ η2 is significant at 0.1853
The test is significant at 0.1846 (adjusted for ties)
```

APPENDIX 2.6: Hyperbola analysis datasheet for 500 MHz

Date	F	Reflector #	Depth (m)	Velocity (m/ns^{-1})	ε_r	GPR θv	Average of TDR measured θv (m^3/m^3) Overall	Upto 20 cm	10cm	20cm	30cm	Across	Along
10/3/2017	500	2	0.45	0.101	8.82	0.1648	0.1736	0.1711	0.1653	0.1770	0.1786	0.1680	0.1793
		3	0.40	0.103	8.48	0.1578	0.1504	0.1513	0.1591	0.1435	0.1487	0.1537	0.1472
		5	0.34	0.099	9.18	0.1721	0.1593	0.1584	0.1569	0.1599	0.1611	0.1585	0.1602
		6	0.27	0.101	8.82	0.1648	0.1660	0.1691	0.1790	0.1592	0.1596	0.1711	0.1608
		7	0.31	0.104	8.32	0.1544	0.1765	0.1785	0.1803	0.1767	0.1723	0.1775	0.1754
		8	0.50	0.099	9.18	0.1721	0.1213	0.1140	0.1070	0.1209	0.1361	0.1245	0.1182
10/24/2017	500	2	0.45	0.108	7.72	0.1415	0.1492	0.1470	0.1420	0.1521	0.1535	0.1443	0.1540
		3	0.40	0.103	8.48	0.1578	0.1504	0.1513	0.1591	0.1435	0.1487	0.1537	0.1472
		5	0.34	0.106	8.01	0.1478	0.1369	0.1361	0.1348	0.1374	0.1384	0.1361	0.1376
		6	0.27	0.110	7.44	0.1355	0.1365	0.1391	0.1473	0.1310	0.1313	0.1408	0.1323
		7	0.31	0.110	7.44	0.1355	0.1549	0.1567	0.1583	0.1552	0.1513	0.1559	0.1540
		8	0.50	0.090	11.11	0.2094	0.1477	0.1387	0.1302	0.1472	0.1656	0.1515	0.1438
6/29/2018	500	2	0.45	0.099	9.18	0.1721	0.1814	0.1788	0.1726	0.1849	0.1866	0.1755	0.1873
		3	0.40	0.097	9.57	0.1797	0.1714	0.1724	0.1813	0.1635	0.1694	0.1751	0.1677
		5	0.34	0.098	9.37	0.1759	0.1262	0.1230	0.1197	0.1269	0.1334	0.1269	0.1247
		6	0.27	0.103	8.48	0.1578	0.1274	0.1323	0.1291	0.1372	0.1164	0.1323	0.1222
		7	0.31	0.100	9.00	0.1684	0.1519	0.1554	0.1594	0.1502	0.1440	0.1448	0.1601
		8	0.50	0.085	12.46	0.2337	0.1648	0.1548	0.1453	0.1642	0.1848	0.1690	0.1605

APPENDIX 3.1: Graphs of measured data

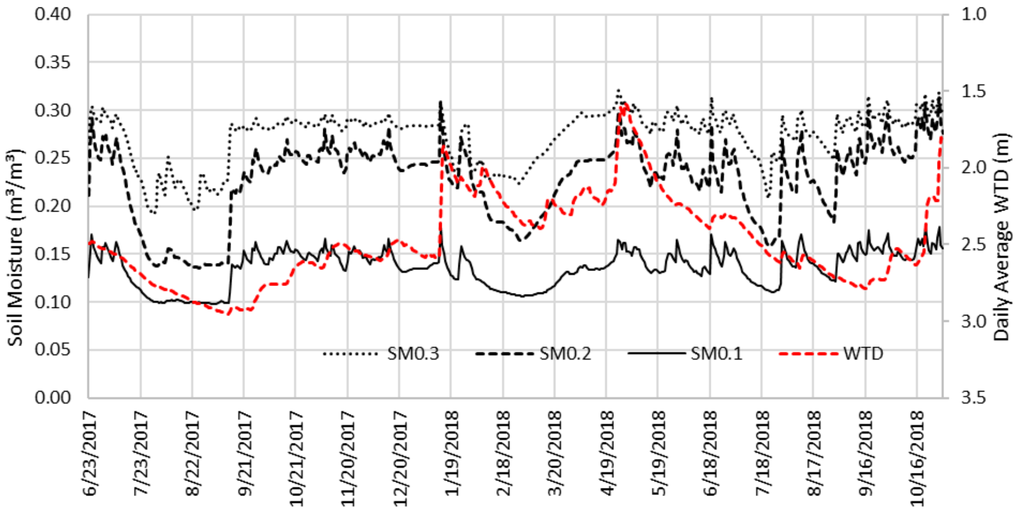

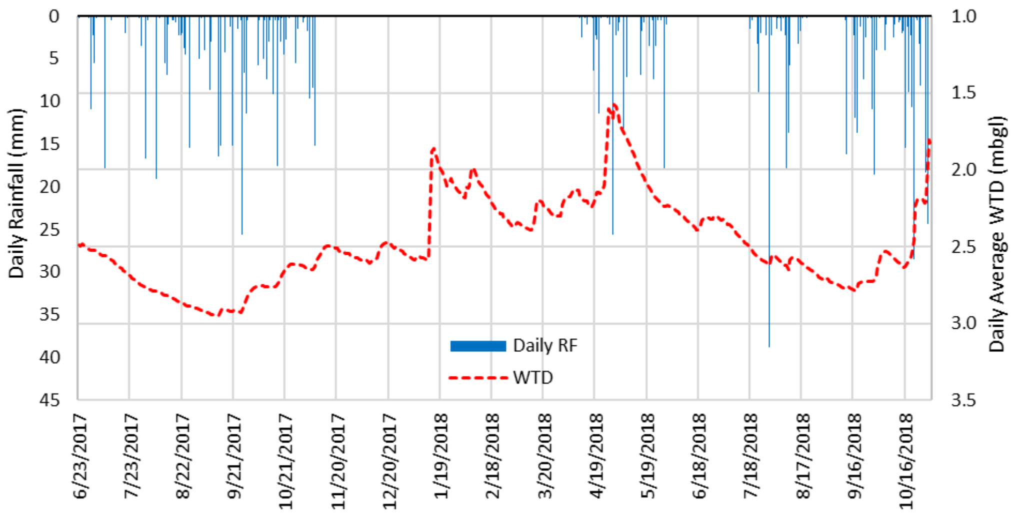

Temporal variation of water table depth (WTD) and soil moisture (SM) at three depths measured near the borehole (above), daily rainfall and daily average WTD fluctuation (below) throughout the study period.

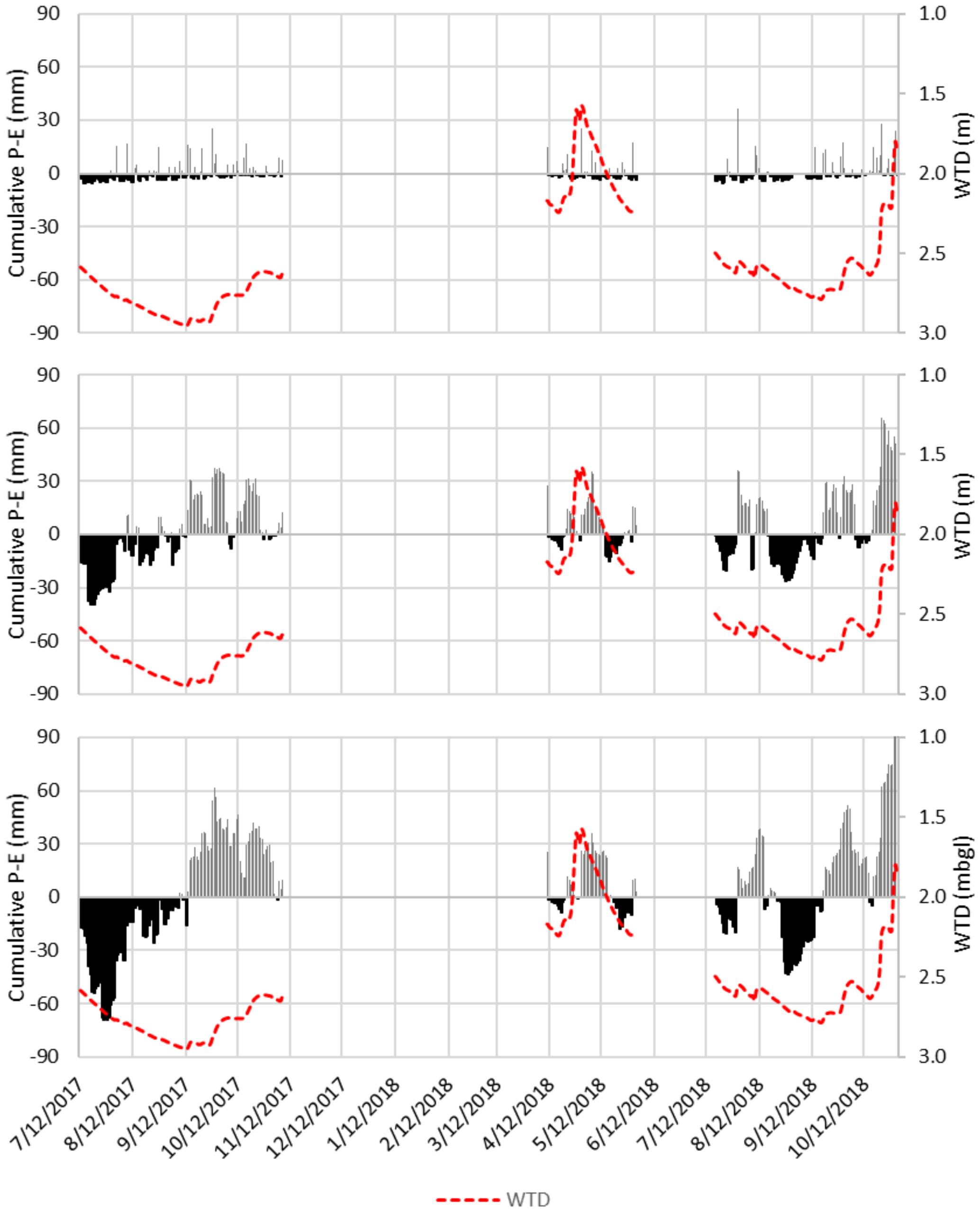

Time lag for water table response to cumulative P-E (daily mean precipitation minus daily mean evapotranspiration); one day time lag (above), 8-days time lag (middle), and 16-days time lag (below).

APPENDIX 3.2: Statistical analysis of Chapter 3

Comparing the slopes of regression line and prediction line with 1:1 line

To test whether the slopes for two independent populations are equal, following null and alternative hypotheses were tested:

H_0: $\beta_1 = \beta_2$ i.e. $\beta_1 - \beta_2 = 0$

H_1: $\beta_1 \neq \beta_2$ i.e. $\beta_1 - \beta_2 \neq 0$

The test statistic is

$$t = \frac{b_1 - b_2}{\sqrt{s_{b_1}^2 + s_{b_2}^2}} \sim T(n_1 + n_2 - 4)$$

n= sample size; b_1 and b_2 are slopes

$$s_b = \frac{s_{y \cdot x}}{s_x \sqrt{n-1}}$$

$s_{y.x}$= standard error of predicted y for each x in the regression
s_x = standard deviation

If the null hypothesis is true then

$$\beta_1 - \beta_2 \sim N\left(0, s_{b_1 - b_2}\right)$$

Where

$$s_{b_1 - b_2} = \sqrt{s_{b_1}^2 + s_{b_2}^2}.$$

Comparison of regression line and 1:1 line

	Regression	1:1 Line
n	16	16
b	1.012	1.000
$s_{y.x}$	0.086	0.000
s_x	0.264	0.264
s_b	0.085	0.000

s_{b1-b2}	0.085
t	0.146
df	28
α	0.050
p-value	0.885
t-critical	2.048
significant	No

Since t < t-critical and p-value> α, two slopes are not significantly different at α=0.05.

Comparison of prediction line and 1:1 line

	Regression	1:1 Line
n	8	8
b	1.597	1.000
$s_{y.x}$	0.086	0.000
s_x	0.171	0.171
s_b	0.169	0.000

s_{b1-b2}	0.169
t	3.536
df	12
α	0.050
p-value	0.004
t-critical	2.179
significant	Yes

Since t > t-critical and p-value< α, two slopes are significantly different at α=0.05.